**Title**
A Micro-Mechanically Based Continuum Model for Strain-Induced Crystallization in Natural Rubber



**Author**
Mistry, Sunny Jigger

**Publication Date**
2014

Peer reviewed|Thesis/dissertation

**A Micro-Mechanically Based Continuum Model for Strain-Induced Crystallization in Natural Rubber**

by

Sunny Jigger Mistry

A dissertation submitted in partial satisfaction of the
requirements for the degree of
Doctor of Philosophy

in

Engineering - Mechanical Engineering

in the

Graduate Division

of the

University of California, Berkeley

Committee in charge:

Professor Sanjay Govindjee, Co-Chair
Professor Panayiotis Papadopoulos, Co-chair
Professor James Casey
Professor Daryl Chrzan

Spring 2014

**A Micro-Mechanically Based Continuum Model for Strain-Induced Crystallization in Natural Rubber**

## Abstract

A Micro-Mechanically Based Continuum Model for Strain-Induced Crystallization in Natural Rubber

by

Sunny Jigger Mistry

Doctor of Philosophy in Engineering - Mechanical Engineering

University of California, Berkeley

Professor Sanjay Govindjee, Co-Chair

Professor Panayiotis Papadopoulos, Co-chair

Recent experimental results show that strain-induced crystallization can substantially improve the crack growth resistance of natural rubber. While this might suggest superior designs of tires or other industrial applications where elastomers are used, a more thorough understanding of the underlying physics of strain-induced crystallization in natural rubber has to be developed before any design process can be started. The objective of this work is to develop a computationally-accessible micro-mechanically based continuum model, which is able to predict the macroscopic behavior of strain crystallizing natural rubber. While several researchers have developed micro-mechanical models of partially crystallized polymer chains, their results mainly give qualitative agreement with experimental data due to a lack of good micro-macro transition theories or the lack of computational power. However, recent developments in multiscale modeling in polymers provide new tools to continue this early work. In this thesis, a new model is proposed to model strain-induced crystallization in natural rubber. To this end, a micro-mechanical model of a constrained partially crystallized polymer chain with an extended-chain crystal is derived and connected to the macroscopic level using the non-affine micro-sphere model. On the macroscopic level, a thermodynamically consistent framework for strain-crystallizing materials is developed, and a description of the crystallization kinetics is introduced. For that matter, an evolution law for crystallization based on the gradient of the macroscopic Helmholtz free energy function (chemical potential) in combination with a simple threshold function is used. A numerical implementation of the model is proposed and its predictive performance assessed using published data.

To my parents

# Contents

# List of Figures

# List of Tables

## Acknowledgments

This thesis marks the end of an unforgettable and incredibly rewarding journey as a Ph.D. student at UC Berkeley. I would like to thank the countless wonderful people I met along the way who contributed to this great time in many ways. I would also like to take this opportunity to thank some of them here.

First and foremost, I am deeply indebted to my Ph.D. advisor Professor Sanjay Govindjee for his endless patience, his support, and most importantly for giving me the opportunity to work with him and learn from his vast knowledge of mechanics. I still remember taking my first lecture on nonlinear continuum mechanics with him 7.5 years ago in Zurich, and being clueless, but instantly intrigued by the subject. Ever since then, I have thoroughly enjoyed all the enlightening and interesting interactions with him, be it in his lectures, as his GSI, in the research meetings, the lunches/dinners, or the fun BBQs at his place. I will always treasure these moments.

I am profoundly grateful to Professor James Casey and Professor Panos Papadopoulos for being on my qualifying exam and dissertation committee. Their genuine enthusiasm for mechanics has always reflected in their highly instructive and ever so enjoyable courses. I would like to thank Professor Daryl Chrzan who agreed to join my dissertation committee on a short notice. I also wanted to thank Professors Tarek Zohdi and Per-Olof Persson for being members of my qualifying exam committee and excellent teachers. Moreover, I thoroughly enjoyed the well-taught courses by Professors Francisco Armero, David Steigmann, and James Sethian.

I heartily thank my current and former labmates Ahmed Bakhaty, Paul Drazin, Giuseppe Montella, Max Igelbüscher, Koki Sagyiama, Toby Mitchell, Tobias Nösekabel, and Tsuyoshi Koyama for many fruitful discussions and making research in a windowless lab fun. Special thanks go to Aurélie Azoug for her motherly reminders of waking up earlier and working more. Even though I never admitted it, I secretly appreciated them.

Throughout my journey as a Ph.D. student, I have been blessed with great friends in my life. They have shared the laughs, their knowledge, their time, the happiness and the inevitable ups and downs of the academic and non-academic life with me, but most importantly they have made me a better person. I am forever indebted to Gerd Brandstetter, Giangiacomo Palombo, Ahmet Can Tanyeri, Amy Nemirovsky, Marco Broccardo, Amaury de Closset, Satomi Nakao, Lisa Buchanan, Adrian Sulc, Eleanor Freund, Michalis Charilaou, Komal Ahmad, Miguel Yupangco, Brett Collins, Debanjan Mukherjee, Chantal & Philippe Hugi, Hiva Esmaeili, Eric Wayman, Michael Hartmann, Jyothi Krishnan, Pedram Hassanzadeh, Francesca & Cristina Verones, Neil Hodge, Flavia Marisi, Harm Schütt, Kranthi Mandadapu, Isabella Reichert, Mahendra Prasad, Sandro De Zanet,...

Above all, I owe heartfelt gratitude to my family, my parents, my brother, and my sister-in law. Without their unwavering support, unconditional love and constant encouragement, I would not be the person I am today.

Berkeley, April 2014 Sunny J. Mistry

# Chapter 1

# Introduction

Historically, the prediction of a material's behavior is closely related to expensive laboratory equipment. However with the comparatively cheap computational power readily available nowadays, numerical methods play an increasingly significant role in the modeling of a wide range of materials. Of particular interest are materials where the macroscopic behavior is driven by the formation and evolution of microstructure. Being able to predict the physics of the microstructure and its macroscopic effects is crucial to the thorough understanding of the material and to the design of new tailored materials. The goal of this thesis is to develop a computationally-accessible micro-mechanically motivated constitutive model for strain-induced crystallization in natural rubber.

## 1.1 Motivation

The study of strain-induced crystallization (SIC) in natural rubber (NR) dates back almost a century to Katz (1925). Using X-ray diffraction, he discovered that NR undergoes a transformation from an initially amorphous solid state to a semi-crystalline state when subjected to strain. Ever since, SIC in NR has been a topic within the complex subject of rubber elasticity, not only because NR is widely used in industrial applications such as tires, seals, and medical devices, but also because its study might deepen the understanding of the Mullins' effect (Govindjee and Simo, 1991) and provide additional insight into the superior crack growth resistance of natural rubber (Le Cam and Toussaint, 2010). Despite this apparent significance, only scant work has been done in the development of a micro-mechanically based continuum model of SIC in NR.

The phenomenon of SIC in NR can be observed and measured in several different ways. In (Gent, 1954) the author uses a hydrostatic weighing technique (Gee et al., 1950) to measure the decrease in volume of a vulcanized rubber sample when it is stretched. Thereby the volume reduction is identified to be proportional to the evolution of the degree of crystallinity in the material. A 1% change in volume is determined to occur for 11.7% crystallinity by comparing it with early X-ray scattering results from Goppel (1949a,b); Arlman (1949);

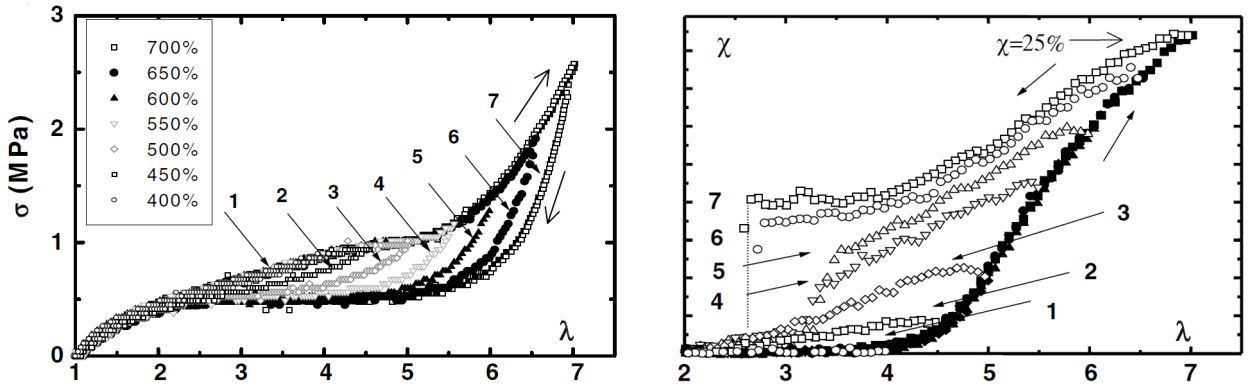


Figure 1.1: Typical experimental results (taken from Albouy et al. (2005)) for a vulcanized natural rubber sample: (left) the typical stress-stretch hysteresis loop for uniaxial loading cycles; (right) the degree of crystallinity $\chi$ measured using an in-situ synchrotron wide-angle X-ray diffraction method.

Goppel, J.M. and Arlman, J.J. (1949); Arlman and Goppel (1951). Another approach is chosen by Wildschut (1946), where stress-relaxation at a constant stretch is measured as a function of decreasing temperature. The author observes that the stress-relaxation can be used as a measure for the degree of crystallinity. Both of the suggested techniques proved to be rather time consuming and only provided coarse measures of crystallinity.

The state of the art in measuring degrees of crystallinity today are in-situ synchrotron wide-angle X-ray diffraction methods as used in Toki et al. (2000); Murakami et al. (2002); Toki et al. (2003); Trabelsi et al. (2003); Toki et al. (2005); Chenal et al. (2007). In Figure 1.1, experimental results from Albouy et al. (2005) are shown to point out some typical features of the macroscopic behavior of vulcanized natural rubber. The stress-strain curves show a characteristic *hysteresis loop* consisting of *S-shaped* loading/unloading curves and an *upturn in stress* towards higher stretches. The degree of crystallinity only starts evolving at stretches of around 4 and reaches maximum levels of 20% to 25%.

On the microscopic scale, NR consists of highly flexible, mobile and long polymer chains that build random network microstructures through cross-links, when vulcanized. SIC from that perspective can be seen in the following way: When a stretch is applied on the macroscopic scale, the polymer chains in the network start to stretch as well and start aligning occasionally, building crystalline structures. The higher the applied stretch will be, the more chains will build regular aligned crystal structures. A sketch of this strain-induced change of microstructure is shown in Figure 1.2. It is also important to note that this crystallizing process is observed at room temperature.

The task at hand for this thesis is to predict the behavior of SIC in NR as shown in Figure 1.1 by connecting the microscopic and the macroscopic viewpoints. The focus hereby

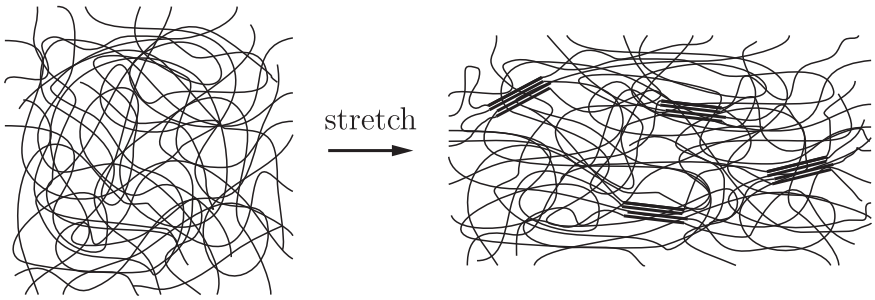


Figure 1.2: Sketch of SIC in NR for part of a typical random network microstructure: when a stretch is applied to a undeformed amorphous solid state (left), polymer chains start aligning and building crystalline structures at room temperature.

is on modeling the evolution of the microstructure and linking it to its macroscopic behavior in a thermodynamically consistent and computationally accessible way.

## 1.2 State of the Art

In order to develop a model of SIC in NR that takes advantage of the evolution of the microstructure to predict the macroscopic behavior, the following three equally important parts have to be considered:

1. A micro-mechanical model of a partially crystallized polymer chain (see Figure 1.2).
2. A description of the crystallization kinetics in polymers, i.e. the time evolution of the degree of crystallinity within the material (see right plot in Figure 1.1).
3. A micro-to-macro transition that connects micro-kinematic variables of the single chain with macroscopic continuum deformation measures.

While extensive work has been done on each of the separate parts, very little work has been done in combining them into a multiscale model. Thus, the main contributions to each of the three parts are summarized next.

The cornerstone of modeling SIC was laid by Flory's statistical mechanical theory of extended chain crystallization (Flory, 1947). In this theory he uses a Gaussian distribution function to model the partially crystallized polymer chains and assumes that the crystallized part of the chain is oriented in the direction of stretch. There is no evolution of the degree of crystallinity involved, since equilibrium crystallization is assumed. All the relations in Flory's model are derived for uniaxial loading using an affine deformation assumption, which is known to result in inaccurate predictions for large deformations. Some years later, Gaylord (1976) and Gaylord and Lohse (1976) developed an improved theory of SIC with two modified assumptions. Unlike Flory, the authors took chain folding into account, which adds insight

about crystal morphologies and orientation, and used a non-Gaussian distribution function derived by Wang and Guth (1952) to model the polymer chains. At the same time another model was proposed by Smith (1976). He relaxed Flory's condition that the extended crystal has to be oriented in the direction of stretch by saying that the direction a chain takes through a crystal is determined by the first few links of a chain entrapped within the crystal itself. Even though all of the above mentioned models have good qualitative agreement with experimental data, they are not able to fully reproduce the behavior as shown in Figure 1.1. The reasons for this are two fold. First, all of the models assume equilibrium crystallization and thus do not consider the time evolution of crystallinity. Second, all of them lack a satisfactory micro-to-macro transition, which accurately models the random network microstructure of NR. However, all of them share the fact that they develop detailed micro-mechanical models of a partially crystallized polymer chains.

Crystallization kinetics itself is a widely studied phenomenon, e.g. in the study of phase changes in metals. Roughly speaking there are three different approaches. One of the most extensively used approaches to describe the process of crystallization is the model of Avrami (1939, 1940, 1941). Based on geometric considerations of nucleation and crystal growth, the equation of Avrami is given by the exponential law $\omega \propto 1 - \mathrm{e}^{-kV_t}$, where $\omega$ is the degree of crystallinity, $k$ is the average density of nuclei, and $V_t$ is the volume a crystal would occupy after a time t. Here $V_t$ depends on the growth rate and the shape of the crystal. Some years later a similar equation was obtained by Evans (1945) and applied to temperature-induced crystallization of Nylon 6,6 by Allen (1952). Gent (1954) was the first to extend the treatment of Avrami to stretched natural rubber vulcanizates and approximate the time functions governing crystal growth. A second and widely used approach is taken by Becker (1938), Turnbull and Fisher (1949), and Hoffman and Weeks (1962). They use an Arrhenius equation to describe the crystallization process, $\dot{\omega} \propto \exp\left(-\Delta F/(k_B T)\right)$, where $\dot{\omega}$ is the rate of crystallization and $\Delta F$ the free energy change upon crystallization. A third approach first discussed for polymer crystallization by Roe and Krigbaum (1965) is based on a micro-mechanical model of a partially crystallized polymer chain and uses its free energy gradient (chemical potential) $\dot{\omega} \propto -\partial F/\partial\omega$ as the driving force for crystallization. All of the three mentioned models have in common that they regard crystallization as a subject in itself and thus do not conisder its effects on the macorscopic scale for natural rubber.

The lack of a satisfactory micro-to-macro transition has also been a challenging topic within the micro-mechanically based modeling of rubber elasticity. A good overview of constitutive models can be found in Boyce and Arruda (2000). More recently Miehe, Goktepe, and Lulei (2004) have extended the micro-plane model of Bazant and Oh (1985) to the so-called non-affine micro-sphere model of rubber elasticity. This is a microscopically motivated finite deformation model for rubberlike materials. The model combines three special features: Firstly, it includes a non-affine stretch component, where micro and macro stretches are linked through a fluctuation field on a micro-sphere. The fluctuation field itself is determined by a minimization of the macroscopic free energy. Secondly, polymer cross-links and entanglements are also considered using the so-called tube model of rubber elasticity, where the movement of a single chain is restricted by a tube-like constraint (Doi and Edwards,

1986). Thirdly, since closed-form solutions to the averaging integrals over a sphere are not available, a 21-point integration scheme, as derived in the original micro-plane model of Bazant and Oh (1985), is used.

## 1.3 Outline

The objective of this work is to leverage these ideas and develop a computationally-accessible micro-mechanically based continuum model, that is able to predict the macroscopic behavior of NR as shown in Figure 1.1. The organization of the presented thesis is as follows. In **Chapter 2** the basic concepts of continuum mechanics that build the macroscopic framework for the modeling process in mind, are outlined. In particular, key deformation measures are introduced, balance principles derived, and the Second Law of Thermodynamics is discussed. **Chapter 3** presents the fundamentals of statistical mechanics, providing the tools to physically understand and mathematically model polymeric materials from a microstructural point of view. **Chapter 4** shows how to connect macroscopic deformation measures with kinematic variables of a random network microstructure of polymers, and provides a way to incorporate microstructural information about polymer chains into a continuum constitutive relation for rubberlike materials using the non-affine micro-sphere model. In **Chapter 5** all the previously introduced ideas are used to propose a new model for SIC in NR. In particular, on the microscopic level, the free energy of an unconstrained semi-crystalline polymer chain with extended crystals is derived and connected to the macroscopic level using the non-affine micro-sphere model. On the macroscopic level, a thermodynamically consistent framework for strain-crystallizing materials is developed, and an evolution law for the degree of crystallinity based on the macroscopic Helmholtz free energy is introduced, where the free energy gradient is used as a driving force. Moreover, a threshold function for the evolution law inspired by phase change evolution in martensitic alloys (Govindjee and Miehe, 2001) is introduced. Finally in **Chapter 6**, a computationally-accessible algorithmic setting of the proposed model is laid out, and its predictive performance is assessed by using published data. Moreover, the physical meaning of the model parameters are emphasized in a comparison to the recent work of Kroon (2010).

# Chapter 2

# Continuum Mechanics

In this chapter, the basic concepts of continuum mechanics will be introduced. This review is not intended to be comprehensive, but rather meant to introduce the relevant notation and set the framework for the following chapters. The material treated here is mainly based on the lecture notes of Govindjee (2006), Papadopoulos (2013) and Naghdi (2001). For a more thorough treatment of the subject matter the reader is referred to the works by Chadwick (1999), Gurtin (1982), Ogden (1997), or Holzapfel (2000). The more advanced reader interested in the mathematical foundations of mechanics and its connection to geometry is referred to the monographs by Truesdell and Toupin (1960), Truesdell and Noll (1965), Bishop and Goldberg (2012), and Marsden and Hughes (1994).

## 2.1 Kinematics of Deformation

Kinematics is "the branch of mechanics concerned with the motion of objects without reference to the forces which cause the motion."[1] To this end the notion of *bodies*, *configurations*, their associated *motions* and *deformation measures* will be discussed here.

### 2.1.1 Description of Motion

Let a *continuum body* $\mathcal{B}$ be defined as a collection of infinitely many *material particles*[2] (or material points or particles) $P \in \mathcal{B}$ and let a subset of $\mathcal{B}$ be denoted by $\mathcal{S}$. Furthermore, let $x$ be the point in the three-dimensional Euclidean point space $\mathcal{E}^3$ occupied by a particle $P \in \mathcal{B}$ at time $t \in \mathbb{R}_+$, and let $\mathbf{x}$ be its location relative to a fixed origin $O$ in the vector space $E^3$. This assignment of particles $P \in \mathcal{B}$ to position vectors in $E^3$ is called a *configuration*

[1] "kinematics". Oxford Dictionaries. Oxford University Press.`http://www.oxforddictionaries.com/us/definition/english/kinematics` (accessed November 18, 2013).

[2] This term should not be confused with a point mass in the Newtonian sense.

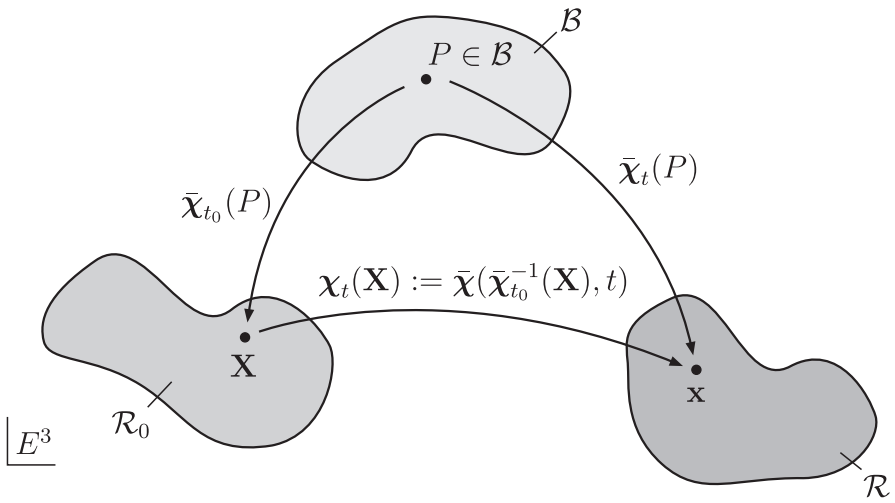


Figure 2.1: Mapping of a physical body $\mathcal{B}$ to its reference configuration $\mathcal{R}_0$ at time $t_0$ with positions $\mathbf{X}$ and its current configuration $\mathcal{R}$ at time $t$ with positions $\mathbf{x}$.

*mapping* (or configuration) of $\mathcal{B}$ at time t and is described by an invertible relation

$$\bar{\boldsymbol{\chi}} : (P, t) \in \mathcal{B} \times \mathbb{R}_+ \to E^3, \tag{2.1}$$

such that

$$\mathbf{x} = \bar{\boldsymbol{\chi}}(P, t) = \bar{\boldsymbol{\chi}}_t(P). \tag{2.2}$$

Given $\bar{\boldsymbol{\chi}}_t$, the body $\mathcal{B}$ may be mapped to its configuration $\mathcal{R}_t = \bar{\boldsymbol{\chi}}_t(\mathcal{B}, t)$ at time $t$. Similarly, $\mathcal{S} \subset \mathcal{B}$ can be mapped to its configuration $\mathcal{P}_t = \bar{\boldsymbol{\chi}}_t(\mathcal{S}, t)$. Since the configuration mapping $\bar{\boldsymbol{\chi}}_t$ is invertible, the position $\mathbf{x} = \bar{\boldsymbol{\chi}}_t(P) \in \mathcal{R}_t$ can uniquely be associated to a particle $P \in \mathcal{B}$ according to $P = \bar{\boldsymbol{\chi}}_t^{-1}(\mathbf{x})$ and the interpenetration of particles (matter) is excluded. The *motion* of the body $\mathcal{B}$ can thus be defined as a one parameter family of configurations $\mathcal{R}_t$ represented by $\bar{\boldsymbol{\chi}}_t$. This description however is of limited use because there is no straightforward way of labeling the particles of the body. A more useful description of the motion of $\mathcal{B}$ is found by looking at two of its configurations.

Let the configuration of the body $\mathcal{B}$ at an arbitrary time $t_0$ be denoted as the *reference configuration* $\mathcal{R}_0 := \bar{\boldsymbol{\chi}}_{t_0}(\mathcal{B})$, also referred to as the *Lagrangian configuration*. Similarly, let the configuration at time $t$ be denoted as the *current configuration* $\mathcal{R} := \mathcal{R}_t = \bar{\boldsymbol{\chi}}_t(\mathcal{B})$ (and likewise $\mathcal{P} := \mathcal{P}_t = \bar{\boldsymbol{\chi}}_t(\mathcal{S})$), also termed *spatial* or *Eulerian configuration*. The points occupied by a particle $P \in \mathcal{B}$ can then be labeled by the referential position $\mathbf{X} := \bar{\boldsymbol{\chi}}_{t_0}(P) \in \mathcal{R}_0$ and the current position $\mathbf{x} := \bar{\boldsymbol{\chi}}_t(P) \in \mathcal{R}$, respectively. By exploiting the invertibility of $\bar{\boldsymbol{\chi}}_{t_0}$, the motion of a body can also be described by a mapping $\boldsymbol{\chi}_t$ between $\bar{\boldsymbol{\chi}}_{t_0}(P)$ and $\bar{\boldsymbol{\chi}}_t(P)$ as

$$\mathbf{x} = \bar{\boldsymbol{\chi}}_t(P) = \bar{\boldsymbol{\chi}}(\bar{\boldsymbol{\chi}}_{t_0}^{-1}(\mathbf{X}), t) =: \boldsymbol{\chi}(\mathbf{X}, t) = \boldsymbol{\chi}_t(\mathbf{X}). \tag{2.3}$$

The so-called *deformation map* $\boldsymbol{\chi}_t$

$$\boldsymbol{\chi}_t(\mathbf{X}) := \begin{cases} E^3 \times \mathbb{R}_+ & \to E^3 \\ (\mathbf{X}, t) & \mapsto \mathbf{x} = \boldsymbol{\chi}_t(\mathbf{X}), \end{cases} \tag{2.4}$$

represents the *referential* or *Lagrangian description* of the body motion and maps a referential position $\mathbf{X} \in \mathcal{R}_0$ of a particle $P \in \mathcal{B}$ to the current position $\mathbf{x} \in \mathcal{R}$ at time $t$, see Figure 2.1. Also note the invertibility of the mapping $\boldsymbol{\chi}$

$$\mathbf{X} = \bar{\boldsymbol{\chi}}_{t_0}(P) = \bar{\boldsymbol{\chi}}_{t_0}(\bar{\boldsymbol{\chi}}_t^{-1}(\mathbf{x})) = \boldsymbol{\chi}_t^{-1}(\mathbf{x}). \tag{2.5}$$

To further distinguish between referential and spatial quantities, let $\{\mathbf{E}_1, \mathbf{E}_2, \mathbf{E}_3\}$ and $\{\mathbf{e}_1, \mathbf{e}_2, \mathbf{e}_3\}$ be fixed right-hand orthonormal bases for the reference and the current configuration, respectively. Using these bases, the position vectors $\mathbf{X}$ and $\mathbf{x}$, and the motion $\boldsymbol{\chi}_t$ can be expressed as

$$\mathbf{X} = X_A \mathbf{E}_A, \quad \mathbf{x} = x_i \mathbf{e}_i, \quad \text{and} \quad x_i \mathbf{e}_i = \chi_i(X_A \mathbf{E}_A, t)\mathbf{e}_i, \tag{2.6}$$

where the *Einstein summation convention* is used. The velocity and acceleration vectors are given by

$$\mathbf{v} = \frac{\partial \boldsymbol{\chi}(\mathbf{X}, t)}{\partial t} \quad , \quad \mathbf{a} = \frac{\partial^2 \boldsymbol{\chi}(\mathbf{X}, t)}{\partial t^2}, \tag{2.7}$$

respectively. With the definition of the body motion (2.4) at hand, fundamental finite *deformation measures* can be introduced.

### 2.1.2 Deformation Measures

The key deformation measure used in finite deformation kinematics is the *deformation gradient*. It is defined as the gradient of the deformation map (2.4) with respect to the reference position $\mathbf{X} \in \mathcal{R}_0$,

$$\mathbf{F} := \frac{\partial \boldsymbol{\chi}(\mathbf{X}, t)}{\partial \mathbf{X}} = \frac{\partial \chi_i(X_B, t)}{\partial X_A}\, \mathbf{e}_i \otimes \mathbf{E}_A = F_{iA} \mathbf{e}_i \otimes \mathbf{E}_A, \tag{2.8}$$

which can also be written as $\mathbf{F} = \mathrm{Grad}(\boldsymbol{\chi}_t) = \nabla_{\mathbf{X}} \boldsymbol{\chi}_t$. Since the motion $\boldsymbol{\chi}_t$ is invertible, the inverse $\nabla_{\mathbf{x}} \boldsymbol{\chi}_t^{-1}(\mathbf{x}) = \mathbf{F}(\mathbf{X}, t)^{-1}$ exists[3] and $\det \mathbf{F} \neq 0$ has to be satisfied. The deformation gradient $\mathbf{F}$ can be considered as a *linear map* of a differential material line element[4] $\mathrm{d}\mathbf{X}$ in the reference configuration into another differential line element $\mathrm{d}\mathbf{x}$ in the current configuration. A simple application of the chain rule can establish this,

$$\mathrm{d}\mathbf{x} = \frac{\partial \boldsymbol{\chi}(\mathbf{X}, t)}{\partial \mathbf{X}}\, \mathrm{d}\mathbf{X} = \mathbf{F} \mathrm{d}\mathbf{X}. \tag{2.9}$$

[3] Can be shown using the inverse function theorem from Rudin (1976, Chapter 9).

[4] A volume, surface, or curve which consists of the same material points in all configurations is called *material*.

Typically, d$\mathbf{X}$ will stretch and rotate to d$\mathbf{x}$ when $\mathbf{F}$ is applied. In order to extract stretch-related information from $\mathbf{F}$, the splits $\mathrm{d}\mathbf{X} = \mathbf{M}dS$ and $\mathrm{d}\mathbf{x} = \mathbf{m}ds$ are introduced, where essentially d$\mathbf{X}$ and d$\mathbf{x}$ are decomposed into its unit directions $\mathbf{M}$ and $\mathbf{m}$, and lengths $dS$ and $ds$, respectively. This allows the stretch of an infinitesimal line element d$\mathbf{X}$ to be defined as $\lambda = \frac{ds}{dS}$. Using the *stretch* $\lambda$, (2.9) can be rewritten as

$$\mathrm{d}\mathbf{x} = \mathbf{F}\mathrm{d}\mathbf{X} = \mathbf{F}\mathbf{M}dS = \mathbf{m}ds, \tag{2.10}$$

and thus

$$\lambda\mathbf{m} = \mathbf{F}\mathbf{M}. \tag{2.11}$$

The stretch can then easily be extracted by

$$\begin{aligned}(\lambda\mathbf{m}) \cdot (\lambda\mathbf{m}) = \lambda^2(\mathbf{m}\cdot\mathbf{m}) = \lambda^2 &= (\mathbf{F}\mathbf{M}) \cdot (\mathbf{F}\mathbf{M}) \\ &= \mathbf{M} \cdot (\mathbf{F}^\top\mathbf{F})\mathbf{M} \\ &= \mathbf{M} \cdot \mathbf{C}\mathbf{M},\end{aligned} \tag{2.12}$$

where $\mathbf{C}$ is the *right Cauchy-Green tensor*, defined as

$$\mathbf{C} := \mathbf{F}^\top\mathbf{F} = F_{iA}F_{iB}\,\mathbf{E}_A \otimes \mathbf{E}_B = C_{AB}\,\mathbf{E}_A \otimes \mathbf{E}_B. \tag{2.13}$$

The *symmetric* and *positive-definite* kinematic measure $\mathbf{C}$ allows the determination of the stretch $\lambda$ of an infinitesimal material line element d$\mathbf{X}$, given its direction $\mathbf{M}$.

Another important kinematic quantity is found, when the difference in the squares of the lengths of d$\mathbf{X}$ and d$\mathbf{x}$ is considered,

$$\begin{aligned}ds^2 - dS^2 &= (\mathrm{d}\mathbf{x}\cdot\mathrm{d}\mathbf{x}) - (\mathrm{d}\mathbf{X}\cdot\mathrm{d}\mathbf{X}) \\ &= (\mathbf{F}\mathrm{d}\mathbf{X})\cdot(\mathbf{F}\mathrm{d}\mathbf{X}) - (\mathrm{d}\mathbf{X}\cdot\mathrm{d}\mathbf{X}) \\ &= \mathrm{d}\mathbf{X}\cdot(\mathbf{F}^\top\mathbf{F})\,\mathrm{d}\mathbf{X} - (\mathrm{d}\mathbf{X}\cdot\mathrm{d}\mathbf{X}) \\ &= \mathrm{d}\mathbf{X}\cdot(\mathbf{C})\,\mathrm{d}\mathbf{X} - (\mathrm{d}\mathbf{X}\cdot\mathrm{d}\mathbf{X}) \\ &= \mathrm{d}\mathbf{X}\cdot(\mathbf{C}-\mathbf{I})\,\mathrm{d}\mathbf{X} \\ &= \mathrm{d}\mathbf{X}\cdot 2\mathbf{E}\,\mathrm{d}\mathbf{X},\end{aligned} \tag{2.14}$$

where

$$\mathbf{E} := \frac{1}{2}(\mathbf{C}-\mathbf{I}) = \frac{1}{2}(\mathbf{F}^\top\mathbf{F}-\mathbf{I}) = \frac{1}{2}(F_{iA}F_{iB}-\delta_{AB})\,\mathbf{E}_A \otimes \mathbf{E}_B \tag{2.15}$$

is the *Green-Lagrange strain tensor*[5]. Note that the tensor $\mathbf{E}$ is symmetric and vanishes, when the body is not undergoing any deformation ($\mathbf{F} = \mathbf{I}$) or when $\mathbf{F}$ is a rotation ($\mathbf{F}^\top\mathbf{F} = \mathbf{I}$). To summarize, neither $\mathbf{C}$ nor $\mathbf{E}$ provide information about the rotation of d$\mathbf{X}$. In order to

[5]It is also sometimes referred to as the *Green-St.Venant strain tensor.*

have a quantity that yields rotation-related information based on $\mathbf{F}$, the *polar decomposition theorem* is used. It states that any invertible tensor $\mathbf{F}$ can be uniquely decomposed into

$$\mathbf{F} = \mathbf{RU} = R_{iB}U_{BA}\,\mathbf{e}_i \otimes \mathbf{E}_A, \tag{2.16}$$

where $\mathbf{R}$ is an *orthogonal tensor* ($\mathbf{R}^\top\mathbf{R} = \mathbf{R}\mathbf{R}^\top = \mathbf{I}$) and $\mathbf{U}$ is a symmetric positive definite tensor. Combining the polar decomposition theorem and the definition of $\mathbf{C}$ (2.13) yields the relation

$$\mathbf{C} = \mathbf{F}^\top\mathbf{F} = (\mathbf{RU})^\top(\mathbf{RU}) = \mathbf{U}^\top\mathbf{R}^\top\mathbf{RU} = \mathbf{U}^2, \tag{2.17}$$

where $\mathbf{U}$ is called the *right stretch tensor*. This relation implies that $\mathbf{U}$ can also be used to determine the stretch of $\mathrm{d}\mathbf{X}$. Since $\mathbf{U} = \sqrt{\mathbf{C}}$, the rotation $\mathbf{R}$ of an infinitesimal material line element $\mathrm{d}\mathbf{X}$ can simply extracted by $\mathbf{R} = \mathbf{F}\mathbf{U}^{-1}$.

Once the deformation gradient $\mathbf{F}$ (the mapping of $\mathrm{d}\mathbf{X}$ into $\mathrm{d}\mathbf{x}$) is defined, two other fundamental maps can be introduced. To this end, consider the transformation of an infinitesimal material volume element $dV$ in the reference configuration to its spatial counterpart $dv$, where $dV$ and $dv$ denote the volume of the parallelepipeds

$$dV = \mathrm{d}\mathbf{X}^1 \cdot (\mathrm{d}\mathbf{X}^2 \times \mathrm{d}\mathbf{X}^3) \quad \text{and} \quad dv = \mathrm{d}\mathbf{x}^1 \cdot (\mathrm{d}\mathbf{x}^2 \times \mathrm{d}\mathbf{x}^3). \tag{2.18}$$

Each $\mathrm{d}\mathbf{X}^i$ gets mapped according to (2.9) as $\mathrm{d}\mathbf{x}^i = \mathbf{F}\mathrm{d}\mathbf{X}^i$. Thus using the triple product, $dv$ is rewritten as

$$\begin{aligned} dv &= \mathrm{d}\mathbf{x}^1 \cdot (\mathrm{d}\mathbf{x}^2 \times \mathrm{d}\mathbf{x}^3) \\ &= (\mathbf{F}\mathrm{d}\mathbf{X}^1) \cdot ((\mathbf{F}\mathrm{d}\mathbf{X}^2) \times (\mathbf{F}\mathrm{d}\mathbf{X}^3)) \\ &= \det\left[[F_{iA}dX^1_A], [F_{iA}dX^2_A], [F_{iA}dX^3_A]\right] \\ &= \det\left[F_{iA}[dX^1_A, dX^2_A, dX^3_A]\right] \\ &= (\det\mathbf{F})\det\left[[dX^1_A], [dX^2_A], [dX^3_A]\right] \\ &=: J\,dV, \end{aligned} \tag{2.19}$$

where $J$ is defined as

$$J = \det\mathbf{F} \tag{2.20}$$

and referred to as *volume map*. If one assumes by convention that $dV > 0$ (and $J > 0$), then $dv < 0$ cannot be reached by a continuous motion starting in the reference configuration (since $J$ would have to go through 0, which would violate the assumption of invertibility). Hence, for the motion to be physically admissible, in addition to $\det\mathbf{F} \neq 0$,

$$J = \det\mathbf{F} > 0 \tag{2.21}$$

has to hold true. A motion is called *isochoric* (or *volume-preserving*) if $J = 1$ for all $dV$ at all times.

Next, consider the transformation of an infinitesimal material surface element $dA$ in the reference configuration to its current image $da$, where $dA$ and $da$ denote the surface area of the parallelograms defined by

$$\mathrm{d}\mathbf{A} = \mathrm{d}\mathbf{X}^1 \times \mathrm{d}\mathbf{X}^2 = \mathbf{N}dA \quad \text{and} \quad \mathrm{d}\mathbf{a} = \mathrm{d}\mathbf{x}^1 \times \mathrm{d}\mathbf{x}^2 = \mathbf{n}da. \tag{2.22}$$

The vectors $\mathbf{N}$ and $\mathbf{n}$ are the unit normals to the corresponding surface elements. Using (2.19), for any $\mathrm{d}\mathbf{X}$ with $\mathbf{N} \cdot \mathrm{d}\mathbf{X} > 0$ it follows that

$$\begin{aligned} dv &= \mathrm{d}\mathbf{x} \cdot (\mathrm{d}\mathbf{x}^1 \times \mathrm{d}\mathbf{x}^2) = \mathrm{d}\mathbf{x} \cdot \mathbf{n}da = (\mathbf{F}\mathrm{d}\mathbf{X}) \cdot \mathbf{n}da \\ &= J\,dV = J\mathrm{d}\mathbf{X} \cdot (\mathrm{d}\mathbf{X}^1 \times \mathrm{d}\mathbf{X}^2) = J\mathrm{d}\mathbf{X} \cdot (\mathbf{N}dA), \end{aligned} \tag{2.23}$$

which implies

$$(\mathbf{F}\mathrm{d}\mathbf{X}) \cdot \mathbf{n}da = J\mathrm{d}\mathbf{X} \cdot (\mathbf{N}dA). \tag{2.24}$$

Since the above equation holds for any infinitesimal material line element $\mathrm{d}\mathbf{X}$, one may write

$$\mathbf{n}da = J\mathbf{F}^{-\top}\mathbf{N}dA, \tag{2.25}$$

a result known as *Nanson's formula*, where the quantity $J\mathbf{F}^{-\top}$ is called the *co-factor* of the deformation gradient or $\operatorname{cof}\mathbf{F}$ and acts as a *normal map*. Moreover, dotting each side with itself and taking the square root leads to

$$\frac{|da|}{|dA|} = J\sqrt{\mathbf{N} \cdot (\mathbf{C}^{-1}\mathbf{N})}, \tag{2.26}$$

which is a measure for the change in area, also called the *area stretch*.

### 2.1.3 Superposed Rigid-Body Motion

A motion of the body $\mathcal{B}$ is called rigid if the distance between any two material points stays the same at all times. Let $\mathbf{X}$ and $\boldsymbol{Y}$ be two position vectors of material points in the reference configuration, and denote their current counterparts by $\mathbf{x} = \boldsymbol{\chi}(\mathbf{X}, t)$ and $\boldsymbol{y} = \boldsymbol{\chi}(\boldsymbol{Y}, t)$. Moreover, define another invertible motion $\boldsymbol{\chi}^+$ with $\mathbf{x}^+ = \boldsymbol{\chi}^+(\mathbf{X}, t) \in \mathcal{R}^+$ and $\boldsymbol{y}^+ = \boldsymbol{\chi}^+(\boldsymbol{Y}, t) \in \mathcal{R}^+$, such that $\boldsymbol{\chi}$ and $\boldsymbol{\chi}^+$ only differ by a rigid-body motion. Notice by looking at Figure 2.2, that

$$\begin{aligned} \mathbf{x}^+ &= \boldsymbol{\chi}^+(\mathbf{X}, t) = \boldsymbol{\chi}^+(\boldsymbol{\chi}_t^{-1}(\mathbf{x}), t) = \bar{\boldsymbol{\chi}}^+(\mathbf{x}, t) = \bar{\boldsymbol{\chi}}^+(\boldsymbol{\chi}_t(\mathbf{X}), t), \\ \boldsymbol{y}^+ &= \boldsymbol{\chi}^+(\boldsymbol{Y}, t) = \boldsymbol{\chi}^+(\boldsymbol{\chi}_t^{-1}(\boldsymbol{y}), t) = \bar{\boldsymbol{\chi}}^+(\boldsymbol{y}, t) = \bar{\boldsymbol{\chi}}^+(\boldsymbol{\chi}_t(\boldsymbol{Y}), t), \end{aligned} \tag{2.27}$$

and that the superposed motion $\bar{\boldsymbol{\chi}}^+(\mathbf{x}, t)$ is also invertible for fixed $t$.

Since the configurations $\mathcal{R}$ and $\mathcal{R}^+$ only differ by a rigid-body motion,

$$\begin{aligned} (\mathbf{x} - \boldsymbol{y}) \cdot (\mathbf{x} - \boldsymbol{y}) &= (\mathbf{x}^+ - \boldsymbol{y}^+) \cdot (\mathbf{x}^+ - \boldsymbol{y}^+) \\ &= \left[\bar{\boldsymbol{\chi}}^+(\mathbf{x}, t) - \bar{\boldsymbol{\chi}}^+(\boldsymbol{y}, t)\right] \cdot \left[\bar{\boldsymbol{\chi}}^+(\mathbf{x}, t) - \bar{\boldsymbol{\chi}}^+(\boldsymbol{y}, t)\right], \end{aligned} \tag{2.28}$$

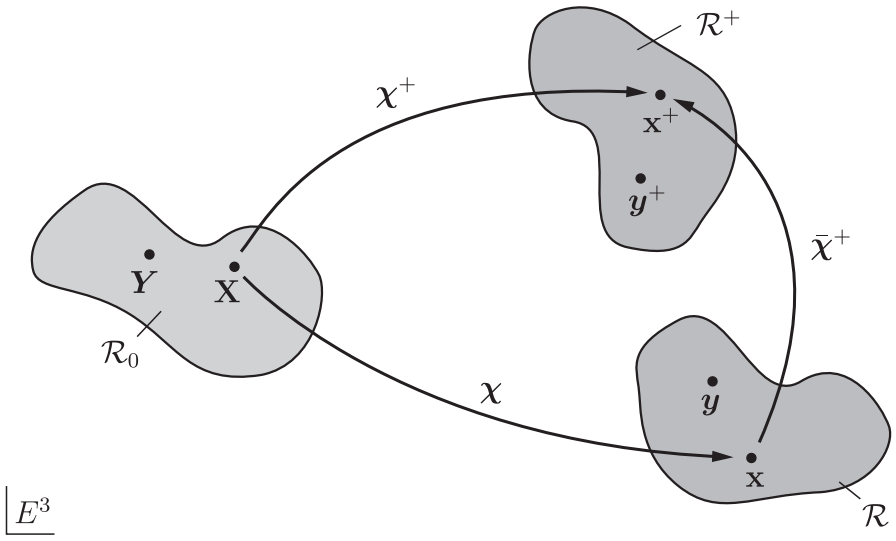


Figure 2.2: Configurations associated with the motions $\boldsymbol{\chi}$, $\boldsymbol{\chi}^+$, and the superposed rigid motion $\bar{\boldsymbol{\chi}}^+$.

has to hold for all $\mathbf{x}$, $\boldsymbol{y}$ in $\mathcal{R}$ at time $t$. Taking derivatives of (2.28) with respect to $\mathbf{x}$ and then $\boldsymbol{y}$, yields

$$\left[\frac{\partial \bar{\boldsymbol{\chi}}^+(\mathbf{x},t)}{\partial \mathbf{x}}\right]^\top = \left[\frac{\partial \bar{\boldsymbol{\chi}}^+(\boldsymbol{y},t)}{\partial \boldsymbol{y}}\right]^{-1}. \tag{2.29}$$

Since $\mathbf{x}$ and $\boldsymbol{y}$ are chosen independently, the left- and the right-hand side of (2.29) can only be a function of time, thus

$$\left[\frac{\partial \bar{\boldsymbol{\chi}}^+(\mathbf{x},t)}{\partial \mathbf{x}}\right]^\top = \left[\frac{\partial \bar{\boldsymbol{\chi}}^+(\boldsymbol{y},t)}{\partial \boldsymbol{y}}\right]^{-1} = \mathbf{Q}^\top(t). \tag{2.30}$$

One can then conclude that $\frac{\partial \bar{\boldsymbol{\chi}}^+(\mathbf{x},t)}{\partial \mathbf{x}} = \frac{\partial \bar{\boldsymbol{\chi}}^+(\boldsymbol{y},t)}{\partial \boldsymbol{y}} = \mathbf{Q}(t)$, and that $\mathbf{Q}(t)$ is an orthogonal tensor with $\mathbf{Q}^\top(t)\mathbf{Q}(t) = \mathbf{I}$. In order to figure out if $\mathbf{Q}(t)$ is proper or improper orthogonal, observe that

$$\mathbf{F}^+ = \frac{\partial \boldsymbol{\chi}^+}{\partial \mathbf{X}} = \frac{\partial \boldsymbol{\chi}^+}{\partial \mathbf{x}}\frac{\partial \boldsymbol{\chi}}{\partial \mathbf{X}} = \mathbf{Q}\mathbf{F}. \tag{2.31}$$

Since the determinants of both $\mathbf{F}$ and $\mathbf{F}^+$ have to be positive by (2.21), $\det \mathbf{Q}$ has to be positive as well, thus $\det \mathbf{Q} = 1$ and $\mathbf{Q}$ is *proper orthogonal*. From (2.30) it can be concluded that

$$\mathbf{x}^+ = \bar{\boldsymbol{\chi}}^+(\mathbf{x},t) = \mathbf{Q}(t)\mathbf{x} + \mathbf{c}(t), \tag{2.32}$$

which is the general form of the superposed rigid motion.

**Remark 2.1.** *Another way of looking at the motions $\boldsymbol{\chi}$ and $\boldsymbol{\chi}^+$ is to regard them as the motions of a body recorded by two observers (see e.g. Holzapfel (2000, Chap. 5)). The recorded*

*motions will differ by a rigid motion (2.32), which represents the relative motion of the two observers to each other.*

## 2.2 Basic Physical Principles

In this section the fundamental balance laws including the conservation of mass, and balance of linear momentum, angular momentum and energy are introduced. These laws must be satisfied at all times and are required to set up initial boundary value problems in thermomechanics. In order to derive these balance laws, the divergence theorem and the Reynolds' transport theorem are reviewed first.

### 2.2.1 Divergence Theorem

Let $\mathcal{P}_0 \subseteq \mathcal{R}_0$ be a bounded closed region with a smooth boundary $\partial\mathcal{P}_0$, and define a vector function per unit reference area $\mathbf{v}(\mathbf{X}) : \mathcal{P}_0 \to E^3$. Then, the divergence of $\mathbf{v}$ satisfies

$$\int_{\mathcal{P}_0} \mathrm{Div}\,(\mathbf{v}(\mathbf{X}))\; dV = \int_{\partial\mathcal{P}_0} \mathbf{v}(\mathbf{X}) \cdot \mathbf{N}\; dA = \int_{\partial\mathcal{P}_0} \mathbf{v}(\mathbf{X}) \cdot \,\mathrm{d}\mathbf{A}, \tag{2.33}$$

where $\mathbf{N}$ is the outward normal vector to the surface $\partial\mathcal{P}_0$ and where $\mathrm{Div}\,(\mathbf{v}(\mathbf{X})) := \mathrm{tr}(\mathrm{Grad}(\mathbf{v}(\mathbf{X}))) = \nabla_{\mathbf{X}} \cdot \mathbf{v}(\mathbf{X}) = \partial v_A/\partial X_A$. Equation (2.33) is known as the classical *divergence theorem* (or *Gauss' divergence theorem*) and relates the flux of $\mathbf{v}$ through the surface $\partial\mathcal{P}_0$ to the behavior of $\mathbf{v}$ in $\mathcal{P}_0$. For a second order tensor function $\mathbf{T} : \mathcal{P}_0 \to \mathcal{L}(E^3, E^3)$ the theorem would read

$$\int_{\mathcal{P}_0} \mathrm{Div}\,(\mathbf{T}(\mathbf{X}))\; dV = \int_{\partial\mathcal{P}_0} \mathbf{T}(\mathbf{X})\,\mathbf{N}\; dA = \int_{\partial\mathcal{P}_0} \mathbf{T}(\mathbf{X})\; \mathrm{d}\mathbf{A}, \tag{2.34}$$

where $\mathrm{Div}(\mathbf{T}(\mathbf{X})) = (\partial T_{AB}/\partial X_B)\,\mathbf{E}_A$. In the general case of a k-th order Tensor $T_{IJ\ldots P}$ the integral theorem in component form (for the sake of clarity) is given by

$$\int_{\mathcal{P}_0} T_{IJ\ldots P,Q}\; dV = \int_{\partial\mathcal{P}_0} T_{IJ\ldots P} N_Q\; dA, \tag{2.35}$$

where $N_Q$ are the components of the normal vector to $\partial\mathcal{P}_0$.

### 2.2.2 Reynolds' Transport Theorem

Let the particles occupying the region $\mathcal{P}_0 \subseteq \mathcal{R}_0$ with the boundary $\partial\mathcal{P}_0$ at time $t_0$ occupy the closed and bounded region $\mathcal{P} \subseteq \mathcal{R}$ with the smooth boundary $\partial\mathcal{P}$ at time $t$, see Figure 2.3. Moreover, let $\phi$ be a scalar field defined by a referential or a spatial function

$$\phi = \hat{\phi}(\mathbf{X}, t) = \tilde{\phi}(\mathbf{x}, t), \tag{2.36}$$

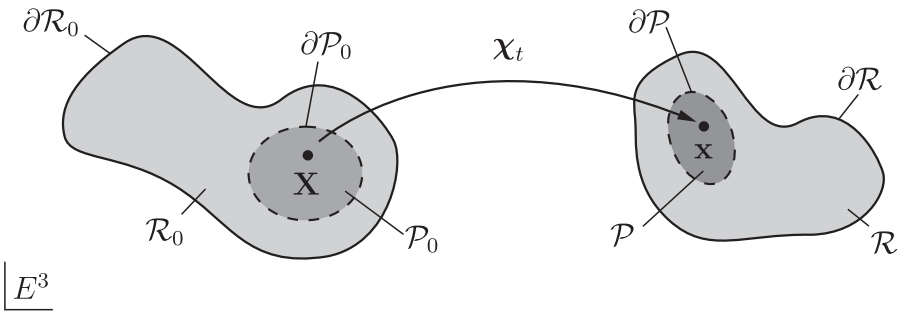


Figure 2.3: Region $\mathcal{P}_0 \subseteq \mathcal{R}_0$ with the boundary $\partial\mathcal{P}_0$ at time $t_0$ and its spatial counterpart $\mathcal{P} \subseteq \mathcal{R}$ and $\partial\mathcal{P}$ at time $t$.

where both $\hat{\phi}$ and $\tilde{\phi}$ are continuously differentiable in both variables. When discussing balance laws, the ability to manipulate material time derivatives of volume integrals defined in a subset $\mathcal{P}$ of the current configuration $\mathcal{R}$ is crucial. The *Reynolds's transport theorem* provides exactly that. Namely, it states that

$$\frac{d}{dt}\int_{\mathcal{P}} \tilde{\phi}\, dv = \int_{\mathcal{P}} \left(\dot{\phi} + \tilde{\phi}\,\mathrm{div}\,\mathbf{v}\right)\, dv, \tag{2.37}$$

which can be proven by the usual approach of mapping the integral on the left-hand side to the (fixed) reference configuration, interchanging the differentiation and integration operations, evaluating the integrand, and then mapping the integral back to the current configuration. The Reynolds' transport theorem (2.37) can also be restated in various forms,

$$\begin{aligned}
\frac{d}{dt}\int_{\mathcal{P}} \tilde{\phi}\, dv &= \int_{\mathcal{P}} \left(\dot{\phi} + \tilde{\phi}\,\mathrm{div}\,\mathbf{v}\right)\, dv \\
&= \int_{\mathcal{P}} \left[\frac{\partial\tilde{\phi}}{\partial t} + \frac{\partial\tilde{\phi}}{\partial\mathbf{x}}\cdot\mathbf{v} + \tilde{\phi}\,\mathrm{div}\,\mathbf{v}\right]\, dv \\
&= \int_{\mathcal{P}} \left[\frac{\partial\tilde{\phi}}{\partial t} + \mathrm{div}(\tilde{\phi}\mathbf{v})\right]\, dv \\
&= \int_{\mathcal{P}} \frac{\partial\tilde{\phi}}{\partial t}\, dv + \int_{\partial\mathcal{P}} \tilde{\phi}\,\mathbf{v}\cdot\mathbf{n}\, da,
\end{aligned} \tag{2.38}$$

where the divergence theorem (2.33) was used in the last step. Note that (2.37) and (2.38) work for vector and tensor functions without any changes.

### 2.2.3 Conservation of Mass

The mass $m(\mathcal{S})$ of any part $\mathcal{S}$ of the body $\mathcal{B}$ is defined in terms of the *referential mass density* $\rho_0 = \rho_0(\mathbf{X}, t)$ as

$$m(\mathcal{S}) = \int_{\mathcal{P}_0} \rho_0\, dV, \tag{2.39}$$

where $\mathcal{P}_0$ is the region occupied by $\mathcal{S}$ in the reference configuration. Alternatively, in terms of the *spatial mass density* $\rho(\mathbf{x}, t)$, the mass is defined as

$$m(\mathcal{S}) = \int_{\mathcal{P}} \rho \, dv, \tag{2.40}$$

where $\mathcal{P}$ is the region occupied by $\mathcal{S}$ in the current configuration. The *conservation of mass* states that for any part $\mathcal{S}$ of the body $\mathcal{B}$, the mass $m(\mathcal{S})$ remains constant at all times, and hence

$$\frac{d}{dt} m(\mathcal{S}) = \frac{d}{dt} \int_{\mathcal{P}} \rho \, dv = 0. \tag{2.41}$$

This equation is an *integral* or *global form* of the conservation of mass in the spatial description. A simple application of the Reynold's transport theorem (2.38) then yields,

$$\int_{\mathcal{P}} \left( \dot{\rho} + \rho \operatorname{div} \mathbf{v} \right) \, dv = 0, \tag{2.42}$$

and using the localization theorem (see e.g. Gurtin et al. (2010, Chap.153)), it can be rewritten in a *local form* as,

$$\dot{\rho} + \rho \operatorname{div} \mathbf{v} = 0, \tag{2.43}$$

also known as the "continuity" equation.

A global form of the balance of mass in the referential description can be obtained by using (2.40), (2.39), and (2.19)

$$m(\mathcal{S}) = \int_{\mathcal{P}} \rho \, dv = \int_{\mathcal{P}_0} \rho J \, dV = \int_{\mathcal{P}_0} \rho_0 \, dV, \tag{2.44}$$

from which it follows that

$$\int_{\mathcal{P}_0} \left( \rho J - \rho_0 \right) \, dV. \tag{2.45}$$

Localization of this equation yields the local form of mass conservation in referential description,

$$\rho_0 = \rho J. \tag{2.46}$$

### 2.2.4 Balance of Linear Momentum

The *linear momentum* of any part $\mathcal{S}$ of the body $\mathcal{B}$ is defined in terms of the velocity (2.7) as

$$\int_{\mathcal{P}} \rho \mathbf{v} \, dv, \tag{2.47}$$

where $\mathcal{P}$ is the region occupied by $\mathcal{S}$ in the current configuration. In order to formulate the balance law, two types of external forces acting on $\mathcal{S}$ at any time $t$ are admitted: (i) *body forces* per unit mass (e.g. gravitational, magnetic) denoted by $\mathbf{b} = \mathbf{b}(\mathbf{x}, t)$, which are exerted

on the interior of $\mathcal{S}$, and (ii) *contact forces* per unit area $\mathbf{t} = \mathbf{t}(\mathbf{x}, t; \mathbf{n}) = \mathbf{t}_{(\mathbf{n})}(\mathbf{x}, t)$, which act on the boundary surface $\partial\mathcal{S}$ and depend on the outward unit normal $\mathbf{n}$ to that surface[6]. These contact forces are also referred to as the *traction vectors* or *stress vectors*. Similar to (i) and (ii), body couples (per unit mass) and surface couples (per unit area) could also be introduced, but they are typically omitted in classical continuum mechanics.

The *balance of linear momentum* states that the material derivative of the linear momentum of $\mathcal{S}$ at a time $t$ is equal to the total external force acting on it at that time. Mathematically the postulate reads

$$\frac{d}{dt}\int_{\mathcal{P}} \rho\mathbf{v}\, dv = \int_{\mathcal{P}} \rho\mathbf{b}\, dv + \int_{\partial\mathcal{P}} \mathbf{t}_{(\mathbf{n})}\, da, \tag{2.48}$$

which can be rewritten using Reynold's theorem (2.38) and the balance of mass (2.43) as,

$$\int_{\mathcal{P}} \rho\mathbf{a}\, dv = \int_{\mathcal{P}} \rho\mathbf{b}\, dv + \int_{\partial\mathcal{P}} \mathbf{t}_{(\mathbf{n})}\, da. \tag{2.49}$$

In the special case where the acceleration $\mathbf{a}$ vanishes, the balance of linear momentum simply says that the sum of all external forces has to vanish, which leads to the classical mechanical equilibrium of statics.

**Remark 2.2.** *Throughout this thesis, quasistatic conditions will be assumed. This means that any type of loads are applied very slowly such that the body can be assumed to be in mechanical equilibrium at all times. In terms of the motion of the body, this assumption means that the inertial terms in* (2.49) *can be neglected,*

$$\mathbf{a} = \frac{\partial^2\boldsymbol{\chi}(\mathbf{X}, t)}{\partial t^2} \approx \mathbf{0}. \tag{2.50}$$

*For the sake of consistency, all the derivations in this chapter are carried out including the inertial terms.*

### 2.2.5 Balance of Angular Momentum

The *angular momentum* of any part $\mathcal{S}$ of the body $\mathcal{B}$ with respect to the origin in $E^3$ is defined in terms of the velocity (2.7) and the position vector $\mathbf{x}$ (2.6) as

$$\int_{\mathcal{P}} \mathbf{x} \times \rho\mathbf{v}\, dv, \tag{2.51}$$

where $\mathcal{P}$ is the region occupied by $\mathcal{S}$ in the current configuration. The *balance of angular momentum* then states that the rate of change of the angular momentum of $\mathcal{S}$ at a time $t$

[6]The dependence of the contact forces on the position and the normal vector is also known as *Cauchy's hypothesis*.

is equal to the moment of all external force acting on it at that time. Mathematically the postulate reads

$$\frac{d}{dt}\int_{\mathcal{P}} \mathbf{x}\times\rho\mathbf{v}\;dv = \int_{\mathcal{P}} \mathbf{x}\times\rho\mathbf{b}\;dv + \int_{\partial\mathcal{P}} \mathbf{x}\times\mathbf{t}_{(\mathbf{n})}\;da, \tag{2.52}$$

which can be rewritten using Reynold's theorem (2.38) and the balance of mass (2.43) as,

$$\int_{\mathcal{P}} \mathbf{x}\times\rho\mathbf{a}\;dv = \int_{\mathcal{P}} \mathbf{x}\times\rho\mathbf{b}\;dv + \int_{\partial\mathcal{P}} \mathbf{x}\times\mathbf{t}_{(\mathbf{n})}\;da. \tag{2.53}$$

The two balance laws (2.49) and (2.53) are also referred to as *Euler's laws*.

Again, in the special case where the acceleration $\mathbf{a}$ vanishes, the balance of angular momentum simply says that the sum of all external moments has to vanish, which leads to the classical mechanical equilibrium of statics.

### 2.2.6 Stress Vector and Stress Tensor

In order to find the local forms of the two preceding balance laws (2.49) and (2.53), the contact force terms have to be written as volume integrals. This can be achieved by way of *Cauchy's lemma* and *Cauchy's theorem*. Cauchy's lemma states that the stress vectors acting on opposite sides of the same surface at a point are equal in magnitude and opposite in direction,

$$\mathbf{t}(\mathbf{x},t:\mathbf{n}) = -\mathbf{t}(\mathbf{x},t:-\mathbf{n}). \tag{2.54}$$

Even though this lemma looks very similar to Newton's third law in particle mechanics (action-reaction principle), Cauchy's lemma can be derived from the linear momentum balance (see e.g. Gurtin (1982, Chap. 5)) and is thus not a principle.

Furthermore, Cauchy's theorem then states that at every point on $\mathcal{S}$, the spatial traction vector is a linear map of the corresponding outward unit normal,

$$\mathbf{t}_{(\mathbf{n})}(\mathbf{x},t) = \mathbf{T}(\mathbf{x},t)\,\mathbf{n}(\mathbf{x},t), \tag{2.55}$$

where the tensor $\mathbf{T}$ is called the *Cauchy stress* tensor. The theorem can be proven using linear momentum balance (2.49) and Cauchy's lemma (2.54) (see e.g. Gurtin et al. (2010, §19.5), or Gurtin (1982, §14)). While the spatial traction vector $\mathbf{t}$ measures current force per unit of current area $da$, it is also possible and desirable to resolve the current traction vector on the reference area $dA$. To this end, a *(nominal) traction vector* $\mathbf{p} = \mathbf{p}(\mathbf{X},t;\mathbf{N}) = \mathbf{p}_{(\mathbf{N})}(\mathbf{X},t)$ is introduced measuring the current force per unit reference area $dA$. The spatial and nominal traction are then related by

$$\mathrm{d}\mathbf{f} = \mathbf{t}_{(\mathbf{n})}\,da = \mathbf{p}_{(\mathbf{N})}\,dA, \tag{2.56}$$

where $\mathrm{d}\mathbf{f}$ is the current force. Similarly to Cauchy's theorem, it can immediately be concluded that

$$\mathbf{p}_{(\mathbf{N})}(\mathbf{X},t) = \mathbf{P}(\mathbf{X},t)\,\mathbf{N}(\mathbf{X}), \tag{2.57}$$

where $\mathbf{P}(\mathbf{X}, t)$ is called the *first Piola-Kirchhoff stress* and $\mathbf{N}$ is the reference unit normal. Using (2.56) with (2.55) and (2.57), and recalling Nanson's formula (2.25) yields the relation

$$\mathbf{PN}\, dA \;=\; \mathbf{Tn}\, da \;=\; \mathbf{T}J\mathbf{F}^{-\top}\mathbf{N}\, dA, \tag{2.58}$$

such that

$$J\mathbf{T} = \mathbf{P}\mathbf{F}^{\top}. \tag{2.59}$$

Returning to the global form of linear momentum balance (2.49), the contact force term can easily be rewritten as a volume integral by using Cauchy's theorem (2.55) and applying the divergence theorem (2.34), leading to

$$\int_{\mathcal{P}} (\rho\mathbf{a} - \rho\mathbf{b} - \operatorname{div}\mathbf{T})\, dv = 0. \tag{2.60}$$

The local form in the spatial description then reads,

$$\operatorname{div}\mathbf{T} + \rho\mathbf{b} = \rho\mathbf{a} \quad \Leftrightarrow \quad T_{jl,l} + \rho b_j = \rho a_j. \tag{2.61}$$

By the same token, the global form of angular momentum balance (2.53) can be written in index notation as

$$\int_{\mathcal{P}} T_{ji}e_{ijk} + x_i e_{ijk}\,(T_{jl,l} + \rho b_j - \rho a_j)\, dv = 0. \tag{2.62}$$

Recalling the local form of linear momentum balance (2.61), the local form of the angular momentum balance in the spatial description reads,

$$T_{ji}e_{ijk} = 0 \quad \Leftrightarrow \quad \mathbf{T} = \mathbf{T}^{\top}. \tag{2.63}$$

In order to derive the equivalent statements in the reference configuration, the balance laws (2.49) and (2.53) have to be pulled back by applying (2.19), (2.46), and (2.56), leading to

$$\int_{\mathcal{P}_0} \rho_0\mathbf{a}\, dV = \int_{\mathcal{P}_0} \rho_0\mathbf{b}\, dV + \int_{\partial\mathcal{P}_0} \mathbf{p}_{(\mathbf{N})}\, dA, \tag{2.64}$$

and

$$\int_{\mathcal{P}_0} \mathbf{x}\times\rho_0\mathbf{a}\, dV = \int_{\mathcal{P}_0} \mathbf{x}\times\rho_0\mathbf{b}\, dV + \int_{\partial\mathcal{P}_0} \mathbf{x}\times\mathbf{p}_{(\mathbf{N})}\, dA. \tag{2.65}$$

The local forms in the referential description are then derived in the same way as in the corresponding spatial description by applying (2.57) and (2.34) to (2.64), resulting in

$$\int_{\mathcal{P}_0} (\rho_0\mathbf{a} - \rho_0\mathbf{b} - \operatorname{Div}\mathbf{P})\; dV = 0, \tag{2.66}$$

and its local counterpart

$$\operatorname{Div}\mathbf{P} + \rho_0\mathbf{b} = \rho_0\mathbf{a} \quad \Leftrightarrow \quad P_{jA,A} + \rho_0 b_j = \rho_0 a_j. \tag{2.67}$$

By the same token, the global form of angular momentum balance (2.65) can be written in index notation as

$$\int_{\mathcal{P}_0} F_{iA}P_{jA}e_{ijk} + x_i e_{ijk}\left(P_{jA,A} + \rho_0 b_j - \rho_0 a_j\right) dV = 0, \tag{2.68}$$

and localized to yield,

$$F_{iA}P_{jA}e_{ijk} = 0 \quad \Leftrightarrow \quad \mathbf{F}\mathbf{P}^\top = \mathbf{P}\mathbf{F}^\top. \tag{2.69}$$

### 2.2.7 Balance of Energy

In order to account for the interconvertibility of mechanical work and heat, the *balance of energy*, also referred to as the *First Law of Thermodynamics*, has to be introduced. It states that the time rate of change of the total energy $K(\mathcal{P}) + U(\mathcal{P})$ is equal to the the sum of the work rate $R(\mathcal{P})$ and the rate of heating $H(\mathcal{P})$,

$$\frac{d}{dt}\left[K(\mathcal{P}) + U(\mathcal{P})\right] = R(\mathcal{P}) + H(\mathcal{P}). \tag{2.70}$$

The *kinetic energy* of $\mathcal{S}$ occupying $\mathcal{P}$ is defined as $K(\mathcal{P}) = \int_{\mathcal{P}} \frac{1}{2}\rho\mathbf{v}\cdot\mathbf{v}\ dv$, and its stored internal energy is denoted by $U(\mathcal{P}) = \int_{\mathcal{P}} \rho\epsilon\ dv$, where an *internal energy* per unit mass $\epsilon = \epsilon(\mathbf{x}, t)$ is assumed to exist. The rate of work done by all external forces is defined as $R(\mathcal{P}) = \int_{\mathcal{P}} \rho\mathbf{b}\cdot\mathbf{v}\ dv + \int_{\partial\mathcal{P}} \mathbf{t}\cdot\mathbf{v}\ da$, and the rate of heating $H(\mathcal{P}) = \int_{\mathcal{P}} \rho r\ dv - \int_{\partial\mathcal{P}} \mathbf{q}\cdot\mathbf{n}\ da$ is composed of the *heat supply* per unit mass $r = r(\mathbf{x}, t)$ and the *outward normal heat flow*[7] $\mathbf{q}(\mathbf{x}, t)\cdot\mathbf{n}$. The global balance in the current configuration (2.70), can be localized using (2.19), (2.46), (2.34), and (2.61), resulting in

$$\rho\dot{\epsilon} = \mathbf{T}\cdot\mathbf{D} + \rho r - \operatorname{div}\mathbf{q}, \tag{2.71}$$

where $\mathbf{D}$ is defined as the symmetric part of the velocity gradient $\boldsymbol{L} := \nabla_{\mathbf{x}}\mathbf{v}$. Through a similar derivation, the first law of thermodynamics can be reformulated in the reference configuration as

$$\rho_0\dot{\epsilon} = \mathbf{S}\cdot\dot{\mathbf{E}} + \rho_0 r - \operatorname{Div}\mathbf{q}_0, \tag{2.72}$$

where $\mathbf{q}_0 = \mathbf{q}J\cdot\mathbf{F}^{-\top}$ and the *symmetric second Piola-Kirchhoff stress*

$$\mathbf{S} = \mathbf{S}^\top := \mathbf{F}^{-1}\mathbf{P} = J\mathbf{F}^{-1}\mathbf{T}\mathbf{F}^{-\top} \tag{2.73}$$

are used. Note that the *stress power* term $\mathbf{T}\cdot\mathbf{D}$ is transformed as

$$\begin{aligned}\int_{\mathcal{P}} \mathbf{T}\cdot\mathbf{D}\ dv &= \int_{\mathcal{P}} \mathbf{T}\cdot\boldsymbol{L}\ dv = \int_{\mathcal{P}} \left(\frac{1}{J}\mathbf{P}\mathbf{F}^\top\right)\cdot\boldsymbol{L}\ dv = \int_{\mathcal{P}_0} \left(\mathbf{P}\mathbf{F}^\top\right)\cdot\boldsymbol{L}\ dV \\ &= \int_{\mathcal{P}_0} \operatorname{tr}\left[\left(\mathbf{P}\mathbf{F}^\top\right)\boldsymbol{L}^\top\right]\ dV = \int_{\mathcal{P}_0} \operatorname{tr}\left[\mathbf{P}(\boldsymbol{L}\mathbf{F})^\top\right]\ dV = \int_{\mathcal{P}_0} \operatorname{tr}\left[\mathbf{P}\dot{\mathbf{F}}^\top\right]\ dV \\ &= \int_{\mathcal{P}_0} \mathbf{P}\cdot\dot{\mathbf{F}}\ dV,\end{aligned} \tag{2.74}$$

[7] The existence of the heat flux vector $\mathbf{q}$ can be proven using a tetrahedron argument as used in Cauchy's theorem.

and,

$$\begin{aligned}\int_{\mathcal{P}} \mathbf{T}\cdot\mathbf{D}\, dv &= \int_{\mathcal{P}_0} \mathbf{P}\cdot\dot{\mathbf{F}}\, dV = \int_{\mathcal{P}_0} (\mathbf{FS})\cdot\dot{\mathbf{F}}\, dV = \int_{\mathcal{P}_0} \mathbf{S}\cdot(\mathbf{F}^\top\dot{\mathbf{F}})\, dV \\ &= \int_{\mathcal{P}_0} \mathbf{S}\cdot\frac{1}{2}(\dot{\mathbf{F}}^\top\mathbf{F}+\mathbf{F}^\top\dot{\mathbf{F}})\, dV \\ &= \int_{\mathcal{P}_0} \mathbf{S}\cdot\frac{1}{2}\dot{\mathbf{C}}\, dV = \int_{\mathcal{P}_0} \mathbf{S}\cdot\dot{\mathbf{E}}\, dV.\end{aligned} \tag{2.75}$$

### 2.2.8 Summary

Before the Second Law of Thermodynamics and considerations associated with it are introduced in the next section, kinematic definitions and balance principles in the referential description under quasistatic conditions are briefly summarized:

The deformation map and the deformation gradient

$$\mathbf{x} = \boldsymbol{\chi}_t(\mathbf{X}) \quad \text{and} \quad \mathbf{F} = \nabla_{\mathbf{X}}\boldsymbol{\chi}_t$$

The conservation of mass

$$\rho_0 = \rho J$$

The balance of linear momentum

$$\operatorname{Div}\mathbf{P} + \rho_0\mathbf{b} = 0$$

The balance of angular momentum

$$\mathbf{FP}^\top = \mathbf{PF}^\top$$

The balance of energy

$$\rho_0\dot{\epsilon} = \rho_0 r - \operatorname{Div}\mathbf{q}_0 + \mathbf{S}\cdot\dot{\mathbf{E}}$$

**Box 2.1:** Summary of kinematic definitions and balance principles.

## 2.3 Thermoelasticity

A very popular approach to introduce thermoelasticity is discussed in Coleman and Noll (1963), where entropy is simply admitted as a primitive variable and then subjected to the Clausius-Duhem inequality. In a similar fashion, Green and Naghdi (1977) also admits entropy and postulates a balance of entropy. In both cases, no prescription to physically determine the entropy is offered. However, Serrin (1996), Rivlin (1973, 1975); Rivlin et al.

(1997), and Casey and Krishnaswamy (1998) take an approach where entropy is not a priori assumed to exist and construct an entropy function, which helps to add meaning to a rather abstract quantity. The notion of entropy will be discussed from a microscopic point of view in Section 3.2.4. In this section the main ideas from Casey (1998) for thermoelastic materials are introduced.

In addition to the equations summarized in Box 2.1, let the absolute temperature history of the body $\mathcal{B}$ be described by the function

$$T = \Theta(\mathbf{X}, t) \geq 0 \quad \forall\, t, \tag{2.76}$$

with the pair $(\boldsymbol{\chi}, \Theta)$ being called a *process*. Moreover, let a thermoelastic material be given by the constitutive equations

$$\epsilon = \hat{\epsilon}(\mathbf{E},\, T), \quad \mathbf{S} = \hat{\mathbf{S}}(\mathbf{E},\, T), \quad \mathbf{q}_0 = \hat{\mathbf{q}}_0(\mathbf{E},\, T,\, \boldsymbol{g}_0), \tag{2.77}$$

where $\boldsymbol{g}_0 = \operatorname{Grad} T = \partial\Theta/\partial\mathbf{X}$. It is assumed that $\hat{\mathbf{q}}_0$ satisfies the condition

$$\hat{\mathbf{q}}_0(\mathbf{E},\, T,\, 0) = \mathbf{0}, \tag{2.78}$$

and that for any fixed value of the temperature, the stress-strain relation is invertible, yielding the form

$$\mathbf{E} = \hat{\mathbf{E}}(\mathbf{S},\, T). \tag{2.79}$$

The pair $(\mathbf{E},\, T)$ can be viewed as a point in a seven-dimensional Euclidean vector space, called the *strain-temperature space*, and likewise, the pair $(\mathbf{S},\, T)$ can be viewed as a point in the seven-dimensional *stress-temperature space*. As time advances, both pairs trace out curves in their corresponding spaces.

In order to derive an entropy function, let the body undergo a *homothermal process* from an arbitrary time $t_0 (< t)$ to $t$. Since $\boldsymbol{g}_0 = \mathbf{0}$ in such a process, the heat flux vanishes according to (2.78). Therefore, the balance of energy from Box 2.1 reduces to

$$\rho_0 \dot{\epsilon} = \rho_0 r + \mathbf{S} \cdot \dot{\mathbf{E}} \quad (\text{homothermal process}). \tag{2.80}$$

As a next step, the *Clausius integral* is assumed to be path-independent in strain-temperature space,

$$\int_{t_0}^{t} \frac{r}{T}\, dt = \int_{t_0}^{t} \frac{1}{T} \left\{ \dot{\epsilon} - \frac{\mathbf{S} \cdot \dot{\mathbf{E}}}{\rho_0} \right\} dt, \tag{2.81}$$

which is also referred to as *"Part I" of the Second Law of Thermodynamics*. This allows the definition of a function $S = \hat{S}(\mathbf{E},\, T)$ with $\hat{S}(\mathbf{0},\, T_0) = 0$ and $\hat{\epsilon}(\mathbf{0},\, T_0) = 0$, such that

$$\dot{S} = \frac{r}{T} = \frac{1}{T} \left\{ \dot{\epsilon} - \frac{\mathbf{S} \cdot \dot{\mathbf{E}}}{\rho_0} \right\} \tag{2.82}$$

for homothermal processes. By additionally introducing a *Helmholtz free energy* function

$$\psi = \hat{\psi}(\mathbf{E},\, T) = \epsilon - S\,T, \tag{2.83}$$

the *Gibbs equation* can be deduced from (2.82) and (2.83) as

$$\rho_0 \dot{\psi} = \mathbf{S} \cdot \dot{\mathbf{E}} - \rho_0 S\,\dot{T}. \tag{2.84}$$

Thus, assuming the path-independency of the Clausius integral and any homothermal process,

$$\rho_0 \left( \frac{\partial \hat{\psi}}{\partial T} + S \right) \dot{T} + \left( \rho_0 \frac{\partial \hat{\psi}}{\partial \mathbf{E}} - \mathbf{S} \right) \cdot \dot{\mathbf{E}} = 0. \tag{2.85}$$

Since this equality holds for all values of $\dot{\mathbf{E}}$ and $\dot{T}$,

$$S = \hat{S}(\mathbf{E},\, T) = -\frac{\partial \hat{\psi}}{\partial T}(\mathbf{E},\, T), \tag{2.86}$$

and

$$\mathbf{S} = \hat{\mathbf{S}}(\mathbf{E},\, T) = \rho_0 \frac{\partial \hat{\psi}}{\partial \mathbf{E}}(\mathbf{E},\, T), \tag{2.87}$$

which are known as the *Gibbs relations*[8]. Even if an arbitrary process of a thermoelastic material is considered (i.e. not homothermal anymore), at each point in the strain-temperature space the constructed entropy function $\hat{S}(\mathbf{E},\, T)$ and Helmholtz free energy $\hat{\psi}(\mathbf{E},\, T)$ can be evaluated. Moreover, the Gibbs relations continue to hold since they do not depend on $\boldsymbol{g}_0$. The balance of energy from Box 2.1 can then be rewritten as

$$\rho_0 \dot{S}\, T = \rho_0 r - \operatorname{Div} \mathbf{q}_0, \tag{2.88}$$

which is often referred to as the *balance of entropy*, but it really is an energy equation.

Once an entropy function is constructed, "Part II" of the Second Law of Thermodynamics can be used by invoking an inequality associated with entropy change. In this case, the version by *Clausius-Duhem* is adopted,

$$\rho_0 \dot{S}\, T \geq \rho_0 r - \operatorname{Div} \mathbf{q}_0 + \frac{\mathbf{q}_0 \cdot \boldsymbol{g}_0}{T}. \tag{2.89}$$

Combining this inequality with the balance of entropy (2.88) yields the classical heat conduction inequality for thermoelastic materials

$$-\mathbf{q}_0 \cdot \boldsymbol{g}_0 \geq 0. \tag{2.90}$$

**Remark 2.3.** *Throughout this thesis, processes are assumed to be isothermal. This assumption means that the temperature distribution of the body $\mathcal{B}$ is kept at a constant temperature $T_0$ through heat exchange with a infinite ambient heat bath of constant temperature $T_0$, yielding*

$$\Theta(\mathbf{X}, t) = T_0 = const. \quad \Rightarrow \quad \dot{\Theta}(\mathbf{X}, t) = 0 \quad and \quad \operatorname{Grad} \Theta(\mathbf{X}, t) = 0. \tag{2.91}$$

[8] If the right Cauchy-Green tensor $\mathbf{C}$ is used in (2.77) instead of $\mathbf{E}$, then the Gibbs relation for the stress would read $\mathbf{S} = \hat{\mathbf{S}}(\mathbf{C},\, T) = 2\rho_0 \frac{\partial \hat{\psi}}{\partial \mathbf{C}}(\mathbf{C},\, T)$

## 2.4 Constitutive Relations

The equations summarized in Box 2.1 are fundamental in describing kinematics, balance principles and kinetics, and hold for any classical continuum at all times. However, these equations do not characterize the type of material the body is made out of. A quick look at the number of equations of the system summarized in Box 2.1

$$\left.\begin{array}{lrl} \text{deformation gradient} & \mathbf{F} = \nabla_{\mathbf{X}} \boldsymbol{\chi}_t & \rightarrow 9 \text{ equations} \\ \text{balance of linear momentum} & \operatorname{Div} \mathbf{P} + \rho_0 \mathbf{b} = 0 & \rightarrow 3 \text{ equations} \\ \text{balance of angular momentum} & \mathbf{F}\mathbf{P}^\top = \mathbf{P}\mathbf{F}^\top & \rightarrow 3 \text{ equations} \end{array}\right\} \rightarrow 15 \text{ equations} \tag{2.92}$$

and its unknowns

$$\left.\begin{array}{lrl} \text{deformation map} & \boldsymbol{\chi}_t & \rightarrow 3 \text{ unknowns} \\ \text{deformation gradient} & \mathbf{F} & \rightarrow 9 \text{ unknowns} \\ \text{Piola-Kirchhoff stress} & \mathbf{P} & \rightarrow 9 \text{ unknowns} \end{array}\right\} \rightarrow 21 \text{ unknowns} \tag{2.93}$$

reveals that the system is short of 6 equations to fully determine a material response. Hence it is necessary to provide 6 more equations in the form of *constitutive laws*, which describe the material of interest. Typically such constitutive equations are functional relationships that relate stress components to strain measures (or their histories or rates).

In order to have *thermodynamically consistent* constitutive relations, the previous section shows that an additional constitutive law for the Helmholtz free energy $\psi$ has to be specified. Moreover, all the constitutive laws have to be consistent with "Part II" of the Second Law of Thermodynamics (2.89), and they also have to be invariant under superposed rigid-body motions (2.32) (which is also often referred to as the *principle of material objectivity*.

There is an enormous amount of constitutive theories around that model all types of material behavior, be it elastic, plastic, viscoelastic, isotropic, anisotropic, etc. However the majority of the theories follow a so-called *phenomenological approach*, which tries to fit mathematical equations to experimental data obtained at the macroscopic level. The phenomenological approach however, does not relate the continuum deformation mechanisms to the microscopic structure of the material. Since the main goal of this work is to find a *microscopically based continuum constitutive law*, Chapter 3 will deal with the modeling of materials on a microscale, Chapter 4 with the transition from the microscale back to the macroscale for rubber-like materials, and Chapter 5 will take all these ideas and set up a constitutive model that allows the prediction of evolution of strain-induced crystallization in natural rubber.

# Chapter 3

# Statistical Mechanics

It is well-known that a macroscopic system is a collection of atoms or molecules whose motion is governed by some laws (e.g. Newton's laws) with appropriate interparticle interactions. However, it is immensely difficult to determine the state of the macroscopic system by finding out positions and momenta of all its atoms because of three reasons. The first obvious difficulty is the enormous number of degrees of freedom in a macroscopic system (e.g. one cubic centimeter of iron roughly contains $9 \cdot 10^{22}$ atoms and thus has $5.4 \cdot 10^{23}$ degrees of freedom). Secondly, it is currently not possible to determine the initial conditions for each and every atom in the system which constitutes a lack of information. Thirdly, the exact nature of the interparticle interactions is also not known. In order to circumvent this problem of partial information and too many degrees of freedom, statistical principles are used to give answers in an average sense.

While the previous chapter provides a framework for the mechanical behavior of solids from the *continuum* (or *macroscopic*) viewpoint, this chapter introduces some basic concepts of statistical mechanics to motivate the macroscopic behavior from the *atomistic* (or *microscopic*) viewpoint. The material treated here mainly follows Weiner (1983) and the lecture notes of Govindjee (2007). For additional thorough treatments of the subject the reader is referred to Chandler (1987) and Reif (1965). The more advanced reader interested in the foundations of statistical mechanics is referred to the works by Khinchin (2013), Landau and Lifshitz (1980), Gibbs (2010), and Penrose (1979).

## 3.1 Concepts of Classical Statistical Mechanics

As the name suggests, classical statistical mechanics combines concepts from classical mechanics and statistical principles. In this section the basic notions of Hamiltonian mechanics, phase functions, time averages, microcanonical and canonical distributions are introduced.

### 3.1.1 Hamiltonian Mechanics

The typical formulation of classical mechanics used in the subject of statistical mechanics is Hamiltonian mechanics. In *Hamiltonian mechanics* the *state* of a *mechanical system* at time $t$ with $N$ particles and $n = 3N$ degrees of freedom is described by all its positions $q_i$ and momenta $p_i$

$$y = (q, p) = (q_1, \ldots, q_n, p_1, \ldots, p_n) \in \Gamma, \tag{3.1}$$

where $\Gamma$ is a $2n$-dimensional Euclidean space called *phase space* which consist of all possible states of the system. The evolution of this system is then governed by Hamilton's equations

$$\dot{q}_i = \frac{\partial H}{\partial p_i}, \quad \dot{p}_i = -\frac{\partial H}{\partial q_i}, \quad (1 \leq i \leq n), \tag{3.2}$$

where $H(q, p)$ is the *Hamiltonian function* (or simply *Hamiltonian*). It maps states (or points) $y = (q, p)$ in the phase space to the real numbers

$$H : \Gamma \to \mathbb{R}, \tag{3.3}$$

and represents the *total energy* of a system in state $(q, p)$. Since the system in (3.2) only contains first order equations, the given values of $(q, p)$ for some time $t = t_0$, determine the states of the system at any other time $t$. The curve in phase space that is then uniquely described by this initial state is called a *trajectory* of the system. In general, the Hamiltonian of a system will not only depend on the microscopic positions and momenta, but also on *macroscopic controlling parameters* of kinematic or kinetic nature. A kinematic example would be the volume of a gas in a cylinder closed by a movable piston. Generally the macroscopic controlling parameters will be denoted as $\mathcal{A}_1, \ldots, \mathcal{A}_\nu$ in the kinematic case and $\mathcal{F}_1, \ldots, \mathcal{F}_\nu$ in the kinetic case. The Hamiltonian can then be written as

$$\begin{aligned} H &= H(q, p\,; \mathcal{A}) = H(q, p\,; \mathcal{A}_1, \ldots, \mathcal{A}_\nu), \text{ or} \\ H &= H(q, p\,; \mathcal{F}) = H(q, p\,; \mathcal{F}_1, \ldots, \mathcal{F}_\nu). \end{aligned} \tag{3.4}$$

However, in this section the controlling parameters are considered fixed and are thus omitted in the Hamiltonian.

### 3.1.2 Phase Functions and Time Averages

A *phase function* of a system of particles with $n$ degrees of freedom is defined as any of its properties whose value at a time $t$ is completely determined by its positions and momenta in its phase space (also referred to as the *microstate* of the system at time $t$). Thus it can be written as[1] $F(q_1, \ldots, q_n, p_1, \ldots, p_n) = F(q, p)$. Straightforward examples of phase functions

[1]Phase functions in general will also depend on the macroscopic controlling parameters, but they are assumed to be constant in this section and are therefore omitted here.

are the kinetic energy of a system, $K(p) = \frac{1}{2}\sum_{i=1}^{n} p_i^2/m_i$, or the total energy of the system, $H(q,p)$. It is well known that the value of a phase function will fluctuate wildly while the system follows a trajectory in phase space given by (3.2). The period of such fluctuations is typically on the order of picoseconds. Thus, any measurement on a macroscopic time interval will be a time average of the phase function

$$\hat{F} = \lim_{T\to\infty} \frac{1}{T} \int_0^T F\left(q(t), p(t)\right)\, dt. \tag{3.5}$$

As mentioned in the introduction to this chapter, the calculation of the trajectory $(q(t), p(t))$ in phase space is an impossible task, because of the system's large number of degrees of freedom, the lack of information about initial conditions, and the unknown nature of interparticle interactions. However, this problem can be circumvented by the following postulate: For any given system with positions and momenta $(q,p)$ and a corresponding phase space $\Gamma$, it is possible to find a so-called *distribution function* $\rho(q,p)$ with the property,

$$\rho \geq 0, \tag{3.6}$$

and the normalization condition

$$\int_\Gamma \rho(q,p)\, dq\, dp = 1, \tag{3.7}$$

such that for any phase function of the system,

$$\bar{F} := \int_\Gamma F(q,p)\, \rho(q,p)\, dq\, dp = \hat{F}, \tag{3.8}$$

where $\bar{F}$ is called the *phase average* of the phase function. It is crucial to note that (3.8) states that the phase average and the time average for any phase function of the system are equal. Such a system is said to be *ergodic*[2].

In order to gain a better understanding of $\rho(q,p)$ for an ergodic system, consider the phase function

$$F(q,p) := \begin{cases} 1 & \text{if} \quad (q,p) \in D \\ 0 & \text{if} \quad (q,p) \notin D, \end{cases} \tag{3.9}$$

where $D$ is any region in $\Gamma$. Then,

$$\bar{F} = \int_\Gamma F(q,p)\, \rho(q,p)\, dq\, dp = \int_D \rho(q,p)\, dq\, dp, \tag{3.10}$$

and

$$\hat{F} = \lim_{T\to\infty} \frac{1}{T} \int_0^T F\left(q(t), p(t)\right)\, dt =: \frac{t_D}{T}, \tag{3.11}$$

[2]For a detailed study of the ergodic hypothesis, see Penrose (1979).

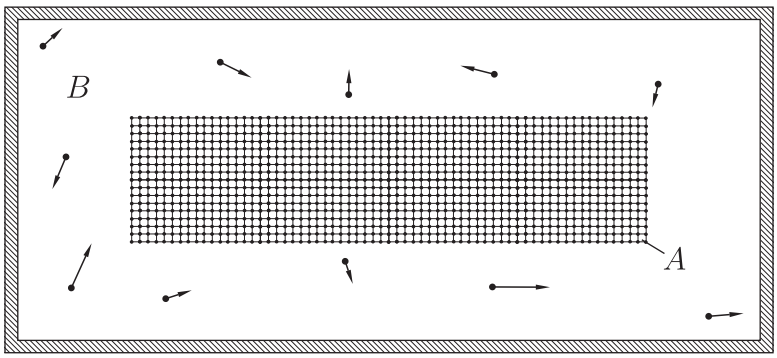


Figure 3.1: Isolated system $A + B$ with crystal $A$ and gaseous ambient $B$.

where $t_D/T$ is the fraction of time the system spends in region $D$. Using ergodicity, it follows that

$$\frac{t_D}{T} = \int_D \rho(q,p)\, dq\, dp. \tag{3.12}$$

In other words, the integral of $\rho(q,p)$ over an arbitrary region $D \in \Gamma$ describes the fraction of time spent in that region. Moreover, the distribution function $\rho(q,p)$ will in general also depend on macroscopic controlling parameters.

The ergodic hypothesis (3.8) is a very important tool in that it allows the calculation of any phase function's time average (3.5), which corresponds to the measured macroscopic value of a microscopic property, solely by a volume integral. Thus, it is essential to determine the explicit form of the distribution function for a system under certain macroscopic conditions. In order to achieve this, first, the phase space dynamics of an isolated[3] system containing a crystal (system A) and a gaseous ambient (system B) are considered (see Figure 3.1) and its corresponding distribution function derived. Second, the distribution function for the isolated system $A + B$ is used to derive the distribution function for a single system $A$ interacting with a surrounding ambient.

### 3.1.3 Characteristics of Phase Space

#### 3.1.3.1 Liouville's Theorem

In statistical mechanics a single system is also often referred to as a *replica*, and a collection of replicas of a given system is then called an *ensemble*, where every replica is governed by the same Hamiltonian.

*Liouville's theorem* comes in two forms. The first form is a global statement and the second form is a local statement. *The first form* states that *the motion in its phase space*

[3]An isolated system has a Hamiltonian that only depends on the positions and momenta of the system itself.

*of an ensemble of replicas of an isolated Hamiltonian system is volume preserving.* To prove this consider a collection of replicas occupying a region $D_0$ at time $t_0$ with coordinates $Y = y(t_0) = (q(t_0), p(t_0))$. At a later time $t$, this ensemble will occupy the region $D_t$ with the coordinates $y(t)$. The rate of change of the volume of $D_t$ can then be written as

$$\begin{aligned}\frac{d}{dt}\mathrm{vol}(D_t) &= \frac{d}{dt}\int_{D_t} dy \\ &= \frac{d}{dt}\int_{D_0} \det\left(\frac{\partial y_i}{\partial Y_J}\right) dY \\ &= \int_{D_0} \det\left(\frac{\partial y_i}{\partial Y_J}\right)\left(\frac{\partial Y_K}{\partial y_j}\right)\frac{\partial \dot{y}_j}{\partial Y_K}\, dY \\ &= \int_{D_t}\left(\frac{\partial \dot{y}_j}{\partial y_j}\right) dy,\end{aligned} \tag{3.13}$$

which has the same appearance as the statement $\dot{J} = J \operatorname{div} \mathbf{v}$ in continuum mechanics but with the Einstein summation convention ranging from 1 to $2n$. Returning to the $(q, p)$ notation, the integrand of the right-hand side of (3.13) yields

$$\frac{\partial \dot{y}_j}{\partial y_j} = \sum_{j=1}^{n} \frac{\partial \dot{q}_j}{\partial q_j} + \frac{\partial \dot{p}_j}{\partial p_j} = \sum_{j=1}^{n} \frac{\partial^2 H}{\partial p_j\, \partial q_j} - \frac{\partial^2 H}{\partial q_j\, \partial p_j} = 0, \tag{3.14}$$

where Hamilton's equations (3.2) and sufficient smoothness of $H$ are used. This completes the proof of the first form of Liouville's theorem.

*The second form* of Liouville's theorem states that $\rho$ *is constant along the trajectory of an isolated system in phase space.* As before, consider a region $D_0$ occupied by an ensemble of replicas at time $t_0$. At a later time $t$, these replicas will occupy the region $D_t$. Noting that the fraction of time spent in $D_0$ and $D_t$ is the same, (3.12) can be used to write

$$\begin{aligned}0 &= \frac{d}{dt}\int_{D_t} \rho(y)\, dy \\ &= \frac{d}{dt}\int_{D_0} \rho(y) \det\left(\frac{\partial y_i}{\partial Y_J}\right) dY \\ &= \int_{D_0} \frac{d\rho}{dt}(y) \det\left(\frac{\partial y_i}{\partial Y_J}\right) + \rho(y)\frac{d}{dt}\left\{\det\left(\frac{\partial y_i}{\partial Y_J}\right)\right\} dY \\ &= \int_{D_0} \frac{d\rho}{dt}(y) \det\left(\frac{\partial y_i}{\partial Y_J}\right) dY \\ &= \int_{D_t} \frac{d\rho}{dt}(y)\, dy,\end{aligned} \tag{3.15}$$

which has the same appearance as the balance of mass (2.43) in continuum mechanics with

$\operatorname{div} \mathbf{v} = 0$. Since $D_t$ is arbitrary, (3.15) yields

$$\begin{aligned} 0 = \frac{d\rho}{dt} &= \frac{\partial \rho}{\partial t} + \sum_{i=1}^{n} \frac{\partial \rho}{\partial q_i}\frac{\partial q_i}{\partial t} + \frac{\partial \rho}{\partial p_i}\frac{\partial p_i}{\partial t} \\ &= \frac{\partial \rho}{\partial t} + \sum_{i=1}^{n} \frac{\partial \rho}{\partial q_i}\frac{\partial H}{\partial p_i} - \frac{\partial \rho}{\partial p_i}\frac{\partial H}{\partial q_i} \\ &=: \frac{\partial \rho}{\partial t} + \{\rho, H\}\,, \end{aligned} \tag{3.16}$$

where the Poisson bracket $\{\rho, H\}$ was introduced.

**Remark 3.1.** *In general the Poisson bracket of any two functions over phase space is defined as*

$$\{F, G\} = \sum_{i=1}^{n} \frac{\partial F}{\partial q_i}\frac{\partial G}{\partial p_i} - \frac{\partial F}{\partial p_i}\frac{\partial G}{\partial q_i}, \tag{3.17}$$

*and it is skew-symmetric,* $\{F, G\} = -\{G, F\}$.

**Remark 3.2.** *For a function over the phase space which does not explicitly depend on time,* $F : \Gamma \to \mathbb{R}$*, the following holds*

$$\frac{dF}{dt} = \{F, H\}\,. \tag{3.18}$$

**Remark 3.3.** *Statistical equilibrium (or equilibrium) of an ensemble of replicas is defined by the condition*

$$\frac{\partial \rho}{\partial t} = 0 \quad \text{or} \quad \{\rho, H\} = 0. \tag{3.19}$$

*Therefore one has statistical equilibrium when the distribution function at any point in phase space remains constant. Throughout this work the equilibrium condition will be assumed (i.e. no explicit time dependence of* $\rho$*). The term* $\partial\rho/\partial t$ *in (3.16) is just kept to retain the clarity of the derivation.*

#### 3.1.3.2 Constant Energy Surfaces

The rate of change of the Hamiltonian $H(q, p)$ along the trajectory of an isolated system is given by

$$\frac{dH}{dt} = \{H, H\} = 0, \tag{3.20}$$

where (3.2) and the remarks above were used. This result means that $H(q, p) = E$ is a constant along the trajectory of an isolated system, and that the trajectory is confined to the $(2n - 1)$ -dimensional hypersurface $S = S(E)$ defined by $H(q, p) = E$.

#### 3.1.3.3 Metrically Indecomposable Energy Surfaces

A constant energy surface $S(E)$ is said to be *metrically indecomposable* if it cannot be represented as a sum of of two regions $S_1$ and $S_2$ with nonzero areas

$$S = S_1 + S_2, \tag{3.21}$$

such that a trajectory that starts in $S_1$ remains in $S_1$ for all time and a trajectory that begins in $S_2$ always stays in $S_2$.

### 3.1.4 Microcanonical Distribution

Recall that for an isolated system as in Figure 3.1 the Hamiltonian $H(y)$ and the distribution function $\rho(y)$ are constant along its trajectory. Moreover, the evolution of the trajectory is required to remain within the hypersurface $S(E) = \{y \,|\, H(y) = E\}$. If the hypersurface $S(E)$ is metrically indecomposable and $\rho(y)$ is assumed to be continuous on $S(E)$, then one can prove[4] that $\rho(y) = C$, a constant, on $S(E)$ and zero otherwise. Thus, the *microcanonical distribution* (or *microcanonical ensemble*) is defined by the following limit

$$\rho(y) := \lim_{\Delta \to 0} \begin{cases} \dfrac{1}{V(E+\Delta) - V(E)} & \text{if} \quad E \le H(y) \le E + \Delta \\ 0 & \text{otherwise,} \end{cases} \tag{3.22}$$

where $V(E)$ denotes the volume of the set $V_E$ defined by

$$V_E := \{y : H(y) \le E\}\,. \tag{3.23}$$

For any phase function $F(y)$ the phase average $\bar{F}$ can now be computed using (3.8) and (3.22),

$$\begin{aligned} \bar{F} &= \lim_{\Delta \to 0} \left[ \int_{V_{E+\Delta}} \rho F \, dy - \int_{V_E} \rho F \, dy \right] \\ &= \frac{\lim_{\Delta \to 0} \left[ \int_{V_{E+\Delta}} F \, dy - \int_{V_E} F \, dy \right] / \Delta}{\lim_{\Delta \to 0} \left[ \int_{V_{E+\Delta}} dy - \int_{V_E} dy \right] / \Delta} \\ &= \frac{\frac{d}{dE} \int_{V_E} F \, dy}{\frac{d}{dE} V(E)} \\ &= \frac{1}{\Omega(E)} \frac{d}{dE} \int_{V_E} F \, dy, \end{aligned} \tag{3.24}$$

[4] See Khinchin (2013, §6) or Weiner (1983, §2.5).

where $\Omega(E)$ is called the *structure function* of the system and is defined as

$$\Omega(E) := \frac{d}{dE}V(E) = V'(E). \tag{3.25}$$

**Remark 3.4.** *In the special case where phase functions only depend on $H(y)$, that is $F(y) = F(H(y))$, volume integrals over phase space can be simplified to*

$$\int_{V_E} F(y)\,dy = \int_0^E F(\hat{E})V'(\hat{E})\,d\hat{E} = \int_0^E F(\hat{E})\Omega(\hat{E})d\hat{E}. \tag{3.26}$$

### 3.1.5 Systems in Weak Interaction

The Hamiltonian for an isolated system as in Figure 3.1 can be written as

$$H_{A+B}(y_A, y_B) = H_A(y_A) + H_B(y_B) + H_{AB}(y_A, y_B), \tag{3.27}$$

where $y_A$ and $y_B$ denote the positions and momenta of systems $A$ and $B$. The Hamiltonians $H_A(y_A)$ and $H_B(y_B)$ describe the systems $A$ and $B$ separately, and $H_{AB}(y_A, y_B)$ describes the interaction of the two systems.

The systems $A$ and $B$ are said to be in *weak interaction* if the interaction Hamiltonian $H_{AB}$ can be neglected for the purpose of integrating over phase space. Only for that specific use of the Hamiltonian, $H_{A+B}$ can be simplified to

$$H_{A+B}(y_A, y_B) = H_A(y_A) + H_B(y_B). \tag{3.28}$$

#### 3.1.5.1 Structure Function of Systems in Weak Interaction

In order to calculate the structure function of the system $A + B$ in weak interaction, the volume $V_E(A + B)$ of the region

$$V_E^{A+B} = \{(y_A, y_B) : H_A(y_A) + H_B(y_B) \leq E\} \tag{3.29}$$

has to be calculated and then differentiated with respect to the total energy $E$. The volume can be expressed as

$$V_E(A+B) = \int_{V_E^A} \int_{V^B_{E-H_A(y_A)}} dy_B\,dy_A = \int_{V_E^A} V_B(E - H_A(y_A))\,dy_A, \tag{3.30}$$

which can be rewritten using (3.26) as

$$V_E(A+B) = \int_0^E V_B(E - E_A)\Omega_A(E_A)\,dE_A. \tag{3.31}$$

A differentiation with respect to $E$ then yields

$$\Omega_E(A+B) = \int_0^E \Omega_B(E - E_A)\Omega_A(E_A)\,dE_A, \tag{3.32}$$

which states that the structure function of the system $A + B$ in weak interaction is equal to the convolution of the structure functions of $A$ and $B$.

#### 3.1.5.2 Distribution Function for Component of an Isolated System

Until now, only the distribution function of the isolated system $A + B$ (3.22) has been considered. The goal within this section however is to find the distribution function for a single component $A$ (or $B$) of the system. This can be achieved by integrating the distribution function $\rho_{A+B}$ over $\Gamma_B$

$$\rho_A(y_A) = \int_{\Gamma_B} \rho_{A+B}\, dy_B. \tag{3.33}$$

To this end, a characteristic function $\phi(y_A)$ is defined as

$$\phi(y_A) := \begin{cases} 1 & \text{for} \quad y_A \in M_A \\ 0 & \text{for} \quad y_A \notin M_A, \end{cases} \tag{3.34}$$

where $M_A$ is an arbitrary region in $V_E^A$. Using $\phi(y_A)$, (3.33), and (3.24) one can write

$$\begin{aligned}
\int_{M_A} \rho_A(y_A)\, dy_A &= \int_{\Gamma_A} \phi(y_A)\rho_A(y_A)\, dy_A \\
&= \int_{\Gamma_A} \phi(y_A) \left( \int_{\Gamma_B} \rho_{A+B}(y_A, y_B)\, dy_B \right) dy_A \\
&= \int_{\Gamma_{A+B}} \phi(y_A)\rho_{A+B}(y_A, y_B)\, dy_B\, dy_A \\
&= \frac{1}{\Omega_{A+B}(E)} \frac{d}{dE} \int_{V_E^{A+B}} \phi(y_A)\, dy_B\, dy_A \\
&= \frac{1}{\Omega_{A+B}(E)} \frac{d}{dE} \int_{V_E^A} \phi(y_A) \int_{V_{E-H_A(y_A)}} dy_B\, dy_A \\
&= \frac{1}{\Omega_{A+B}(E)} \frac{d}{dE} \int_{V_E^A} \phi(y_A) V_B(E - H_A(y_A))\, dy_A \\
&= \frac{1}{\Omega_{A+B}(E)} \frac{d}{dE} \int_{M_A} V_B(E - H_A(y_A))\, dy_A \\
&= \int_{M_A} \frac{\Omega_B(E - H_A(y_A))}{\Omega_{A+B}(E)}\, dy_A.
\end{aligned} \tag{3.35}$$

Since the region $M_A$ is arbitrary it can be concluded that,

$$\rho_A(y_A) := \begin{cases} \dfrac{\Omega_B(E - H_A(y_A))}{\Omega_{A+B}(E)} & \text{for} \quad y_A \in V_E^A \\ 0 & \text{for} \quad y_A \notin V_E^A. \end{cases} \tag{3.36}$$

Using (3.26) and (3.32), the normalization condition (3.7) can be checked easily

$$\begin{aligned}\int_{\Gamma_A} \rho_A(y_A)\, dy_A &= \int_{V_E^A} \rho_A(y_A)\, dy_A \\ &= \int_0^E \rho_A(y_A)\Omega_A(\hat{E}_A)\, d\hat{E}_A \\ &= \frac{1}{\Omega_{A+B}} \int_0^E \Omega_B(E-\hat{E}_A)\Omega_A(\hat{E}_A)\, d\hat{E}_A = 1.\end{aligned} \tag{3.37}$$

Thus, (3.36) is the distribution function for a single component of an isolated system $A+B$ with fixed total energy $E$.

### 3.1.6 Canonical Distribution

Isolated systems $A+B$ with constant total energy as discussed until now are very idealized systems. Every actual physical system will have an exchange of energy with its surroundings to some extent. One way to get a bit closer to reality is to let the degrees of freedom of system $B$ go to infinity and view the system $A$ as part of a much larger system $A+B$. In this case the system $A$ can exchange energy with system $B$, which constitutes its surrounding. In order to arrive at the distribution function for such a system $A$, let $B$ be an ideal gas with $n/3$ atoms with atomic mass $m$ confined to a box of edge $L$ and assume weak interaction between $A$ and $B$. The Hamiltonian of $B$ then reads

$$H_B(q,p) = \chi_B(q) + \frac{1}{2m}\sum_{i=1}^{n} p_i^2, \tag{3.38}$$

where the potential $\chi_B(q)$ is given by

$$\chi_B(q) = \begin{cases} 0 & \text{if particle inside the box} \\ \infty & \text{if particle outside the box,} \end{cases} \tag{3.39}$$

representing the effect of the confining box. Next, consider the volume $V_B(E)$ of the region $V_E^B$ defined by $H_B \leq E$, which is needed to calculate the structure function $\Omega_B(E)$. The volume can be calculated as the product of an n-dimensional hypercube of edge $L$ in $q$-space, and an n-dimensional hypersphere of radius $\sqrt{2mE}$ in $p$-space

$$V_B(E) = L^n \cdot \frac{\pi^{n/2}(\sqrt{2mE})^n}{(n/2)!} = C_0 E^{n/2}, \tag{3.40}$$

where all the constants are combined into $C_0$. Taking a derivative of the volume with respect to $E$ yields the structure function

$$\Omega_B(E) = \frac{n}{2} C_0 E^{n/2-1}. \tag{3.41}$$

To continue, the distribution function in (3.36) is rewritten as

$$\rho_A(y_A) = \frac{\Omega_B(E - H_A(y_A))}{\Omega_{A+B}(E)} \cdot \frac{\Omega_B(E)}{\Omega_B(E)} = C\frac{\Omega_B(E - H_A(y_A))}{\Omega_B(E)}, \tag{3.42}$$

where $C = \Omega_B(E)/\Omega_{A+B}(E)$ is independent of $y_A$. A substitution of (3.41) into (3.42) results in

$$\rho_A(y_A) = C\left(1 - \frac{H_A(y_A)}{E}\right)^{(n/2)-1}. \tag{3.43}$$

Before the limit of this expression for $n \to \infty$ is taken, an important quantity used to characterize the ambient $B$ is introduced: the energy of $A + B$ per number of degree of freedom of $B$,

$$\frac{\theta}{2} := \frac{E}{n}. \tag{3.44}$$

Using this definition of $\theta$, the limit of (3.42) works out to be

$$\lim_{n\to\infty} C\left(1 - \frac{2H_A(y_A)}{\theta n}\right)^{(n/2)-1} = Ce^{-H_A(y_A)/\theta}. \tag{3.45}$$

Thus, the distribution function for a system $A$ in weak interaction with a large system $B$ can be written as

$$\rho_A(y_A) = Ce^{-H_A(y_A)/\theta} \tag{3.46}$$

and is called a *canonical distribution* (or *canonical ensemble*).

## 3.2 Corresponding Concepts in Thermoelasticity and Statistical Mechanics

In this section the canonical and microcanonical distribution functions will be used to motivate macroscopic concepts introduced in Sections 2.2.7 and 2.3 from an atomistic point of view. To this end, the canonical ensemble (3.46) will be rewritten as

$$\rho(q, p; \mathcal{A}, \theta) = \exp\left\{\frac{\psi - H(q, p; \mathcal{A})}{\theta}\right\}, \tag{3.47}$$

where $\psi$ can be determined from the normalization condition and will depend on the macroscopic kinematic controlling parameters $\mathcal{A}_1, \ldots, \mathcal{A}_\nu$ (or the conjugate generalized forces $\mathcal{F}_1, \ldots, \mathcal{F}_\nu$) and $\theta$. Moreover, for specific macroscopic quantities, for example, $\mathcal{F}_\alpha(\mathcal{A}, \theta)$, the corresponding microscopic phase functions will be denoted as $\mathcal{F}^m_\alpha(q, p)$, with $m$ referring to microscopic.

### 3.2.1 Temperature

Consider three systems: a system $A$ in equilibrium with its ambient and described by

$$\rho_A(y_A; \mathcal{A}_A, \theta_A) = \exp\left\{\frac{\psi_A - H(y_A; \mathcal{A}_A)}{\theta_A}\right\}, \tag{3.48}$$

a second system $B$ in equilibrium with its ambient and described by

$$\rho_A(y_B; \mathcal{A}_B, \theta_B) = \exp\left\{\frac{\psi_B - H(y_B; \mathcal{A}_B)}{\theta_B}\right\}, \tag{3.49}$$

and a third system composed of $A$ and $B$ in equilibrium with an ambient described by

$$\rho_{A+B} = \exp\left\{\frac{\psi_{A+B} - H_{A+B}(y_A, y_B; \mathcal{A}_A, \mathcal{A}_B)}{\theta_{A+B}}\right\}. \tag{3.50}$$

System $A$ is said to be in *thermal equilibrium* with system $B$ if,

$$\rho_A \cdot \rho_B = \rho_{A+B}. \tag{3.51}$$

By plugging in the distribution functions, the condition above can be rewritten as

$$\frac{H_{A+B}}{\theta_{A+B}} = \frac{H_A}{\theta_A} + \frac{H_B}{\theta_B}. \tag{3.52}$$

Moreover, if a weak interaction between $A$ and $B$ is assumed (3.28), the thermal equilibrium condition reads,

$$\frac{H_A + H_B}{\theta_{A+B}} = \frac{H_A}{\theta_A} + \frac{H_B}{\theta_B}. \tag{3.53}$$

Since $H_A$ and $H_B$ are independent, the condition can only be satisfied if

$$\theta_{A+B} = \theta_A = \theta_B, \tag{3.54}$$

holds true for all values of $y_A$ and $y_B$. Thus it is clear that the microscopic parameter $\theta$ functions like macroscopic temperature.

### 3.2.2 Quasi-Static Process

The concept of a quasi-static process from a macroscopic point of view is based on the idea that any mechanical loads $\mathcal{A}_\alpha(t)$ (or $\mathcal{F}_\alpha$(t)) or thermal loads $\theta(t)$ are applied very slowly such that the body is in a state of equilibrium for all $t$. The microscopic analog of a quasi-static process is found by assuming that the canonical distribution

$$\rho(q, p; \mathcal{A}(t), \theta(t)) = \exp\left\{\frac{\psi - H(q, p; \mathcal{A}(t))}{\theta(t)}\right\}, \tag{3.55}$$

can be applied for all $t$, where $t$ represents a macroscopic time scale.

### 3.2.3 Balance of Energy

The macroscopic balance of energy (2.71) is often mentioned in thermodynamics textbooks as

$$dU = dQ + dW, \tag{3.56}$$

where $dU$ corresponds to $\rho\dot{\epsilon}$, $dQ$ to $\rho r - \mathrm{div} q$, and $dW$ to $\mathbf{T} \cdot \mathbf{D}$. In order to identify corresponding microscopic quantities, the focus will be on quasi-static adiabatic ($dQ = 0$) processes. The statistical mechanical analog is an isolated system with a constant total energy $H(q, p; \mathcal{A}) = E$, driven by the macroscopic functions $\mathcal{A}_\alpha(t)$, $E(t)$. Such a system will be described by a microcanonical ensemble $\rho_{mc}(q, p; \mathcal{A}, E)$ that is normalized to *unity* when integrated over the *constant energy surface* $S(E; \mathcal{A})$

$$\int_{S(E,\mathcal{A})} \rho_{mc}(q, p; \mathcal{A}, E)\, dS = 1. \tag{3.57}$$

Furthermore, let the phase function for the generalized forces $\mathcal{F}_\alpha$ (conjugate to $\mathcal{A}_\alpha$) be defined as[5]

$$\mathcal{F}^m_\alpha(q, p; \mathcal{A}) = \frac{\partial H}{\partial \mathcal{A}_\alpha}(q, p; \mathcal{A}), \quad \alpha = 1 \ldots, \nu. \tag{3.58}$$

The rate of work done on the isolated system during a quasi-static process can then be written as

$$\begin{aligned} \dot{W} &= \mathcal{F}_\alpha \dot{\mathcal{A}}_\alpha \\ &= \int_{S(E;\mathcal{A})} \mathcal{F}^m_\alpha \rho_{mc}\, dS \cdot \dot{\mathcal{A}}_\alpha \\ &= \int_{S(E;\mathcal{A})} \frac{\partial H}{\partial \mathcal{A}_\alpha} \dot{\mathcal{A}}_\alpha \rho_{mc}\, dS \\ &= \int_{S(E;\mathcal{A})} \dot{H} \rho_{mc}\, dS, \end{aligned} \tag{3.59}$$

where $\dot{H} = (\partial H/\partial \mathcal{A}_\alpha)\dot{\mathcal{A}}_\alpha$ is the rate of change of $H$ at fixed $(q, p)$ and the implied Einstein summation convention is ranging from 1 to $\nu$.

Moreover, let the phase average of $H$ with respect to $\rho_{mc}$ be denoted as

$$\bar{H}(\mathcal{A}, E) = \int_{S(E,\mathcal{A})} H(q, p; \mathcal{A}) \rho_{mc}(q, p; \mathcal{A}, E)\, dS. \tag{3.60}$$

[5]The definition is motivated by the fact that the change in total energy due to an incremental change in the controllable parameters $d\mathcal{A}_\alpha$ at fixed $(q, p)$ should be equal to the work done by the generalized forces $\mathcal{F}^m_\alpha$. A simple chain rule yields $dH = \frac{\partial H}{\partial \mathcal{A}_\alpha} d\mathcal{A}_\alpha = \mathcal{F}^m_\alpha d\mathcal{A}_\alpha$, and thus $\mathcal{F}^m_\alpha = \frac{\partial H}{\partial \mathcal{A}_\alpha}$.

Then, the differentiation of $\bar{H}$ with respect to $t$ gives

$$\begin{aligned}\frac{d}{dt}\bar{H} = \dot{\bar{H}} &= \frac{d}{dt}\int_{S(E;\mathcal{A})} H\rho_{mc}\, dS \\ &= \int_{S(E;\mathcal{A})} \dot{H}\rho_{mc}\, dS + E\frac{d}{dt}\int_{S(E;\mathcal{A})} \rho_{mc}\, dS \\ &= \int_{S(E;\mathcal{A})} \dot{H}\rho_{mc}\, dS,\end{aligned} \tag{3.61}$$

where the normalization condition (3.57) was used in the last step. Thus, combining (3.56), (3.59), and (3.61) yields

$$\dot{W} = \dot{U} = \dot{\bar{H}} = \int_{S(E;\mathcal{A})} \dot{H}\rho_{mc}\, dS \tag{3.62}$$

during an adiabatic quasi-static process. This leads to the conclusion that the Hamiltonian $H(q,p;\mathcal{A})$ acts as the microscopic counterpart to the internal energy, that is,

$$U^m(q,p;\mathcal{A}) := H(q,p;\mathcal{A}). \tag{3.63}$$

Since a phase function is generally independent of the type of ensemble used, the internal energy for a canonical ensemble can also be calculated using (3.63).

Next, consider a system in equilibrium with an ambient at temperature $\theta$ undergoing a quasi-static process described by $\mathcal{A}_\alpha(t)$, $\theta(t)$. Such a system will be governed by a canonical distribution $\rho(q,p;\mathcal{A},\theta)$. Using the fact that the phase average of the Hamiltonian $H(q,p;\mathcal{A})$ gives the internal energy $U(\mathcal{A},\theta)$, one can write

$$\begin{aligned}\dot{U} &= \frac{d}{dt}\int_\Gamma H\rho\, dq\, dp \\ &= \int_\Gamma \dot{H}\rho + H\dot{\rho}\, dq\, dp \\ &= \int_\Gamma \frac{\partial H}{\partial \mathcal{A}_\alpha}\dot{\mathcal{A}}_\alpha\rho + H\dot{\rho}\, dq\, dp \\ &= \int_\Gamma \mathcal{F}^m_\alpha\dot{\mathcal{A}}_\alpha\rho + H\dot{\rho}\, dq\, dp \\ &= \dot{\mathcal{A}}_\alpha\int_\Gamma \mathcal{F}^m_\alpha\rho\, dq\, dp + \int_\Gamma H\dot{\rho}\, dq\, dp \\ &= \mathcal{A}_\alpha\dot{\mathcal{F}}_\alpha + \int_\Gamma H\dot{\rho}\, dq\, dp = \dot{W} + \int_\Gamma H\dot{\rho}\, dq\, dp.\end{aligned} \tag{3.64}$$

Thus, comparing (3.56) and the last line in (3.64) yields

$$\dot{Q} = \int_\Gamma H\dot{\rho}\, dq\, dp, \tag{3.65}$$

which means that *heat transfer* on a microscopic scale is the *changing of the distribution* of the system in phase space. On the other hand, it is seen from (3.62), that *mechanical work* is done because of a change of the Hamiltonian at a given point in phase space.

**Remark 3.5.** *In the case of a microcanonical distribution, it can be shown using Liouville's theorem that the heat flow (3.65) reduces to zero,*

$$\dot{\rho} = 0 \quad \Rightarrow \quad \dot{Q} = 0, \tag{3.66}$$

*which is consistent with the adiabatic assumption.*

## 3.2.4 Second Law of Thermodynamics

### 3.2.4.1 Entropy

The key concept to explain the second law of thermodynamics, as mentioned in Section 2.3, is entropy. From the macroscopic point of view it is frequently introduced as

$$dS := \frac{dQ}{T} \quad \text{or} \quad \dot{Q} = T\dot{S}, \tag{3.67}$$

for quasi-static processes, with $S$ denoting the entropy and $T$ an absolute temperature scale, such that $S = 0$ at absolute zero (compare with (2.81) and (2.82)). In order to identify corresponding microscopic quantities, consider again a system in equilibrium with an ambient at temperature $\theta$ undergoing a quasi-static process described by $\mathcal{A}_\alpha(t)$, $\theta(t)$ and define the *index of probability* as

$$\eta(q, p;\, \mathcal{A}, \theta) = \frac{\psi(\mathcal{A},\, \theta) - H(q, p; \mathcal{A})}{\theta} \tag{3.68}$$

such that the canonical ensemble can be rewritten as

$$\rho(q, p;\, \mathcal{A}, \theta) = \exp\{\eta(q, p;\, \mathcal{A}, \theta)\}. \tag{3.69}$$

Using the normalization condition (3.7), observe that

$$\frac{d}{dt}\int_\Gamma e^\eta \, dy = \int_\Gamma \dot{\eta} e^\eta \, dy = 0, \tag{3.70}$$

and thus

$$\dot{\bar{\eta}}\frac{d}{dt}\bar{\eta} = \frac{d}{dt}\int_\Gamma \eta e^\eta \, dy = \int_\Gamma \dot{\eta} e^\eta + \eta\dot{\eta} e^\eta \, dy = \int_\Gamma \eta\dot{\eta} e^\eta \, dy. \tag{3.71}$$

Going back to the heat flow (3.65), it is rewritten as

$$\dot{Q} = \int_\Gamma H\dot{\rho}\, dy = \int_\Gamma H\dot{\eta} e^\eta \, dy = \int_\Gamma (H - \psi)\,\dot{\eta} e^\eta \, dy = -\int_\Gamma \eta\theta\dot{\eta} e^\eta \, dy = -\theta\dot{\bar{\eta}} \tag{3.72}$$

using (3.68) the fact that $\psi = \psi(\mathcal{A}, \theta)$, and thus

$$\int_\Gamma \psi \dot{\eta} e^\eta \, dy = \psi \int_\Gamma \dot{\eta} e^\eta \, dy = 0. \tag{3.73}$$

Comparing (3.67) and (3.72), it is clear that $\theta$ corresponds to an absolute temperature scale and $\bar{\eta}$ to entropy. Usually the conversion used for the temperature is $\theta = kT$ where $k = 1.38 \times 10^{-23}$J/K is known as Boltzmann's constant. It immediately follows that

$$\bar{\eta}(\mathcal{A}, T) = -\frac{S(\mathcal{A}, T)}{k} \quad \text{or} \quad S(\mathcal{A}, T) = -k \int_\Gamma \rho \ln \rho \, dy, \tag{3.74}$$

and that the microscopic phase function for entropy reads

$$S^m(q, p; \mathcal{A}, \theta) = -k \ln \rho. \tag{3.75}$$

#### 3.2.4.2 Helmholtz Free Energy

The analog of the Helmholtz free energy in statistical mechanics is obtained by taking the phase average of both sides of (3.68), leading to

$$\bar{\eta}(\mathcal{A}, T) = \frac{\psi(\mathcal{A}, T) - \bar{H}(\mathcal{A}, T)}{kT} = \frac{\psi(\mathcal{A}, T) - U(\mathcal{A}, T)}{kT}, \tag{3.76}$$

where (3.63) was used, and equating it with (3.74), yielding

$$\psi(\mathcal{A}, T) = U(\mathcal{A}, T) - TS(\mathcal{A}, T). \tag{3.77}$$

This relationship identifies the normalization constant $\psi$ as the Helmholtz free energy function.

### 3.2.5 Partition Function

#### 3.2.5.1 Definition

Recall the normalization condition (3.7)

$$\int_\Gamma \exp\left\{\frac{\psi - H}{kT}\right\} dy = 1 \tag{3.78}$$

and rewrite it using the Helmholtz free energy (3.77) as

$$\exp\left\{-\frac{\psi}{kT}\right\} = \int_\Gamma \exp\left\{-\frac{H}{kT}\right\} dy \tag{3.79}$$

or

$$\psi(\mathcal{A}, T) = -kT \ln Z(\mathcal{A}, T), \tag{3.80}$$

where

$$Z(\mathcal{A}, T) = \int_\Gamma \exp\left\{-\frac{H(q,p;\,\mathcal{A})}{kT}\right\} dy. \tag{3.81}$$

The function $Z(\mathcal{A}, T)$ is called the *partition function* of the system and it plays a fundamental role in connecting the macroscopic behavior of the system with its microscopic model, as is seen in (3.80). Heuristically speaking the partition function is proportional to the volume of accessible microstates in phase space for a given temperature and a set of given controllable parameters.

#### 3.2.5.2 Useful Results and Notation

Some useful expressions introduced in this chapter are rewritten here in terms of the partition function (3.81), highlighting its important role.

**Canonical Distribution** The canonical distribution is often written in terms of the partition function as

$$\rho = \frac{1}{Z}\exp\{-\beta H\}, \tag{3.82}$$

where the common notation $\beta = 1/(kT)$ is used.

**Mean Energy** The phase average of the Hamiltonian can then be written as

$$\bar{H} = \frac{1}{Z}\int_\Gamma H e^{-\beta H}\, dy = -\frac{1}{Z}\frac{\partial}{\partial\beta}\int_\Gamma e^{-\beta H}\, dy = -\frac{\partial}{\partial\beta}\ln Z. \tag{3.83}$$

**Entropy** The entropy as mentioned in (3.74) can also be written in terms of the partition function as

$$S = -k\int_\Gamma \rho\frac{\psi - H}{kT}\, dy = -\frac{\psi}{T} + \frac{\bar{H}}{T} = k\ln Z - \frac{1}{T}\frac{\partial}{\partial\beta}\ln Z. \tag{3.84}$$

**Conjugate Forces** The phase average of the phase functions for generalized forces $\mathcal{F}_\alpha$ as introduced in (3.58) can be written as

$$\begin{aligned}\mathcal{F}_\alpha &= \frac{1}{Z}\int_\Gamma \frac{\partial H}{\partial \mathcal{A}_\alpha}\, e^{-\beta H}\, dy \\ &= \frac{1}{Z}\left(-\frac{1}{\beta}\right)\frac{\partial}{\partial\mathcal{A}_\alpha}\int_\Gamma e^{-\beta H}\, dy \\ &= -\frac{1}{\beta}\frac{\partial}{\partial\mathcal{A}_\alpha}\ln Z = \frac{\partial}{\partial\mathcal{A}_\alpha}\psi.\end{aligned} \tag{3.85}$$

**Canonical Strain Ensemble** When generalized displacements are used as controllable parameters in the Hamiltonian, the notation $H_{\mathcal{A}}(q,p;\mathcal{A})$ is used and the corresponding canonical distribution

$$\rho_{\mathcal{A}}(q,p;\mathcal{A},T) = \exp\frac{\psi_{\mathcal{A}} - H_{\mathcal{A}}(q,p;\mathcal{A})}{kT} \tag{3.86}$$

is referred to as the canonical strain ensemble (or just strain ensemble).

**Canonical Stress Ensemble** When generalized forces are used as controllable parameters in the Hamiltonian, the notation $H_{\mathcal{F}}(q,p;\mathcal{F})$ is used and the corresponding canonical distribution

$$\rho_{\mathcal{F}}(q,p;\mathcal{F},T) = \exp\frac{\psi_{\mathcal{F}} - H_{\mathcal{F}}(q,p;\mathcal{F})}{kT} \tag{3.87}$$

is referred to as the canonical stress ensemble (or just stress ensemble).

## 3.3 Rubber Elasticity

In this section the concepts of equilibrium statistical mechanics introduced so far are used to study the thermoelastic behavior of *amorphous polymeric solids* (or *elastomers*) from the atomistic point of view. Very frequently this topic is also simply referred to as *rubber elasticity*[6]. Typically, rubber elastic materials are characterized by the following four observations, provided that the temperature is above a critical temperature[7]:

1. Rubber shows a large extensibility ranging from $500\% - 1000\%$.
2. Rubber has a low modulus of elasticity ranging from $100kPa - 100MPa$.
3. Rubber contracts upon heating (and expands upon cooling).
4. Rubber releases heat when stretched.

The key to understanding and modeling rubber elastic materials is the fact that, unlike in crystalline solids, there is no potential energy stored in stretched *covalent bonds*, and thus there is no internal energy[8] contribution. However, due to the atomistic nature of rubberlike materials, the main contribution comes from *changes in entropy*. This section will deal with the atomistic structure of single *long-chain molecules* (also called *polymers*) and provide derivations of well-known one-dimensional and three-dimensional chain models clarifying the role of entropy.

[6]Some of the standard works in the field of rubber elasticity are Flory (1953, 1969); Treloar (1975).

[7]The critical temperature is called the *glass transition temperature* and it is different for each elastomer. Below this temperature, elastomers transition into a hard and brittle state and their behavior becomes glasslike.

[8]At very high strains internal energy comes into play again.

### 3.3.1 Atomistic Structure of Long-Chain Molecules

Long-chain molecules in rubber elastic materials mainly consist of carbon atoms which are held together by covalent bonds. In the simplest case of a long-chain molecule, polyethylene, the single carbon-carbon covalent bonds are 1.54Å long and the bond angles (angles between two successive bonds) have a value of 109.5°, as shown in Figure 3.2. The chemical formula

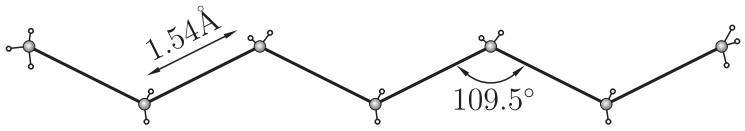


Figure 3.2: Atomistic structure of a polyethylene molecule with *bond length* and *bond angle* for carbon-carbon bonds: the black dots represent the carbon atoms, the smaller hollow dots represent hydrogen atoms, and the covalent bonds are shown as solid lines.

of polyethylene is generally written as $CH_3 - [CH_2]_n - CH_3$, where $n$ is the number of $CH_2$ units (or monomers). Typically the number of monomers in long-chain molecules ranges from $10^2$ to $10^4$. The resulting chain of carbon atoms is then called the *backbone* and the hydrogen atoms are referred to as *side groups*. Oftentimes, different polymer chains only differ in the type of side groups but have the same backbone.

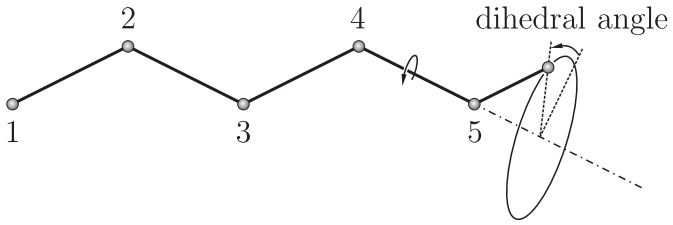


Figure 3.3: Rotation of a backbone atom around bond $4 - 5$ with a constant bond angle.

Covalent bonds between carbon atoms are known to be very strong and highly directional. This means that any small changes in the minimum-energy bond length or the minimum-energy bond angle would result in a large increase of the potential energy of interactions of the backbone atoms. However, there are still a lot of different atomic configurations possible in long-chain molecules while keeping the bond lengths and bond angles constant. By rotating atoms around their *dihedral angle*, as shown in Figure 3.3, many different configurations can be obtained. The potential energy of interaction of the backbone atoms is independent of the dihedral angle. Only the side groups of the long-chain-molecules interact with neighboring side groups and give a contribution to the potential energy of the chain depending on the

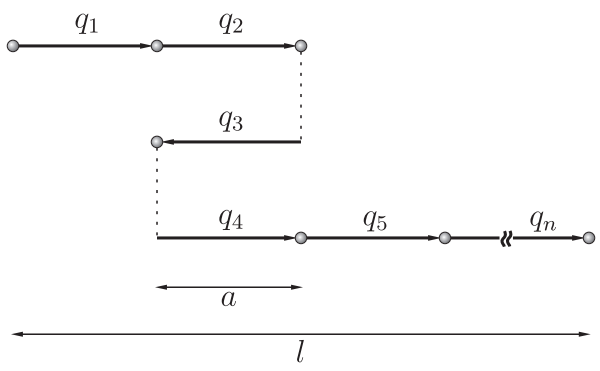


Figure 3.4: One-dimensional freely jointed chain with link length $a$, end-to-end length $l$, and generalized coordinates $q_1 = 1$, $q_2 = 1$, $q_3 = -1$, $q_4 = 1$, $q_5 = 1$, and $q_n = 1$.

dihedral angle. However, for the sake of simplicity, in the following derivations of the one-dimensional and three-dimensional polymer models, the rotational energy barrier around the dihedral angle due to side group interactions will not be considered.

### 3.3.2 One-Dimensional Polymer Model

In order to start a more quantitative discussion about modeling of long-chain molecules, a highly idealized model is considered here, the so-called one-dimensional *freely jointed chain*. In this model, a polymer is viewed as a one-dimensional chain consisting of $n$ rigid links of length $a$ connected by hinges. The hinges are only allowed to be fully opened or fully closed such that the chain is always oriented along a straight line. A configuration of the chain can then be defined by a sequence of generalized coordinates $q_j$, $j = 1, \ldots, n$, where $q_j \in \{+1, -1\}$ as shown in Figure 3.4.

The end-to-end length $l$ is considered a controllable kinematical parameter of the system and has to be an integer multiple of $a$. The potential energy of the chain is then written as

$$V(q_1, \ldots, q_n; l) = \begin{cases} 0 & \text{if} \quad \sum_{j=1}^{n} a q_j = l \quad (\text{if compatible with } l) \\ \infty & \text{if} \quad \sum_{j=1}^{n} a q_j \neq l \quad (\text{if compatible with } l). \end{cases} \tag{3.88}$$

Since no other contributions to the Hamiltonian are considered, the canonical phase space distribution results in

$$\rho(q_1, \ldots, q_n; l, T) = C e^{-V/kT} = \begin{cases} C & \text{if} \quad \sum_{j=1}^{n} a q_j = l \\ 0 & \text{if} \quad \sum_{j=1}^{n} a q_j \neq l. \end{cases} \tag{3.89}$$

In this system, points in phase space are defined by a sequence of discrete values $q = (q_1, \ldots, q_n)$, which means that any integration over the phase space will be written as a

summation. The normalization condition (3.7) then takes the form

$$\sum_q \rho(q; l, T) = 1, \tag{3.90}$$

which results in the normalization constant $C$

$$C = \frac{1}{\Omega(l)}, \tag{3.91}$$

where $\Omega(l)$ is the number of configurations of the chain compatible with the end-to-end length $l$.

The expression for the entropy (3.74) is then also written as a sum for this system

$$\begin{aligned} S(l) &= -k \sum_q \rho \ln \rho \\ &= -k \sum_{q\, comp.\, l} \frac{1}{\Omega(l)} \ln \frac{1}{\Omega(l)} \\ &= k \ln \Omega(l). \end{aligned} \tag{3.92}$$

With the entropy at hand, the Helmholtz free energy (3.77) and the generalized force (3.85) are given as a function of the generalized displacement $l$ as

$$\psi(l, T) = U - TS(l) \quad \text{and} \quad f = \frac{\partial \psi(l, T)}{\partial l}, \tag{3.93}$$

where $f$ denotes the corresponding generalized force. Since the internal energy of this system does not depend on $l$, the force required to keep the end-to-end length at $l$ is

$$f = \frac{\partial \psi}{\partial l} = -kT \frac{\partial}{\partial l} \ln \Omega(l). \tag{3.94}$$

In order to calculate the number of compatible configurations $\Omega(l)$, let $n_+$ be the number of $q_j = +1$ steps and $n_-$ the number of $q_j = -1$ steps. Compatibility with the end-to-end length yields

$$l = (n_+ - n_-)a \quad \text{and} \quad n = n_+ + n_-, \tag{3.95}$$

which can be solved for

$$\begin{aligned} n_+ &= \frac{1}{2}\left(n + \frac{l}{a}\right) \\ n_- &= \frac{1}{2}\left(n - \frac{l}{a}\right). \end{aligned} \tag{3.96}$$

The total number of ways of picking $n_+$ steps from $n$ is then equal to the number of compatible configurations $\Omega(l)$

$$\binom{n}{n_+} = \frac{n!}{n_+!\, n_-!} = \Omega(l), \tag{3.97}$$

and thus,

$$\begin{aligned}\Omega(l) &= \frac{n!}{\left(\frac{1}{2}\left(n+\frac{l}{a}\right)\right)!\,\left(\frac{1}{2}\left(n-\frac{l}{a}\right)\right)!} \\ &= \frac{\Gamma(n+1)}{\Gamma\left(\frac{1}{2}\left(n+\frac{l}{a}\right)+1\right)\Gamma\left(\frac{1}{2}\left(n-\frac{l}{a}\right)+1\right)},\end{aligned} \tag{3.98}$$

where the gamma function $\Gamma(n) = (n-1)!$ is introduced. Using (3.94), the force-extension relation (3.94) reads

$$f = \frac{kT}{2a}\left(\frac{\Gamma'(\frac{1}{2}\left(n+\frac{l}{a}\right)+1)}{\Gamma(\frac{1}{2}\left(n+\frac{l}{a}\right)+1)} - \frac{\Gamma'(\frac{1}{2}\left(n-\frac{l}{a}\right)+1)}{\Gamma(\frac{1}{2}\left(n-\frac{l}{a}\right)+1)}\right). \tag{3.99}$$

**Remark 3.6.** *For large values of $n$, $n_+$, and $n_-$, which characterize a long chain that is far from a fully extended state, the previous result (3.99) is simplified using the approximation*

$$\ln n! = \sum_{i=1}^{n} \ln i \approx \int_1^n \ln x\, dx = n\ln n - n + 1, \tag{3.100}$$

*such that*

$$\ln \Omega(l) \approx (n\ln n - n + 1) - (n_+ \ln n_+ - n_+ + 1) - (n_- \ln n_- - n_- + 1), \tag{3.101}$$

*which yields*

$$f = \frac{kT}{2a}\left(\ln\frac{1+\frac{l}{na}}{1-\frac{l}{na}}\right) \approx \frac{kT}{na^2}\,l \quad \text{for} \quad \frac{l}{na} \ll 1. \tag{3.102}$$

*This force-extension relation is plotted in Figure 3.5, where two things should be noted. Firstly, the non-linear graph ends where the full extension of the chain $l = na$ is reached. In reality it should not end at this point, because the stretching of the covalent bonds would start there. Secondly, if the temperature increases, the force required to maintain a certain end-to-end length increases as well. Thus at a fixed force, a temperature rise would lead to a contraction in length.*

#### 3.3.2.1 Random Walk Interpretation

Another common way of modeling long-chain molecules is by using the mathematical concept of a random walk. For a one-dimensional polymer model, a random walk starting at $x = 0$ and taking steps of length $a$ in either the positive $x$ or the negative $x$ direction with equal probability is considered. The quantity of interest of this random walk is the probability of ending up at a position $x = l$ after $n$ steps.

Observe that a single sequence of $n$ steps has the probability of $(\frac{1}{2})^n$. Thus, all the compatible sequences will have the probability of

$$\left(\frac{1}{2}\right)^n \frac{n!}{n_+!\,n_-!}, \tag{3.103}$$

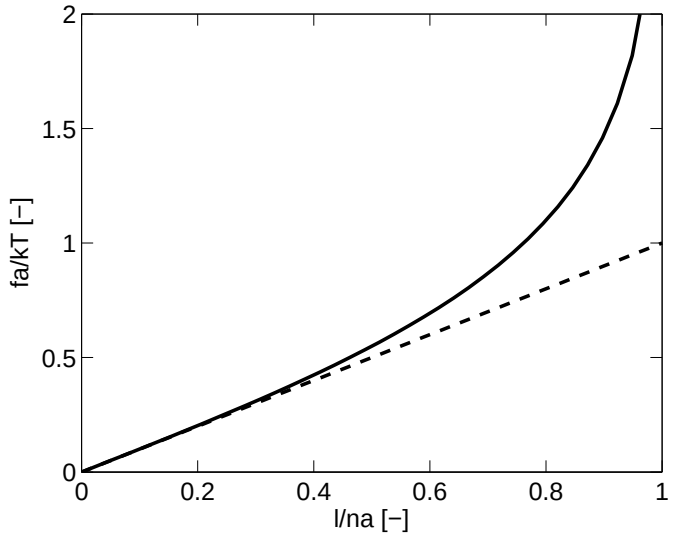


Figure 3.5: The solid line shows the full force-extension relation for a one-dimensional polymer model, the dashed line shows the linear approximation from (3.102).

which can be used to write a probability density as a function of $n_+$ as

$$p(n_+)\,dn_+ = \left(\frac{1}{2}\right)^n \frac{n!}{n_+!\,n_-!}\,dn_+. \tag{3.104}$$

From the compatibility equation in (3.96) it can be be seen that $dn_+ = \frac{1}{2a}\,dl$, and thus using (3.98), the probability density can be written as

$$p(n_+)\,dn_+ = \left(\frac{1}{2}\right)^n \Omega(l)\,\frac{dl}{2a}. \tag{3.105}$$

This leads to the desired probability density (probability per unit distance)

$$p(l;n) = \Omega(l)\frac{1}{2^{n+1}a}. \tag{3.106}$$

Again, for long chains far from a fully extended state, i.e. $n \ll 1$ and $l/(na) \gg 1$ in case of the random walk, Stirling's approximation

$$\ln n! \approx (n+\frac{1}{2})\ln n - n + \frac{1}{2}\ln 2\pi \tag{3.107}$$

can be used in combination with

$$\ln\frac{1}{2}\left(n \pm \frac{l}{a}\right) \cong \pm\frac{l}{na} - \frac{l^2}{2n^2a^2} + \ln\frac{n}{2} \tag{3.108}$$

to obtain the probability density as

$$p(l;n) = \frac{1}{\sqrt{2\pi n a^2}}\, e^{-\frac{l^2}{2na^2}}, \tag{3.109}$$

where $(\sqrt{2\pi n a^2})^{-1}$ is the normalization constant. This well-known probability distribution is a *Gaussian distribution* (or *normal distribution*) with a mean value of $\langle l \rangle = 0$ and a variance of $\langle l^2 \rangle = na^2$.

The Gaussian distribution can also be used to calculate a force-extension relation. To this end, solve (3.106) for $\Omega(l)$ and plug it into (3.94) yielding

$$\begin{aligned} f(l) &= -kT\frac{\partial}{\partial l}\ln\Omega(l) = -kT\frac{\partial}{\partial l}\ln 2^{n+1}ap(l) \\ &= -kT\frac{\partial}{\partial l}\left(\ln p(l) + \ln 2^{n+1}a\right) = -kT\frac{\partial}{\partial l}\ln p(l) \\ &= \frac{kT}{na^2}\, l, \end{aligned} \tag{3.110}$$

which is the exact same relation as calculated in (3.102).

### 3.3.3 Three-Dimensional Polymer Model

Before a three-dimensional model for long-chain molecules is derived, the convolution theorem for Fourier transforms is briefly introduced, since it constitutes an important tool in the study of three-dimensional random walks.

#### 3.3.3.1 Convolution Theorem

Let $x_1$ and $x_2$ be two independent continuous random variables with probability distribution functions $p_1(x_1)$ and $p_2(x_2)$, where $-\infty < x_1, x_2 < \infty$. Moreover, let $y$ be another random variable defined by $y = x_1 + x_2$. The probability distribution function $p(y)$ is then given by

$$p(y) = \int_{-\infty}^{\infty} p_1(x_1)p_2(y - x_1)\, dx_1, \tag{3.111}$$

which is the convolution of $p_1(x_1)$ and $p_2(x_2)$. Similarly, let $P_1(\eta)$, $P_2(\eta)$ be the Fourier transforms of $p_1(x_1)$ and $p_2(x_2)$ defined by

$$P_j(\eta) = \int_{-\infty}^{\infty} e^{-i\eta y} p_j(y)\, dy, \tag{3.112}$$

and its inverse being

$$p_j(y) = \frac{1}{2\pi}\int_{-\infty}^{\infty} e^{i\eta y} P_j(\eta)\, d\eta. \tag{3.113}$$

The convolution theorem then states that the Fourier transform of a convolution is the product of the Fourier transforms, and thus

$$P(\eta) = P_1(\eta)P_2(\eta). \tag{3.114}$$

A simple extension of this result for the case of $y = x_1 + \ldots + x_n$, where $x_1, \ldots, x_n$ are $n$ independent random variables with probability distributions $p_j(x_j)$, yields

$$P(\eta) = \prod_{j=1}^{n} P_j(\eta), \tag{3.115}$$

with $P_j(\eta)$ being the Fourier transform of $p_j(x_j)$. In the case of identical probability distributions $p_j(x_j) = p_1(x_j)$, $j = 1, \ldots, n$

$$P(\eta) = [P_1(\eta)]^n. \tag{3.116}$$

In the case of three-dimensional random variables $\mathbf{r}_1, \ldots, \mathbf{r}_n$, all having the same probability distribution function $p_1(\mathbf{r}_j)$, $j = 1, \ldots, n$, let $\mathbf{r}$ be the sum of all the random variables

$$\mathbf{r} = \mathbf{r}_1 + \mathbf{r}_2 + \ldots + \mathbf{r}_n, \tag{3.117}$$

and $p(\mathbf{r})$ its probability distribution. Using the three-dimensional Fourier transform

$$P(\boldsymbol{\rho}) = \int_{\mathbb{R}^3} e^{-i\boldsymbol{\rho}\cdot\mathbf{r}} p(\mathbf{r})\, d\mathbf{r}, \tag{3.118}$$

with the inverse

$$p(\mathbf{r}) = \frac{1}{(2\pi)^3} \int_{\mathbb{R}^3} e^{i\boldsymbol{\rho}\cdot\mathbf{r}} P(\boldsymbol{\rho})\, d\boldsymbol{\rho}, \tag{3.119}$$

$p(\mathbf{r})$ can be calculated by setting

$$P(\boldsymbol{\rho}) = [P_1(\boldsymbol{\rho})]^n. \tag{3.120}$$

#### 3.3.3.2 Freely Jointed Chain

As in the one-dimensional case, a three-dimensional model for long-chain molecules consists of $n$ freely jointed links $a$. The goal is to find the distribution function $p(\mathbf{r})$ of the end-to-end length $\mathbf{r}$ of the chain. Using the random walk analogy, the problem can be seen as taking $n$ steps of length $a$, with the direction of each step being uniformly distributed on a sphere of radius $a$. Thus for one step, the probability distribution takes the form

$$p_1(\mathbf{r}_1) = \frac{1}{4\pi a^2}\delta(r_1 - a), \tag{3.121}$$

where $r_1 = |\mathbf{r}_1|$, and $\delta(x)$ is a Dirac delta function. Also note that $p_1(\mathbf{r}_1)$ satisfies the normalization condition $\int_{\mathbb{R}^3} p_1(\mathbf{r}_1)\, d\mathbf{r}_1$.

The Fourier transform of $p_1(\mathbf{r}_1)$ can then be calculated as

$$\begin{aligned} P_1(\boldsymbol{\rho}) &= \frac{1}{4\pi a^2} \int_{\mathbb{R}^3} e^{-i\boldsymbol{\rho}\cdot\mathbf{r}_1} \delta(r_1 - a)\, d\mathbf{r}_1 \\ &= \frac{1}{4\pi a^2} \int_0^{2\pi} d\phi \int_0^{\infty} dr_1 \int_0^{\pi} e^{-i\rho r_1 \cos\theta} \delta(r_1 - a) r^2 \sin\theta\, d\theta \\ &= \left( \frac{\sin \rho a}{\rho a} \right), \end{aligned} \tag{3.122}$$

where $\rho = |\boldsymbol{\rho}|$ and the direction of $\boldsymbol{\rho}$ is taken as the polar axis with $\theta$ being the angle between $\boldsymbol{\rho}$ and $\mathbf{r}_1$. By using (3.120), it follows that

$$P(\boldsymbol{\rho}) = \left( \frac{\sin \rho a}{\rho a} \right)^n. \tag{3.123}$$

The distribution function $p(\mathbf{r})$ of the end-to-end length $\mathbf{r}$ of the chain is then found by using the inverse Fourier transform,

$$p(\mathbf{r}) = \frac{1}{(2\pi)^3} \int_{\mathbb{R}^3} e^{i\boldsymbol{\rho}\cdot\mathbf{r}} \left( \frac{\sin \rho a}{\rho a} \right)^n d\boldsymbol{\rho}, \tag{3.124}$$

which can be reduced to an integral over $\rho$ by using $\mathbf{r}$ as polar axis

$$p(\mathbf{r}) = \frac{1}{2\pi^2 r} \int_0^{\infty} \sin \rho r \left( \frac{\sin \rho a}{\rho a} \right)^n \rho\, d\rho. \tag{3.125}$$

Since the probability distribution only depends on the length of $\mathbf{r}$, it is spherically symmetric. For large values of $n$, and when the chain is far from a fully extended state, the probability distribution for a freely jointed chain in three dimension can be approximated (see e.g. Weiner (1983, §5.5)) by

$$p(\mathbf{r}) = \left[ \frac{3}{2\pi n a^2} \right]^{3/2} \exp\left\{ -\frac{3r^2}{2na^2} \right\}, \tag{3.126}$$

which is again a *Gaussian distribution*, as already seen in the one-dimensional case (3.109). If the procedure from (3.110) is generalized for three-dimensional chains, the force-extension relation can be calculated as

$$\mathbf{f}(\mathbf{r}) = -kT \frac{\partial}{\partial \mathbf{r}} \ln p(\mathbf{r}) = \frac{3kT}{na^2} \mathbf{r}, \tag{3.127}$$

and is plotted in Figure 3.6. This three dimensional linear force-extension relation is well known and often referred to as a *linear entropic spring*. However, at high levels of stretch, that is when the end-to-end length approaches the fully extended state, the force-extension relation shows a non-linear behavior, where a characteristic upturn due to the limited extensibility of polymer chains is observable (Mark, 1981). For the one-dimensional case the

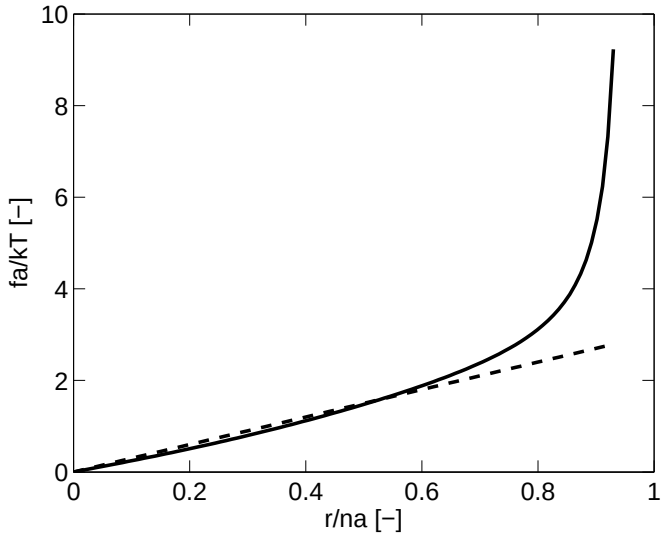


Figure 3.6: The dashed line shows the force-extension relation for the freely jointed three-dimensional chain with a Gaussian distribution (3.126), where $\mathbf{r}$ pointing is the $x$-direction. The solid line shows the force-extension relation for the non-Gaussian distribution (3.128), with $n = 6$.

non-linear behavior was already observed in Figure 3.5. In order to capture this stiffening behavior at high stretches in three-dimensions, an approximation of the probability distribution function (3.125) of the form

$$p(\mathbf{r}) = \left[\frac{3}{2\pi n a^2}\right]^{3/2} \exp\left\{-\frac{3r^2}{2na^2}\right\}\left\{1 - \frac{3}{4n} + \frac{3r^2}{2n^2a^2} - \frac{9r^4}{20n^3a^4}\right\} \tag{3.128}$$

is derived in Wang and Guth (1952). The force extension-relation for this non-Gaussian distribution function ends up being

$$\mathbf{f}(\mathbf{r}) = -kT\frac{\partial}{\partial \mathbf{r}} \ln p(\mathbf{r}) = \frac{kT}{na^2}\left(3 + 4\frac{15 - 9\left(\frac{r}{na}\right)^2 n}{15 - 20n - 30\left(\frac{r}{na}\right)^2 n + 9\left(\frac{r}{na}\right)^4 n^2}\right)\mathbf{r}, \tag{3.129}$$

and is plotted in Figure 3.6 for $n = 6$.

# Chapter 4

# Micro–Macro Mechanics

When dealing with the mechanical behavior of rubber-like materials, the microscopic modeling of a single long-chain molecule is not enough to fully capture their characteristic *S-shaped uniaxial stress response* on a macroscopic scale (see Figure 1.1). The reason is that when polymer chains are *vulcanized* (or *cured*), cross-links at random point along the chains are formed that tie two chains together, resulting in a random polymer network microstructure as shown in Figures 1.2 and 4.1. The portion of the chains between the cross-links typically consist of 100 to 1000 links, depending on the degree of vulcanization. In addition, these three-dimensional amorphous networks contain many defects, such as entanglements, loose ends, closed loops, and interlooping of chains.

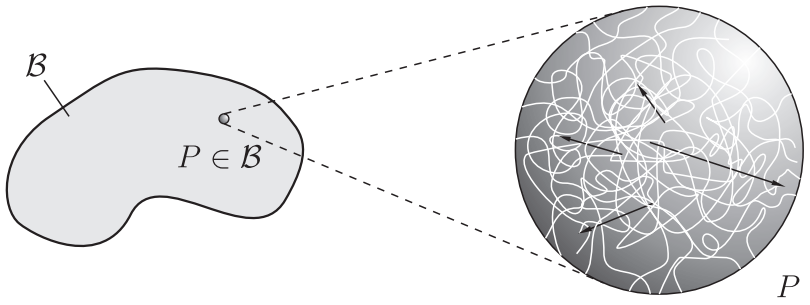


Figure 4.1: Random network microstructure of a continuous rubber elastic solid $\mathcal{B}$ at a material point $P$ consisting of cross-linked polymer chains (white solid lines) with end-to-end vectors (black arrows) plotted for four random chains.

If an amorphous solid is deformed on the macroscopic scale, the average end-to-end length of chains between cross-links will change in some way on the microscopic scale. Thus, in order to achieve an accurate macroscopic stress-strain response for rubber elastic materials, a micro-macro transition connecting the micro-kinematic variables of the single-chain models and the continuum deformation measures has to be constructed, by *modeling the polymer network microstructure*.

This chapter will show how a simple model of a long-chain molecule can be incorporated into a network microstructure model leading to a continuum constitutive relation for rubber-like materials. The ideas of this micro-macro approach are based on the non-affine micro-sphere model of Miehe et al. (2004).

## 4.1 Macroscopic Setting of Model

On the macroscopic (continuum) scale the model assumes a Helmholtz free energy function *per unit volume* that depends on the right Cauchy-Green deformation tensor

$$\Psi = \Psi(\mathbf{C}). \tag{4.1}$$

Following the argument as outlined in Section 2.3, the second Piola-Kirchhoff is given by

$$\mathbf{S} = 2\frac{\partial \Psi(\mathbf{C})}{\partial \mathbf{C}}. \tag{4.2}$$

Note that no dependency on the temperature is mentioned because isothermal conditions are assumed.

Following common practice for isothermal finite strain elasticity, a decoupling of the Helmholtz free energy function into volumetric and isochoric parts is introduced by use of the unimodular part of the deformation gradient as proposed by Flory (1961),

$$\bar{\mathbf{F}} := J^{-1/3}\mathbf{F}, \quad J = \det \mathbf{F}, \tag{4.3}$$

and using the form

$$\Psi = \Psi_{\text{vol}}(J) + \bar{\Psi}\left(\bar{\mathbf{C}}\right), \ \bar{\mathbf{C}} = \bar{\mathbf{F}}^T\bar{\mathbf{F}}, \tag{4.4}$$

with volumetric and isochoric contributions to the free energy function. Applying (4.2) to the decoupled macroscopic free energy leads to the standard result in compressible hyperelasticity (see e.g. Holzapfel (2000, Chap. 6))

$$\mathbf{S} = J\Psi'_{\text{vol}}(J)\mathbf{C}^{-1} + J^{-2/3}\left(\mathbb{I} - \frac{1}{3}\mathbf{C}^{-1}\otimes\mathbf{C}\right) : 2\frac{\partial \bar{\Psi}(\bar{\mathbf{C}})}{\partial \bar{\mathbf{C}}}, \tag{4.5}$$

where the fourth-order unit tensor is given as

$$\mathbb{I} = \frac{1}{2}(\delta_{ik}\delta_{jl} + \delta_{il}\delta_{jk})\,\mathbf{e}_i\otimes\mathbf{e}_j\otimes\mathbf{e}_k\otimes\mathbf{e}_l. \tag{4.6}$$

The volumetric response $\Psi_{\text{vol}}(J)$ can be any scalar valued function which is strictly convex, has unbounded value as $J \to 0$ and $J \to \infty$, and has a unique minimum at $J = 1$. The isochoric response of the material, $\bar{\Psi}\left(\bar{\mathbf{C}}\right)$, contains the microstructural details and is developed in the next two sections. First, a micro-mechanical model of a constrained single long-chain molecule is considered, and then the polymer network structure is modeled using the non-affine micro-sphere model, which provides a bridge between the microscopic and the macroscopic scale.

## 4.2 Micro-Mechanical Setting of Model

In order to develop an expression for the total free energy $\psi$ on the micro-mechanical scale, two contributions are taken into account. Firstly, an unconstrained single chain model as derived in Section 3.3.3 is considered. Secondly, in order to account for hindrances to the motion of a single chain within a polymer network, the chain is assumed to be confined to a tube (Miehe et al., 2004). To this end, an additive split of the total free energy $\psi$ into a contribution due to the unconstrained single chain $\psi_f$, and a contribution due to the tube constraint $\psi_c$

$$\psi = \psi_f + \psi_c, \tag{4.7}$$

is assumed. The analytical expressions for the free energy of an unconstrained single chain $\psi_f$ and the free energy of the tube constraint $\psi_c$ are developed next.

### 4.2.1 Free energy of an unconstrained single chain

In order to find the free energy of an unconstrained single chain, it is assumed that the single chain is long and far from its fully extended state. Thus, the Gaussian distribution (3.126) as derived in Section 3.3.3 is used,

$$p_f(\mathbf{r}) = \left[\frac{3}{2\pi N a^2}\right]^{\frac{3}{2}} \exp\left\{-\frac{3r^2}{2Na^2}\right\}, \tag{4.8}$$

where $b$ denotes the link length and $N$ the total number of links. The free energy is then found by combining (3.94) and (3.110) as

$$\psi_f(\mathbf{r}) = -kT \ln p(\mathbf{r}). \tag{4.9}$$

Introducing the *micro-kinematic stretch* $\lambda$ defined by

$$\lambda := \frac{r}{r_0}, \qquad r_0 = \sqrt{N}a; \qquad \lambda \in \left[0, \sqrt{N}\right), \tag{4.10}$$

the free energy can be written as

$$\psi_f(\lambda) = \frac{3}{2} kT \lambda^2 + \psi_{f0}, \tag{4.11}$$

where $\psi_{f0}$ is a constant.

### 4.2.2 Free energy due to tube constraint

The free energy of the unconstrained single chain in (4.11) does not consider the fact that the motion of a chain in a network is restricted by neighboring chains. In order to take this type of hindered motion of a chain in a network into account, the single chain is assumed

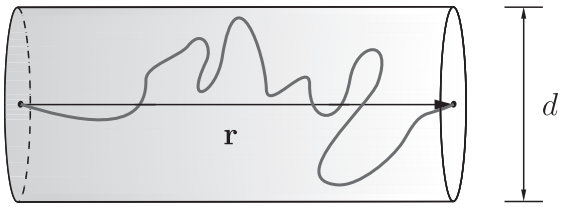


Figure 4.2: Single chain confined to a tube of diameter $d$, with its ends fixed at the center of the tube ends, and an end-to-end vector $\mathbf{r}$.

to be confined to a tube of constant diameter $d$, as depicted in Figure 4.2. Following Miehe et al. (2004), in order to calculate the free energy due to the tube constraint, the probability density is introduced as

$$p_c(\nu) = p_0 \exp\left[-\alpha \left(\frac{r_0}{d_0}\right)^2 \nu\right], \tag{4.12}$$

where $p_0$ is a normalization constant, $\alpha$ is a numerical factor which depends on the tube geometry, and the dimensionless kinematic variable $\nu$ is the micro-kinematic tube area contraction and is defined as

$$\nu := \left(\frac{d_0}{d}\right)^2, \ \nu \in (0, \infty), \tag{4.13}$$

with $d_0$ being the initial diameter of the tube and $d$ the current diameter. By the same token as (4.9), the tube constraint free energy reduces to

$$\psi_c(\nu) = \alpha kTN \left(\frac{a}{d_0}\right)^2 \nu + \psi_{c0}, \tag{4.14}$$

where $\psi_{c0}$ is a constant.

## 4.3 Micro-macro transition

The main idea in the non-affine micro-sphere model is to connect the micro-kinematic variables through an averaging over a unit sphere to macro-kinematic quantities. To this end, the random three-dimensional network microstructure at a material point $P$, that contains many chains between cross-links with end-to-end vectors pointing in every possible direction, is statistically described by a collection of unit end-to-end orientation vectors $\mathbf{M}$ that are uniformly distributed on a unit sphere $S_0$ as shown in Figure 4.3. The unit sphere $S_0$ can be seen as a representative volume element (RVE) containing the distribution of the end-to-end vectors, and the averaging over the distribution can be interpreted as a homogenization of any microscopic network property yielding the macroscopic counterpart.

In this section the polymer network model based on the non-affine micro-sphere model is developed. Given the analytical expressions for the total free energy on the microscale

$$\psi(\lambda, \nu) = \psi_f(\lambda) + \psi_c(\nu), \tag{4.15}$$

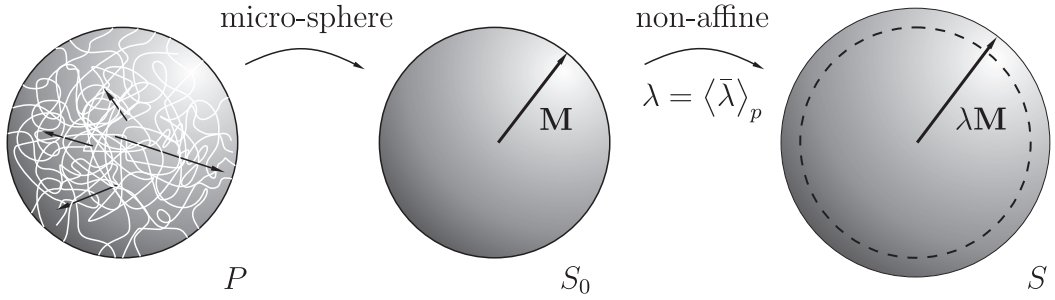


Figure 4.3: The non-affine micro-sphere model: the random network microstructure at a material point $P$ is statistically described by a collection of unit end-to-end orientation vectors $\mathbf{M}$ that are uniformly distributed on a unit sphere $S_0$; the unit sphere $S_0$ is then deformed in a non-affine way according to $\lambda = \langle \bar{\lambda} \rangle_p$; the dashed line in the deformed sphere $S$ represents the undeformed unit sphere $S_0$.

the goal is to find the isochoric contribution to the total macroscopic free energy (4.4). The additive split of the microscopic free energy $\psi$ motivates the following macroscopic split of energy

$$\bar{\Psi}\left(\bar{\mathbf{C}}\right) = \bar{\Psi}_f\left(\bar{\mathbf{C}}\right) + \bar{\Psi}_c\left(\bar{\mathbf{C}}\right). \tag{4.16}$$

To connect the two expressions, a relationship between the micro-kinematic variables $\lambda$ and $\nu$ and macro-kinematic variables like $\bar{\mathbf{C}}$ or $\bar{\mathbf{F}}$ has to be established. In the following two sections the core result of the non-affine micro-sphere model Miehe et al. (2004) is used to link the kinematic variables on the different scales and find the desired macroscopic free energies.

### 4.3.1 Non-affine network model for the unconstrained single chain

Let a macro-stretch $\bar{\lambda}$, induced on the undeformed sphere $S_0$ by $\bar{\mathbf{C}}$ in the direction of a sphere orientation vector $\mathbf{M}$, be defined by

$$\bar{\lambda}(\mathbf{M}) = \sqrt{\mathbf{M} \cdot \bar{\mathbf{C}}\mathbf{M}}, \quad \mathbf{M} \cdot \mathbf{M} = 1. \tag{4.17}$$

In order to find the link between the micro-stretch $\lambda$ of the unconstrained single chain and the macro-stretch $\bar{\lambda}$, allow $\lambda$ to fluctuate around $\bar{\lambda}$ according to

$$\lambda(\mathbf{M}) = \bar{\lambda}(\mathbf{M}) f(\mathbf{M}), \tag{4.18}$$

where $f$ is a stretch-fluctuation field defined on the unit sphere $S_0$. In an affine model the value of $f$ would be unity in all unit sphere directions. However, in the non-affine model, $f$ needs to be determined; this is accomplished by requiring the following constraint to hold

$$\langle \lambda \rangle_p = \langle \bar{\lambda} \rangle_p, \tag{4.19}$$

where $\langle\cdot\rangle_p$ is the $p$-root average over the unit sphere $S_0$

$$\langle\cdot\rangle_p = \left(\frac{1}{|S_0|}\int_{S_0}(\cdot)^p \; dA\right)^{\frac{1}{p}}, \quad |S_0| = 4\pi, \tag{4.20}$$

and $p$ is a model parameter of the micro-macro transition scheme. The macroscopic free energy for an unconstrained single chain is then determined by minimizing its averaged microscopic free energy contribution over the unit sphere $\left\langle n_D\psi_f\left(\bar{\lambda}f\right)\right\rangle$ subject to the constraint (4.19),

$$\bar{\Psi}_f\left(\bar{\mathbf{C}}\right) = \sup_{\kappa}\inf_{f}\left\{\left\langle n_D\psi_f\left(\bar{\lambda}f\right)\right\rangle - \kappa\left(\left\langle\bar{\lambda}f\right\rangle_p - \left\langle\bar{\lambda}\right\rangle_p\right)\right\}, \tag{4.21}$$

where $\langle\cdot\rangle := \langle\cdot\rangle_1$ is an integration over the unit sphere, $\kappa$ a Lagrange multiplier for the constraint (4.19), and $n_D$ is the number of chains in the polymer network per unit volume. The necessary condition for the minimization problem is

$$n_D\frac{\partial\psi_f\left(\bar{\lambda}f\right)}{\partial\lambda} - \kappa\left(\left\langle\bar{\lambda}f\right\rangle_p\right)^{(1-p)}\left(\bar{\lambda}f\right)^{(p-1)} = 0, \tag{4.22}$$

which can be rewritten as

$$\kappa = n_D\frac{\partial\psi_f\left(\bar{\lambda}f\right)}{\partial\lambda}\left(\left\langle\bar{\lambda}f\right\rangle_p\right)^{(p-1)}\left(\bar{\lambda}f\right)^{(1-p)}, \tag{4.23}$$

where $\kappa$ is constant on the sphere. A non-trivial solution can only be derived if $\lambda = \bar{\lambda}f$ is constant. Thus, we find the simple result

$$\lambda = \left\langle\bar{\lambda}\right\rangle_p, \tag{4.24}$$

and the macroscopic free energy contribution from the unconstrained single chain reads

$$\bar{\Psi}_f\left(\bar{\mathbf{C}}\right) = n_D\psi_f\left(\left\langle\bar{\lambda}\right\rangle_p;\omega\right). \tag{4.25}$$

The result in (4.24) states that the micro-stretches in all the unit sphere directions are constant and equal to the p-root average of the macro-stretches as shown in Figure 4.3. Taking a step back in the level of abstraction and looking at a network of chains at a material point $P$, this statement implies that all the different end-to-end vectors of chains between cross-links are stretched by the same amount no matter how the continuum body $\mathcal{B}$ is deformed (compare with Figures 4.1 and 4.3).

### 4.3.2 Non-affine network model for the tube constraint

Let a macro-area stretch $\bar{\nu}$ on the undeformed sphere $S_0$ be defined by

$$\bar{\nu}(\mathbf{N}) = \sqrt{\mathbf{N}\cdot\bar{\mathbf{C}}^{-1}\mathbf{N}}, \quad \mathbf{N}\cdot\mathbf{N} = 1, \tag{4.26}$$

with $\mathbf{N}$ being a unit normal vector to an area element on the undeformed sphere. In order to introduce a non-affine relationship between the micro-tube area contraction $\nu$ as defined in (4.13) and the macro-area stretch $\bar{\nu}$ the power law of Miehe et al. (2004) is used

$$\nu(\mathbf{N}) = (\bar{\nu}(\mathbf{N}))^q \,. \tag{4.27}$$

Since the micro-area stretches actually depend on the different normals of the unit sphere, the macroscopic energy contribution is obtained by integrating all microscopic energy contributions (4.14) over the sphere as,

$$\bar{\Psi}_c\left(\bar{\mathbf{C}}\right) = \left\langle n_D \psi_c\left(\bar{\nu}^q\right)\right\rangle , \tag{4.28}$$

where $q$ is a model parameter.

## 4.4 Macroscopic material response and summary

Now that all the micro- and macro-kinematic measures are connected, and the microscopic energy contributions are averaged over the unit sphere yielding the macroscopic energies, the overall stress response (4.5) can be computed. In this section the derivatives needed for that response are calculated and the model parameters briefly summarized.

### 4.4.1 Derivatives

The non-affine contributions from the unconstrained single chain and the tube constraint can be assembled into the overall isochoric response of the material as follows,

$$\bar{\Psi}\left(\bar{\mathbf{C}}\right) = n_D \psi_f\left(\left\langle\bar{\lambda}\right\rangle_p\right) + \left\langle n_D \psi_c\left(\bar{\nu}^q\right)\right\rangle . \tag{4.29}$$

In order to calculate the second Piola-Kirchhoff stress tensor as given in (4.5), the following derivative is needed,

$$\frac{\partial\bar{\Psi}(\bar{\mathbf{C}})}{\partial\bar{\mathbf{C}}} = \frac{\partial\bar{\Psi}_f(\bar{\mathbf{C}})}{\partial\bar{\mathbf{C}}} + \frac{\partial\bar{\Psi}_c(\bar{\mathbf{C}})}{\partial\bar{\mathbf{C}}}. \tag{4.30}$$

Using the result in (4.24), (4.18), and the chain rule, the contribution from the unconstrained single chain ends up being

$$\left(\frac{\partial\bar{\Psi}_f}{\partial\bar{\mathbf{C}}}\right)_{kl} = \left(\frac{\partial\psi_f}{\partial\lambda}\frac{\partial\lambda}{\partial\bar{\lambda}}\frac{\partial\bar{\lambda}}{\partial\bar{\mathbf{C}}}\right)_{kl} = n_D\frac{\partial\psi_f}{\partial\lambda}\lambda^{1-p}\left\langle\bar{\lambda}^{p-2}M_kM_l\right\rangle , \tag{4.31}$$

and using (4.27) and (4.26), the non-affine tube constraint contribution results in

$$\left(\frac{\partial\bar{\Psi}_c}{\partial\bar{\mathbf{C}}}\right)_{kl} = \left(\frac{\partial\psi_c}{\partial\nu}\frac{\partial\nu}{\partial\bar{\nu}}\frac{\partial\bar{\nu}}{\partial\bar{\mathbf{C}}}\right)_{kl} = -\left\langle n_D\frac{\partial\psi_c}{\partial\nu}q\bar{\nu}^{q-2}\frac{1}{4}\left(C^{-1}_{ik}C^{-1}_{lj} + C^{-1}_{il}C^{-1}_{kj}\right)N_iN_j\right\rangle . \tag{4.32}$$

The only derivatives left to evaluate are $\partial\psi_f/\partial\lambda$ from (4.31) and $\partial\psi_c/\partial\nu$ from (4.32). Using (4.11), the partial derivative reads

$$n_D \frac{\partial \psi_f}{\partial \lambda} = 3\mu\lambda, \qquad \mu := n_D kT, \tag{4.33}$$

where $\mu$, the effective shear modulus is introduced. Using (4.14)

$$n_D \frac{\partial \psi_c}{\partial \nu} = \mu N U, \qquad U := \alpha \left(\frac{a}{d_0}\right)^2, \tag{4.34}$$

where $U$ is the effective tube geometry parameter.

### 4.4.2 Model summary

The non-affine micro-sphere model has a total of *five material parameters*. The material parameters $\mu$, $N$, and $U$ appear in (4.33) and (4.34) and basically define the microscopic response of the constrained polymer chain. The material parameters $p$ and $q$ appear in (4.24) and (4.27) and define the non-affine character of the network model. All the five parameters are summarized in Table 4.1, where also rough descriptions of their phenomenological effects on stress-strain curves are provided.

| # | Parameter | Name | Eq. | Effect |
|---|---|---|---|---|
| 1 | $\mu := n_D kT$ | Shear modulus | (4.33) | Ground state stiffness |
| 2 | $N$ | Number of chain segments | (4.8) | Chain locking response |
| 3 | $p$ | Non-affine stretch parameter | (4.19) | 3D locking characteristic |
| 4 | $U := \alpha\,(a/d_0)^2$ | Tube geometry parameter | (4.34) | Additional constraint stiffness |
| 5 | $q$ | Non-affine tube parameter | (4.27) | Shape of constraint stress |

Table 4.1: Material parameters of the non-affine micro-sphere model.

# Chapter 5

# Micro-Mechanically Based Continuum Model for Strain-Induced Crystallization in Natural Rubber

The three previous chapters describing continuum mechanics, statistical mechanics, and micro-macro mechanics set the stage for this chapter. A fully thermodynamically consistent and micro-mechanically based constitutive law for strain-induced crystallization in natural rubber is developed in three steps. As a first step, a thermodynamically consistent macroscopic framework including evolution of the degree of crystallinity is developed. Secondly, a microscopic model of a partially crystalline chain is derived, and as a last step, the non-affine micro-sphere model is applied to connect the two scales[1].

## 5.1 Macroscopic Setting of Model

In the experimental results shown in Chapter 1, it can be seen that the stress-strain curves for natural rubber form a hysteresis loop and that the measured degree of crystallinity only starts evolving after a certain level of stretch is reached. In order to model this dissipative behavior on a macroscopic scale, the mathematical framework developed for elastic-thermoplastic materials by Casey (1998) is specialized to the case of strain-crystallizing materials.

### 5.1.1 Thermomechanical Development

In the development of this thermodynamically consistent framework, strain-crystallizing materials are conceptually seen as a one-parameter *family* of thermoelastic materials as introduced in Section 2.3. To this end, let $P$ be a point in strain-temperature space defined by the pair $(\mathbf{E}, T)$ of a body $\mathcal{B}$ at material point $X$ and time $t$. $P$ is called a *thermo-elastic*

[1]This chapter follows the ideas the author recently published in Mistry and Govindjee (2014).

*point* if and only if there exists an open set $\mathcal{U}$ containing $P$, such that on $\mathcal{U}$, the constitutive equations (2.77) hold. Moreover, let $\mathcal{E}$ denote the *thermoelastic region* in strain-temperature space defined by the maximal open set $\mathcal{U}$ containing the point $P$. The region $\mathcal{E}$ is assumed to be simply connected and enclosed by a smooth orientable hypersurface $\partial\mathcal{E}$, called the *transformation surface*.

Generally, changing the strain and temperature at $X$ will yield a new thermoelastic region and result in new constitutive equations of type (2.77). It is assumed that this family of thermoelastic materials is parametrized by a scalar variable $\omega$, describing the *degree of crystallinity* in the material as can be measured by experiments (see Chapter 1).

To this end, let the macroscopic response functions for internal energy, stress, and heat flux of the strain-crystallizing material be,

$$\epsilon = \hat{\epsilon}(\mathbf{E},\, T; \omega), \quad \mathbf{S} = \hat{\mathbf{S}}(\mathbf{E},\, T; \omega), \quad \mathbf{q}_0 = \hat{\mathbf{q}}_0(\mathbf{E},\, T,\, \boldsymbol{g}_0; \omega). \tag{5.1}$$

For each fixed value of $\omega$, (5.1) define a unique thermoelastic material, (2.78) will hold, and an inverse of the stress response will exist:

$$\mathbf{E} = \hat{\mathbf{E}}(\mathbf{S},\, T; \omega). \tag{5.2}$$

Moreover, it is assumed that the hypersurface $\partial\mathcal{E}$ at a fixed $\omega$ is determined by means of a *transformation function* $g(\mathbf{E},\, T; \omega)$, as all the points in strain-temperature space that satisfy

$$g(\mathbf{E},\, T; \omega) = 0. \tag{5.3}$$

Points on the transformation surface will be referred to as a strain-crystallizing point. The yield function is chosen such that points inside the thermoelastic region are characterized by $g < 0$. In addition, the quantity

$$\hat{g} = \frac{\partial g}{\mathbf{E}} \cdot \dot{\mathbf{E}} + \frac{\partial g}{\partial T}\dot{T}, \tag{5.4}$$

called a loading indicator, is introduced to define the following loading criteria:

$$\begin{aligned}
&\text{(i)} && g < 0: && \text{thermoelastic point,}\\
&\text{(ii)} && g = 0,\ \hat{g} < 0: && \text{unloading from a strain-crystallizing point,}\\
&\text{(iii)} && g = 0,\ \hat{g} = 0: && \text{neutral loading from a strain-crystallizing point,}\\
&\text{(iv)} && g = 0,\ \hat{g} > 0: && \text{loading from a strain-crystallizing point.}
\end{aligned} \tag{5.5}$$

For the cases (i) to (iii) it assumed that

$$\dot{\omega} = 0. \tag{5.6}$$

In the case of (iv), it is assumed that loading from a strain-crystallizing point leads to strain-crystallizing point, which implies that if

$$g = 0,\ \hat{g} > 0 \quad \Rightarrow \quad \dot{g} = 0 \tag{5.7}$$

also known as the *consistency condition*. In general, it will be assumed that material derivative of $\omega$ will only depend on the variables $(\mathbf{E},\, T; \omega)$, i.e. there is no rate dependency.

In order to get a thermodynamically consistent material response, an entropy function is constructed using the same steps as in Section 2.3 next. To this end, let a homothermal process occur at a fixed $\omega$ for $g \leq 0$ and $\hat{g} \leq 0$. Since in that case (5.6) holds, the full energy balance from Box 2.1 will reduce to (2.80). By invoking "Part I" of the Second Law of Thermodynamics (2.81), a family of thermoelastic entropy functions parametrized by $\omega$ can be written as

$$S = \hat{S}(\mathbf{E},\, T; \omega), \tag{5.8}$$

where the arbitrary integration constants for each thermoelastic material are assumed to be zero. Also, note that for homothermal processes at fixed $\omega$, (2.82) holds. This allows the definition of a Helmholtz free energy

$$\psi = \hat{\psi}(\mathbf{E},\, T; \omega) = \epsilon - ST \tag{5.9}$$

as in (2.83). Thus, since (2.84), (2.85), (2.86), and (2.87) all hold for homothermal processes at fixed $\omega$, it can be concluded that

$$S = \hat{S}(\mathbf{E},\, T; \omega) = -\frac{\partial \hat{\psi}}{\partial T}(\mathbf{E},\, T; \omega), \tag{5.10}$$

and

$$\mathbf{S} = \hat{\mathbf{S}}(\mathbf{E},\, T; \omega) = \rho_0 \frac{\partial \hat{\psi}}{\partial \mathbf{E}}(\mathbf{E},\, T; \omega), \tag{5.11}$$

at fixed $\omega$. The relations (5.10) and (5.11) hold for all thermoelastic processes at fixed $\omega$ since there is no dependency on $\boldsymbol{g}_0$. Moreover they also hold when $\omega$ is changing, because both functions are independent of $\dot{\omega}$. Thus, (5.10) and (5.11) constitute an extension of the Gibbs relations to strain-crystallizing materials.

As a last step, consider an arbitrary strain-crystallizing process. Combining the definition of the Helmholtz free energy function (5.9) with the balance of energy in Box 2.1 yields

$$\rho_0 \left\{ \dot{S}T + S\dot{T} + \frac{\partial \hat{\psi}}{\mathbf{E}} \cdot \dot{\mathbf{E}} + \frac{\partial \hat{\psi}}{\partial T}\dot{T} + \frac{\partial \hat{\psi}}{\partial \omega}\,\dot{\omega} \right\} = \rho_0 r - \operatorname{Div} \mathbf{q}_0 + \mathbf{S} \cdot \dot{\mathbf{E}}. \tag{5.12}$$

By using (5.10) and (5.11), it can be reduced to

$$\rho_0 \dot{S} T = \rho_0 r - \operatorname{Div} \mathbf{q}_0 - \rho_0 \,\frac{\partial \hat{\psi}}{\partial \omega}\,\dot{\omega}. \tag{5.13}$$

Note that when loading is not occurring (i.e. $\dot{\omega} = 0$), (5.13) reduces to (2.88). Assuming now that the Clausius-Duhem inequality (2.89) holds for strain-crystallizing materials, by virtue of (5.13) it will follow that

$$-\rho_0 \,\frac{\partial \hat{\psi}}{\partial \omega}\,\dot{\omega} - \frac{\mathbf{q}_0 \cdot \boldsymbol{g}_0}{T} \geq 0. \tag{5.14}$$

If a homothermal strain-crystallizing process is taken, the inequality above will read

$$\rho_0 \frac{\partial \hat{\psi}}{\partial \omega} \dot{\omega} \leq 0. \tag{5.15}$$

Since none of the terms in (5.15) depend on the temperature gradient, nor on $\dot{\mathbf{E}}$ or $\dot{T}$, the inequality holds for all processes and loading conditions.

As noted before, (5.13) boils down to (2.88) for thermoelastic processes in strain-crystallizing materials, and (2.89) leads to (2.90), which will then hold for a fixed $\omega$. Finally, since none of the quantities in (2.90) depend on $\dot{\mathbf{E}}$ or $\dot{T}$, it will hold for a changing $\omega$ as well.

### 5.1.2 Crystallization Kinetics in Polymers

The goal of *crystallization kinetics* is to find constitutive functions for $\dot{\omega}$ and $g$, which together describe *the time evolution* of the *degree of crystallinity* in the material on a macroscale (as seen in Figure 1.1).

On the microscale, there are two mechanisms that drive the evolution of the degree of crystallinity in natural rubber. The first mechanism assumes that there are a fixed amount of nuclei in the amorphous polymer and the increase in crystallinity stems from crystal growth, which is supported by Chenal et al. (2007). The second mechanism assumes the size of the crystallites to be more or less constant, but suggests a growth in crystallinity through formation of nuclei, which is supported by Murakami et al. (2002). Since the research on this topic as to which mechanism is driving the crystallinity is not conclusive, the first mechanism will be considered for the purpose of the modeling task at hand.

In (Roe and Krigbaum, 1965), the first mechanism of growing crystals is treated by considering a partially crystallized polymer chain from a statistical mechanics point of view. The theory proposes that the driving force for the crystallization comes from the change in free energy of the system that accompanies the increase of the degree of crystallinity, or the free energy gradient.

This idea of a chemical potential on the microscopic scale is applied to the macroscopic framework by assuming that the evolution of the degree of crystallinity $\omega$ is governed by the macroscopic Helmholtz free energy function (5.9) as

$$\dot{\omega} = -A \frac{\partial \hat{\psi}}{\partial \omega}, \quad A \geq 0, \tag{5.16}$$

where the condition $A \geq 0$ follows immediately from (5.15). The degree of crystallinity however, can only evolve once a certain chemical potential threshold is reached. In order to incorporate this into the model, a chemical potential "threshold function" of the form

$$g = \left| \frac{\partial \hat{\psi}}{\partial \omega} \right| - (g_c + \gamma \omega) \leq 0, \tag{5.17}$$

is introduced, where $g_c \geq 0$ denoting a critical chemical potential value (threshold at zero degree of crystallinity) and $\gamma$ a threshold evolution parameter (hardening/softening) are material constants. With these two constitutive equations defined, the only thing left to do is to specify the Helmholtz free energy function (5.9). The idea here is again to base that energy on a micro-mechanical model and average it using the micro-sphere model as introduced in Chapter 4. Before continuing with the micro-mechanical setting of the model, the key macroscopic equations are briefly summarized next.

### 5.1.3 Summary

In order to differentiate between microscopic and macroscopic free energies, boldface letters are used for the latter. Moreover, since isothermal condition are assumed, the dependency of the functional relationships on $T$ will be dropped. Then, by virtue of (5.9), let the model assume a Helmholtz free energy function *per unit volume* that depends on the right Cauchy-Green deformation tensor $\mathbf{C}$ and a measure of the degree of crystallinity $\omega$

$$\Psi = \Psi\left(\mathbf{C}; \omega\right). \tag{5.18}$$

Following the argument as outlined in Section 5.1.1 leading to (5.11), the second Piola-Kirchhoff is given by

$$\mathbf{S} = 2\frac{\partial \Psi(\mathbf{C}; \omega)}{\partial \mathbf{C}}. \tag{5.19}$$

A decoupling of the free energy function (5.18) into volumetric and isochoric parts is introduced based on the same reasoning as for the split in (4.4),

$$\Psi = \Psi_{\text{vol}}(J) + \bar{\Psi}\left(\bar{\mathbf{C}}; \omega\right), \tag{5.20}$$

and leads to an analogous result as in (4.5)

$$\mathbf{S} = J\Psi'_{\text{vol}}(J)\mathbf{C}^{-1} + J^{-2/3}\left(\mathbb{I} - \frac{1}{3}\mathbf{C}^{-1} \otimes \mathbf{C}\right) : 2\frac{\partial \bar{\Psi}(\bar{\mathbf{C}}; \omega)}{\partial \bar{\mathbf{C}}}. \tag{5.21}$$

The evolution of the degree of crystallinity is chosen to be governed by the macroscopic free energy function by setting the rate of the degree of crystallinity to

$$\dot{\omega} = -A\frac{\partial \Psi\left(\mathbf{C}; \omega\right)}{\partial \omega}, \quad A \geq 0, \tag{5.22}$$

where the free energy gradient acts as a driving force for the crystallinity as discussed in Section 5.1.2. In addition, a chemical potential threshold acting as a yield function of the form

$$g = \left|\frac{\partial \Psi\left(\mathbf{C}; \omega\right)}{\partial \omega}\right| - (g_c + \gamma\omega), \tag{5.23}$$

is used to model the crystallization kinetics, with $g_c \geq 0$ and $\gamma$ being material parameters as already described. The associated loading and unloading conditions from (5.5) can then be summarized in the form of Kuhn-Tucker conditions as

$$A \geq 0, \quad g \leq 0, \quad Ag = 0. \tag{5.24}$$

These conditions mean that when the material is crystallizing $A > 0$, $g = 0$ has to hold, and on the other hand when $g < 0$, no crystallization can take place since $A = 0$ has to hold. Moreover, the consistency condition in (5.7) states that when the material is crystallizing,

$$\dot{g} = 0, \quad \text{for} \quad A > 0, \tag{5.25}$$

has to hold, meaning that loading from strain-crystallizing point will lead to another strain-crystallizing point.

Since the volumetric response $\Psi_{\text{vol}}(J)$ can be any scalar function satisfying the conditions noted in the paragraph immediately following (4.5), only the isochoric response of the material, $\bar{\Psi}\left(\bar{\mathbf{C}}; \omega\right)$ is left to be determined. In the next two sections, this isochoric response is developed by first considering a micro-mechanical model of a partially crystalline chain and then bridging scales using the non-affine micro-sphere model.

## 5.2 Micro-mechanical setting of model

In order to develop an expression for the total free energy $\psi$ on the micro-mechanical scale that incorporates crystallization of polymer chains, two contributions are taken into account following the example in Section 4.2. The first contribution will be from the tube constraint dealing with the hindered motion of a polymer chain in a network as introduced in Section 4.2.2. However, for the second contribution, the classical statistical mechanical treatment of polymers (see Section 3.3) will have to be slightly modified. Instead of a fully amorphous polymer chain, an unconstrained semi-crystalline polymer chain will be considered. To this end, an additive split of the total free energy $\psi$ into a contribution due to the unconstrained partially crystallized single chain $\psi_f$, and the contribution due to the tube constraint $\psi_c$ as given in (4.14),

$$\psi = \psi_f + \psi_c, \tag{5.26}$$

is assumed. In the following subsection an analytical expressions for the free energy of an unconstrained partially crystallized single chain $\psi_f$ is developed.

### 5.2.1 Free energy of an unconstrained partially crystallized single chain

In order to set up the *free energy of an unconstrained partially crystallized single chain* $\psi_f$, an approach by Smith (1976) can be adapted. Crystallization is assumed to happen as depicted in Figure 5.1, where the chain has a rigid extended crystal part, two amorphous

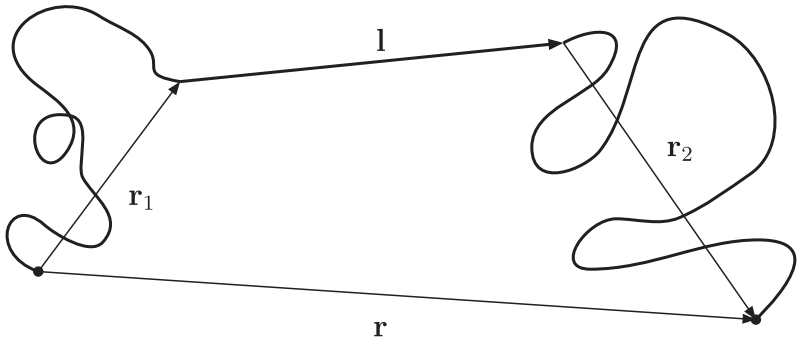


Figure 5.1: Schematic of a partially crystallized chain between two cross-links with end-to-end vectors of the two amorphous subchains $\mathbf{r}_1$, $\mathbf{r}_2$, the crystal vector $\mathbf{l}$, and the chain end-to-end vector $\mathbf{r}$.

subparts, and is composed of $N$ links each of length $a$. The amorphous subchains $\mathbf{r}_1$ and $\mathbf{r}_2$ consist of $N_1$ and $N_2$ links, and the crystallized part of the chain contains $n$ links, such that $|\mathbf{l}| = na$ and $N_1 + N_2 = N - n$. Since the crystal within the chain is assumed to be rigid, the free energy only consists of two contributions: a pure thermodynamic part and an elastic part

$$\psi_f := -\Delta H_u \left(1 - \frac{T}{T_m^0}\right) N\omega + \Delta F_e, \tag{5.27}$$

where $\Delta H_u$ is the heat of fusion per link, $T_m^0$ is the crystallization temperature, $\Delta F_e$ is the elastic contribution, and the parameter $\omega$ is the microscopic degree of crystallinity defined as

$$\omega := \frac{n}{N}, \qquad \omega \in [0, 1]\,. \tag{5.28}$$

Note that $\Delta H_u$ represents, in the spirit of Flory (1947), the total (internal) energy to bring a link into the crystal. This includes both the traditional energy of fusion as well as amorphous-crystalline interface energies (which are expected to be small). The heat of fusion is an admittedly crude modeling device and properly should be viewed as an effective material parameter.

In order to calculate $\Delta F_e$, the overall probability density $p_f$ of the conformation in Figure 5.1 is calculated as the product of the two probability densities $p_1$ and $p_2$ of the amorphous subchains

$$p_f\left(\mathbf{r}_1, \mathbf{r}_2\right) := p_1\left(\mathbf{r}_1\right) p_2\left(\mathbf{r}_2\right). \tag{5.29}$$

Using the kinematic relation $\mathbf{r}_2 = (\mathbf{r} - \mathbf{l}) - \mathbf{r}_1$, $\mathbf{r}_2$ is eliminated from $p_f(\mathbf{r}_1, \mathbf{r}_2)$, resulting in

$$\hat{p}_f\left(\mathbf{r}_1, \mathbf{r}\right) := p_f\left(\mathbf{r}_1, (\mathbf{r} - \mathbf{l}) - \mathbf{r}_1\right). \tag{5.30}$$

Since $\mathbf{r}_1$ is unknown, it is eliminated by integrating $\hat{p}_f(\mathbf{r}_1, \mathbf{r})$ over all possible values of $\mathbf{r}_1$ for fixed $\mathbf{r}$ and $\mathbf{l}$. Thus, we get

$$\tilde{p}_f(\mathbf{r}) := \int_{\mathbb{R}^3} \hat{p}_f(\mathbf{r}_1, \mathbf{r})\, d\mathbf{r}_1. \tag{5.31}$$

Here, $\tilde{p}_f$ is the probability density of the conformation in Figure 5.1, irrespective of the values of $\mathbf{r}_1$ and $\mathbf{r}_2$ in (5.29). Both, the Gaussian (3.126) and the non-Gaussian (3.128) probability densities are considered in what follows. For the *Gaussian model*, where the probability densities for the amorphous subchains $p_1$ and $p_2$ are Gaussian, a straightforward calculation leads to

$$\tilde{p}_f(\mathbf{r}) = \left(\frac{3}{2Na^2\pi(1-\omega)}\right)^{3/2} \exp\left[-\frac{3(\mathbf{r}-\mathbf{l})^2}{2Na^2(1-\omega)}\right]. \tag{5.32}$$

Assuming that the crystal $\mathbf{l}$ has the same direction as $\mathbf{r}$, the probability density can be rewritten as

$$\bar{p}_f(\lambda;\omega) = \left(\frac{3}{2Na^2\pi(1-\omega)}\right)^{3/2} \exp\left[-\frac{3\left(\lambda-\sqrt{N}\omega\right)^2}{2(1-\omega)}\right], \tag{5.33}$$

where the micro-kinematic stretch $\lambda$ is defined as

$$\lambda := \frac{r}{r_0}, \qquad r_0 = \sqrt{N}a; \qquad \lambda \in \left[0, \sqrt{N}\right). \tag{5.34}$$

Thus, combining (4.9) and (5.33), the elastic contribution reads

$$\Delta F_e = -kT \ln\left(\bar{p}_f(\lambda;\omega)\right), \tag{5.35}$$

and the free energy of an unconstrained partially crystallized chain (5.27) has the form

$$\psi_f(\lambda;\omega) := -\Delta H_u\left(1-\frac{T}{T_m^0}\right)N\omega - \frac{3kT}{2}\left[\ln\left(\frac{3}{2Na^2\pi(1-\omega)}\right) - \frac{\left(\lambda-\sqrt{N}\omega\right)^2}{(1-\omega)}\right]. \tag{5.36}$$

The derivation of the results for the *Non-Gaussian model*, where the probability density for the amorphous subchains is non-Gaussian (3.128), is more involved and the expression for $\bar{p}_f$ can be found in the Appendix A.1.

**Remark 5.1.** *The probability density in (5.33) is invariant with respect to changes in position of the extended chain crystal within the single chain. This translational invariance implies that the partially crystallized chain model in Figure 5.1 is equivalent to a single chain consisting of a crystalline part and only one amorphous part.*

**Remark 5.2.** *It should be noted that no straining of the crystal is permitted in the model. In natural rubber, our system of interest, crystallinity is rarely greater than 20%. Thus the crystals, which are substantially stiffer than the surrounding amorphous material, experience low (relative) loads and store little strain energy as the bulk of the motion is accommodated by the softer surrounding material.*

## 5.3 Micro-macro transition

Given the analytical expressions for the total free energy on the microscale from (4.14) and (5.36) as

$$\psi\left(\lambda,\nu;\omega\right)=\psi_f\left(\lambda;\omega\right)+\psi_c\left(\nu\right), \tag{5.37}$$

the isochoric contribution to the total macroscopic free energy (5.20) is calculated next. The additive split of the microscopic free energy $\psi$ motivates the following macroscopic split energy

$$\bar{\Psi}\left(\bar{\mathbf{C}};\omega\right)=\bar{\Psi}_f\left(\bar{\mathbf{C}};\omega\right)+\bar{\Psi}_c\left(\bar{\mathbf{C}}\right). \tag{5.38}$$

To connect the two expressions, a relationship between the micro-kinematic variables $\lambda$ and $\nu$ and macro-kinematic variables like $\bar{\mathbf{C}}$ or $\bar{\mathbf{F}}$ has to be established. In order to bridge these scales, the idea of the non-affine micro-sphere model as outlined in Section 4.3 is applied to a partially crystallized chain. It is important to note here that the variable $\omega$ is assumed to be a measure of the degree of crystallinity on the microscale as well as on the macroscale, and thus an identity map for its micro-macro transition is assumed (see Section 5.3.2 for a remark on this strong assumption of isotropy). In the following subsection a non-affine network model for the unconstrained partially crystallized chain is developed. The macroscopic contribution of the non-affine network model for the tube constraint stays identical to (4.28), with the non-affine relationship (4.27).

### 5.3.1 Non-affine network model for the unconstrained partially crystallized chain

In Section 4.3.1 the non-affine relation between microscopic stretches $\lambda$ and macroscopic stretches $\bar{\lambda}$ is determined by applying the principle of minimal free energy to the undeformed micro-sphere $S_0$ as shown in Figure 4.3. The same approach is chosen for the unconstrained partially crystallized chain. To this end, let the micro-stretches $\lambda$ vary depending on the unit sphere direction $\mathbf{M}$ according to

$$\lambda(\mathbf{M})=\bar{\lambda}(\mathbf{M})f(\mathbf{M}), \tag{5.39}$$

where $f$ is a stretch-fluctuation field that will be determined by the free energy minimization. However, it is assumed that the $p$-root average (4.20) over $S_0$ of the micro stretches and the macro-stretches are the same, which adds the following constraint to the minimization ahead:

$$\left\langle\lambda\right\rangle_p=\left\langle\bar{\lambda}\right\rangle_p, \tag{5.40}$$

where $p$ is a model parameter. The macroscopic free energy and the fluctuation field $f$ for an unconstrained partially crystallized material are then determined by the minimization

$$\bar{\Psi}_f\left(\bar{\mathbf{C}};\omega\right)=\sup_{\kappa}\inf_{f}\left\{\left\langle n_D\psi_f\left(\bar{\lambda}f;\omega\right)\right\rangle-\kappa\left(\left\langle\bar{\lambda}f\right\rangle_p-\left\langle\bar{\lambda}\right\rangle_p\right)\right\}, \tag{5.41}$$

where $\langle\cdot\rangle := \langle\cdot\rangle_1$ is an integration over the unit sphere, $\kappa$ a Lagrange multiplier for the constraint (5.40), and $n_D$ is the number of chains in the polymer network per unit volume. The necessary condition for the minimization problem is

$$n_D \frac{\partial \psi_f\left(\bar{\lambda} f;\omega\right)}{\partial \lambda} - \kappa \left(\left\langle \bar{\lambda} f \right\rangle_p\right)^{(1-p)} \left(\bar{\lambda} f\right)^{(p-1)} = 0, \tag{5.42}$$

which can be rewritten as

$$\kappa = n_D \frac{\partial \psi_f\left(\bar{\lambda} f;\omega\right)}{\partial \lambda} \left(\left\langle \bar{\lambda} f \right\rangle_p\right)^{(p-1)} \left(\bar{\lambda} f\right)^{(1-p)}, \tag{5.43}$$

where $\kappa$ is constant on the sphere. Since $\omega$ is also assumed to be constant on the unit sphere, a non-trivial solution can only be derived if $\lambda = \bar{\lambda} f$ is constant. Thus, we find that the same simple result as in (4.24)

$$\lambda = \left\langle \bar{\lambda} \right\rangle_p, \tag{5.44}$$

still holds and that the macroscopic free energy contribution from the unconstrained partially crystallized chain reads

$$\bar{\Psi}_f\left(\bar{\mathbf{C}};\omega\right) = n_D \psi_f\left(\left\langle \bar{\lambda} \right\rangle_p;\omega\right). \tag{5.45}$$

Given the macroscopic free energies (4.28) and (5.45), the stress response for SIC in natural rubber (5.21), the chemical potential threshold (5.23), and the rate of the degree of crystallinity (5.22) can be calculated by evaluating the necessary derivatives.

**Remark 5.3.** *It should be noted that the modeling framework that has been laid out is restricted to modest degrees of crystallinity – a situation seen in natural rubber where the maximum expected degree of crystallinity is around 20%. At higher values, say approaching 100%, one would expect the material to behave more in line with the Cauchy-Born rule (CBR); see e.g. Ericksen (2008) for a recent commentary on this rule. In a general CBR motion the lattice moves affinely coupled with a non-affine basis (atom) relaxation (Weiner, 1983, §4.3). The micro-sphere model incorporates a relaxation but lacks a mechanism (beyond the averaging constraint) for inter-chain interactions which would allow for the "natural" appearance of CBR-like behavior. Thus the use of the micro-sphere framework for a strain crystallizing model is restricted to materials such as natural rubber that do not exhibit large degrees of crystallization.*

### 5.3.2 The Isotropic Assumption

The model presented in this chapter for SIC in natural rubber is isotropic and this warrants further discussion. When natural rubber crystallizes it forms monoclinic crystals (Bunn, 1942a,b; Toki et al., 2003) and these are principally aligned with the loading axis (Flory, 1947; Toki et al., 2003; Guilie et al., 2013). There is clearly an *induced* anisotropy on the microscale. Since the micro-sphere framework allows one to consider independent directions it would appear that an anisotropic micro-sphere model would be possible. However,

central to the micro-sphere framework is the relaxation in (5.41). This relaxation differentiates the micro-sphere model from the earlier efforts of, say, Treloar and Riding (1979) and Wu and van der Giessen (1993) in which affine assumptions were invoked (i.e. no relaxation) and it is what gives the micro-sphere framework its *superior* modeling capabilities. The addition of anisotropy with relaxation is non-trivial and works dealing with anisotropy and the micro-sphere model invariably assume an affine motion; see e.g. Göktepe and Miehe (2005) or Menzel and Waffenschmidt (2009). In the limiting case of $\omega = 0$, the affine model is known to give a poor result; relaxation is required. The primary question is what is the appropriate variational principle to impose on the micro-sphere model during anisotropic evolution of the microstructure. With an eye towards phase transformations and plastic flow some variational principles have been developed; see e.g. Mielke (2004) and Mielke and Ortiz (2008). Unfortunately, the mathematical structure of these developments is not directly compatible with the micro-sphere framework which lacks a gradient constraint on microstructural state. Kroon (2010) in his strain crystallization model does provide one mechanism for an anisotropic relaxation but it relies on the addition of an *ad hoc* term to the micro-sphere energy. For these reasons, an isotropic model is chosen and the final result is viewed as a single (isotropic) order parameter model which provides a spatially averaged measure of the true state of the material.

## 5.4 Macroscopic material response and summary

In this section the derivatives needed for the macroscopic stress-strain response are calculated and evaluated for the case of the partially crystallized single chain having a Gaussian probability density (3.126). The results for the non-Gaussian case are not mentioned here but will be considered in the next chapter to assess the modeling capacity of the proposed model.

### 5.4.1 Derivatives

At this point, the contribution from the partially crystallized chain and the contribution from the non-affine tube constraint can be assembled into the overall isochoric response of the material

$$\bar{\Psi}\left(\bar{\mathbf{C}};\omega\right) = n_D\psi_f\left(\left\langle\bar{\lambda}\right\rangle_p;\omega\right) + \left\langle n_D\psi_c\left(\bar{\nu}^q\right)\right\rangle. \tag{5.46}$$

In order to calculate the second Piola-Kirchhoff stress tensor as given in (5.21), the following derivative is needed,

$$\frac{\partial\bar{\Psi}(\bar{\mathbf{C}};\omega)}{\partial\bar{\mathbf{C}}} = \frac{\partial\bar{\Psi}_f(\bar{\mathbf{C}};\omega)}{\partial\bar{\mathbf{C}}} + \frac{\partial\bar{\Psi}_c(\bar{\mathbf{C}})}{\partial\bar{\mathbf{C}}}. \tag{5.47}$$

It is important to note that the derivative is taken with respect to $\bar{\mathbf{C}}$ at a *constant degree of crystallinity* $\omega$. Thus, using the result in (5.44), the contribution from the partially

crystallized chain ends up being

$$\left(\frac{\partial\bar{\Psi}_f}{\partial\bar{\mathbf{C}}}\right)_{kl} = \left(\frac{\partial\psi_f}{\partial\lambda}\frac{\partial\lambda}{\partial\bar{\lambda}}\frac{\partial\bar{\lambda}}{\partial\bar{\mathbf{C}}}\right)_{kl} = \frac{1}{2}n_D\frac{\partial\psi_f}{\partial\lambda}\lambda^{1-p}\left\langle\bar{\lambda}^{p-2}M_kM_l\right\rangle, \tag{5.48}$$

and using (4.27), the non-affine tube constraint contribution results in

$$\left(\frac{\partial\bar{\Psi}_c}{\partial\bar{\mathbf{C}}}\right)_{kl} = \left(\frac{\partial\psi_c}{\partial\nu}\frac{\partial\nu}{\partial\bar{\nu}}\frac{\partial\bar{\nu}}{\partial\bar{\mathbf{C}}}\right)_{kl} = -\left\langle n_D\frac{\partial\psi_c}{\partial\nu}q\bar{\nu}^{q-2}\frac{1}{4}\left(C^{-1}_{ik}C^{-1}_{lj}+C^{-1}_{il}C^{-1}_{kj}\right)N_iN_j\right\rangle. \tag{5.49}$$

The only derivatives left to evaluate are $\partial\psi_f/\partial\lambda$ from (5.48), $\partial\psi_c/\partial\nu$ from (5.49), and $\partial\Psi/\partial\omega$ from (5.22) for the evolution of the internal variable $\omega$. For the simple case of the Gaussian probability density (3.126) the derivatives are listed next. The derivatives for the *Non-Gaussian model* with the probability density (3.128) can be calculated using the expression for $\bar{p}_f$ given in APPENDIX A.1. Using (5.36), the partial derivative reads

$$n_D\frac{\partial\psi_f}{\partial\lambda} = \frac{3\mu}{1-\omega}\left(\lambda-\sqrt{N}\omega\right), \qquad \mu := n_DkT, \tag{5.50}$$

where $\mu$, the effective shear modulus is introduced. Using (4.14)

$$n_D\frac{\partial\psi_c}{\partial\nu} = \mu NU, \qquad U := \alpha\left(\frac{a}{d_0}\right)^2, \tag{5.51}$$

where $U$ is the effective tube geometry parameter. The gradient in (5.22) is calculated using (5.20), and (5.46):

$$\begin{aligned}\frac{\partial\Psi(\bar{\mathbf{C}};\omega)}{\partial\omega} &= n_D\frac{\partial\psi_f\left(\left\langle\bar{\lambda}\right\rangle_p;\omega\right)}{\partial\omega}\\ &= -\mu_DN\left(1-\frac{T}{T_m^0}\right)-\frac{3\mu}{2}\left[\frac{1}{1-\omega}+\frac{2\sqrt{N}(\lambda-\omega\sqrt{N})}{1-\omega}\right.\\ &\left.-\frac{(\lambda-\omega\sqrt{N})^2}{(1-\omega)^2}\right]_{\lambda=\left\langle\bar{\lambda}\right\rangle_p},\end{aligned} \tag{5.52}$$

where $\mu_D := n_D\Delta H_u$ is the effective heat of fusion.

### 5.4.2 Model summary

The proposed model has a total of *eight material parameters*, summarized in Table 5.1, in addition to the ambient temperature $T$ and the crystallization temperature $T_m^0$, which are both used in (5.52). Five of the parameters are associated with the non-affine micro-sphere model and three additional parameters are introduced for the crystallization kinetics: $\mu_D$ is the heat of fusion (per unit volume); $g_C$ is the critical threshold value the driving force

| # | Parameter | Name | Eq. | Effect |
|---|---|---|---|---|
| 1 | $\mu := n_D kT$ | Shear modulus | (5.50) | Ground state stiffness |
| 2 | $N$ | Number of chain segments | (3.126) | Chain locking response |
| 3 | $p$ | Non-affine stretch parameter | (5.40) | 3D locking characteristic |
| 4 | $U := \alpha \left(a/d_0\right)^2$ | Tube geometry parameter | (5.51) | Additional constraint stiffness |
| 5 | $q$ | Non-affine tube parameter | (4.27) | Shape of constraint stress |
| 6 | $\mu_D := n_D \Delta H_u$ | Heat of fusion | (5.52) | Heat of fusion |
| 7 | $g_C$ | Critical chemical potential | (5.22) | Threshold at $\omega = 0$ |
| 8 | $\gamma$ | Threshold evolution parameter | (5.22) | Softening/ hardening |

Table 5.1: Material parameters of the proposed model.

$|\partial\Psi/\partial\omega|$ has to reach before the crystallization process can start; $\gamma$ is a hardening/softening parameter, meaning that if $\gamma > 0$, the driving force threshold increases as the degree of crystallinity goes up. On the other hand if $\gamma < 0$, the driving force threshold decreases as the degree of crystallinity goes up, which in turn means that once the crystallization process has started, it becomes progressively easier for the crystallization to continue.

# Chapter 6

# Assessment of Modeling Capacity

While the previous chapter sets up a thermodynamically consistent multiscale model for SIC in NR, this chapter lays out a computationally accessible algorithmic setting of the model, assesses its predictive performance by using published data, and emphasizes the physical meaning of the model parameters[1].

## 6.1 Return mapping algorithm

In this section the algorithmic setting of the proposed constitutive model for strain-induced crystallization is explained. The goal of the numerical implementation is to be able to calculate the evolution of the stress tensor and the degree of crystallinity for a given deformation cycle.

As a first step of the algorithm a trial stress tensor (5.21) is calculated assuming no evolution of crystallinity. In order to do so, the averaging integrals over the unit sphere in (5.48) and (5.49) have to be evaluated. This is done using a 21-point integration scheme as derived in Bazant and Oh (1986). A very thorough and easy-to-follow description of the algorithm using the 21-point integration scheme is provided in Miehe et al. (2004), where the unit sphere $S_0$ is discretized by $m = 21$ orientation vectors $\{\mathbf{r}^i = r_1^i\mathbf{e}_1 + r_2^i\mathbf{e}_2 + r_3^i\mathbf{e}_3\}_{i=1\ldots m}$ and weight factors $\{w^i\}_{i=1\ldots m}$. The spherical averaging (integration) of a microscopic quantity $v$ on the unit sphere is then written as a discrete sum

$$\langle v \rangle = \frac{1}{S_0}\int_{S_0} v(A)\, dA \approx \sum_{i=1}^{m} v^i w^i, \tag{6.1}$$

where $\{v^i\}_{i=1\ldots m}$ represent the microscopic variable $v$ evaluated at points $A^i$ on the unit sphere corresponding to the orientation vector $\mathbf{r}^i$. The integration points and the associated weights are summarized in Table 6.2.

[1]Results in this chapter are reprinted with permission from Mistry and Govindjee (2014)

| | |
|---|---|
| 1. | Given the deformation $\mathbf{C}_{n+1}$, compute the trial state (no evolution of crystallinity): $\omega_{n+1}^{trial} = \omega_n$, $g_{n+1}^{trial} = g(\mathbf{C}_{n+1}, \omega_n)$, $\mathbf{S}_{n+1}^{trial} = \mathbf{S}(\mathbf{C}_{n+1}, \omega_n)$. |
| 2. | Check consistency of crystallization step: if $g_{n+1}^{trial} \leq 0$, then $(\,\cdot\,)_{n+1} := (\,\cdot\,)_{n+1}^{trial}$ & EXIT |
| 3. | else $g_{n+1}^{trial} > 0$, set $g_{n+1} = \left\lvert \frac{\partial \Psi(\langle \bar{\lambda} \rangle_p, \omega_{n+1})}{\partial \omega} \right\rvert - (g_C + \gamma \omega_{n+1}) = 0$, and solve for $\omega_{n+1}$ using a Newton-Raphson scheme, where a Backward-Euler scheme is used to integrate the evolution equation: $\omega_{n+1} = \omega_n - A(t_{n+1} - t_n)(\partial \Psi(\langle \bar{\lambda} \rangle_p, \omega_{n+1})/\partial \omega)$. |
| 4. | Calculate the new $\mathbf{S}_{n+1}$ using the updated $\omega_{n+1}$ |

Table 6.1: Implementation of the return mapping algorithm for strain-induced crystallization.

Once the trial stress tensor $\mathbf{S}_{n+1}^{trial}$ has been computed, a return mapping algorithm is proposed in order to determine the evolution of the degree of crystallinity and to correct the stress computation. The idea is to start with the trial state where the evolution of the degree of crystallinity is frozen, that is $\omega_{n+1}^{trial}$ is assumed to be the same as the previous one $\omega_n$. Next $g_{n+1}^{trial}$ is evaluated using $\omega_{n+1}^{trial}$ and the actual $\mathbf{C}_{n+1}$ as summarized in step 1 of Table 6.1. Since the trial state may or may not be a physically admissible state, the value of the threshold function $g_{n+1}^{trial}$ is checked for consistency. If $g_{n+1}^{trial} \leq 0$, then no evolution of the degree of crystallinity is allowed and the trial state indeed is a physically admissible state. However if $g_{n+1}^{trial} > 0$, the trial step cannot be a solution, and there has to be an evolution of the degree of crystallinity. By numerically solving the equation $g(\mathbf{C}_{n+1}, \omega_{n+1}) = 0$ for $\omega_{n+1}$, an admissible degree of crystallinity $\omega_{n+1}$ and an updated $\mathbf{S}(\mathbf{C}_{n+1}, \omega_{n+1})$ can be computed.

## 6.2 Numerical results and discussion

This section uses published X-ray diffraction measurements carried out by Toki et al. (2003) to test the proposed model. Moreover the proposed model is compared to the recent model of Kroon (2010) and the differences between them are discussed.

### 6.2.1 Model compared to experiments

In the experiments of Toki et al. (2003), strain-induced crystallization is measured using in situ synchrotron wide-angle X-ray diffraction on sulfur (NR-S) and peroxide (NR-P) cured natural rubber as well as sulfur vulcanized synthetic polyisoprene rubber (IR-S). The exper-

| # | $r_1^i$ | $r_2^i$ | $r_3^i$ | $w^i/2$ |
|---|---|---|---|---|
| 1 | 0.0 | 0.0 | 1.0 | 0.0265214244093 |
| 2 | 0.0 | 1.0 | 0.0 | 0.0265214244093 |
| 3 | 1.0 | 0.0 | 0.0 | 0.0265214244093 |
| 4 | 0.0 | 0.707106781187 | 0.707106781187 | 0.0199301476312 |
| 5 | 0.0 | -0.707106781187 | 0.707106781187 | 0.0199301476312 |
| 6 | 0.707106781187 | 0.0 | 0.707106781187 | 0.0199301476312 |
| 7 | -0.707106781187 | 0.0 | 0.707106781187 | 0.0199301476312 |
| 8 | 0.707106781187 | 0.707106781187 | 0.0 | 0.0199301476312 |
| 9 | -0.707106781187 | 0.707106781187 | 0.0 | 0.0199301476312 |
| 10 | 0.836095596749 | 0.387907304067 | 0.387907304067 | 0.0250712367487 |
| 11 | -0.836095596749 | 0.387907304067 | 0.387907304067 | 0.0250712367487 |
| 12 | 0.836095596749 | -0.387907304067 | 0.387907304067 | 0.0250712367487 |
| 13 | -0.836095596749 | -0.387907304067 | 0.387907304067 | 0.0250712367487 |
| 14 | 0.387907304067 | 0.836095596749 | 0.387907304067 | 0.0250712367487 |
| 15 | -0.387907304067 | 0.836095596749 | 0.387907304067 | 0.0250712367487 |
| 16 | 0.387907304067 | -0.836095596749 | 0.387907304067 | 0.0250712367487 |
| 17 | -0.387907304067 | -0.836095596749 | 0.387907304067 | 0.0250712367487 |
| 18 | 0.387907304067 | 0.387907304067 | 0.836095596749 | 0.0250712367487 |
| 19 | -0.387907304067 | 0.387907304067 | 0.836095596749 | 0.0250712367487 |
| 20 | 0.387907304067 | -0.387907304067 | 0.836095596749 | 0.0250712367487 |
| 21 | -0.387907304067 | -0.387907304067 | 0.836095596749 | 0.0250712367487 |

Table 6.2: Spherical integration points and weights.

iments are conducted at 0 °C, where a 25mm sample is uniaxially deformed from a stretch of 1 to a stretch of 6 and back at 10mm/min. One loading cycle thus takes approximately 25 minutes. The data for the NR-S, NR-P, and IR-S samples are plotted as dotted lines in Figures 6.1, 6.2, and 6.3 respectively. Optimized model parameters are found in two steps. In a first step, the evolution of the degree of crystallinity from the experiments is considered as given and only the stress-strain curve is fit. An estimate of the five material parameters of the non-affine micro-sphere model (N, p, $\mu$, q, U) is thus calculated using a least squares fit. As a next step, the remaining three parameters ($\mu_D$, $g_C$, $\gamma$) are fit by hand with only minor changes of the other parameters. This is feasible because of a clear meaning of the three parameters: an increase in $\mu_D$ decreases the maximum degree of crystallinity, and slightly increases the incipient crystallization stretch; an increase in $g_C$ increases the the incipient crystallization stretch and lowers the maximum degree of crystallinity; and an increase in $\gamma$ decreases/delays incipient decrystallization stretch and slightly decreases the maximum degree of crystallinity. The optimized material parameters for the model curves are listed in Table 6.3.

In Figures 6.1(a) Toki's experimental data for the NR-S sample are indicated by the

| | | Gaussian model | | | Non-Gaussian model | | |
|---|---|---|---|---|---|---|---|
| | | NR-S | NR-P | IR-S | NR-S | NR-P | IR-S |
| N | [-] | 195.95 | 191.13 | 199.95 | 175.95 | 191.70 | 191.95 |
| p | [-] | 1.4692 | 1.1594 | 1.4692 | 1.4692 | 1.4941 | 1.46922 |
| $\mu$ | [MPa] | 0.62023 | 1.0191 | 1.02023 | 0.62023 | 1.0878 | 1.02023 |
| q | [-] | 16.933 | 15.048 | 16.200 | 17.053 | 14.766 | 16.260 |
| U | [-] | 3.7578e-8 | 1.9937e-7 | 3.7578e-8 | 3.7578e-8 | 2.3993e-7 | 3.7578e-8 |
| $\mu_D$ | [MPa] | 0.110 | 0.125 | 0.210 | 0.115 | 0.130 | 0.205 |
| $g_C$ | [MPa] | 18 | 34 | 42 | 14 | 34 | 34 |
| $\gamma$ | [MPa] | -65 | -140 | -260 | -45 | -120 | -205 |

Table 6.3: Optimized material parameters for the models with Gaussian and non-Gaussian probability densities. The ambient temperature is $T = 0\,^{\circ}\mathrm{C}$ and the crystallization temperature is assumed to be $T_m^0 = -143.95\,^{\circ}\mathrm{C}$ (isoprene).

dotted line and the prediction by the *Gaussian model* by the solid line. The prediction of the stress-strain hysteresis is in good agreement up to a stretch of 4. Above a stretch of 4, during loading, the proposed model under predicts the stress due to the fact that the crystallization flow-rule is rate independent; this point is supported by the experimental observations of Marchal (2006). Note, that this rate dependency is independent of whether or not the background material model is elastic or viscoelastic. The prediction of the crystallization is seen to be quite good, except for the decrystallization from a stretch of 3 to 1. The prediction there appears to have some type of "inverse yielding" (necking during unloading) as mentioned in Albouy et al. (2005) and Trabelsi et al. (2003) (see Figure 1.1). Note a negative value of $\gamma$ is used which suggests a softening as mentioned in Section 5.4.2. It is also important to point out that the predicted value of $N \approx 196$ is physically sound. Assuming a monomer length of $a = 4$Å, the maximum degree of crystallinity $\omega_{max} \approx 0.15$ gives us an estimated crystallite length of $l_c \approx N\omega_{max}a \approx 118$Å, which falls into the range of reported crystallite lengths of 80Å to 180Å (Chenal et al., 2007; Trabelsi et al., 2003). Lastly it is noted that no relevant differences are found between the prediction generated by the *Non-Gaussian model* in Figure 6.1(b) and the *Gaussian model* in Figure 6.1(a).

In Figure 6.2(a) Toki's experimental data for the NR-P sample is indicated by the dotted line and the prediction by the *Gaussian model* by the solid line. The same remarks as made for the quality of the NR-S fit can be made here as well. However in Figure 6.3(a) the quality of the stress-strain hysteresis fit for Toki's IR-S seems to be better than the quality of the previous two fits. Deviations are only found on the loading curve between stretches of 4 and 6. Additionally the model is able to fully capture the instant start of the decrystallization as seen in the unloading part of the crystallization curve. The same also holds true for the *Non-Gaussian model* in Figure 6.3(b).

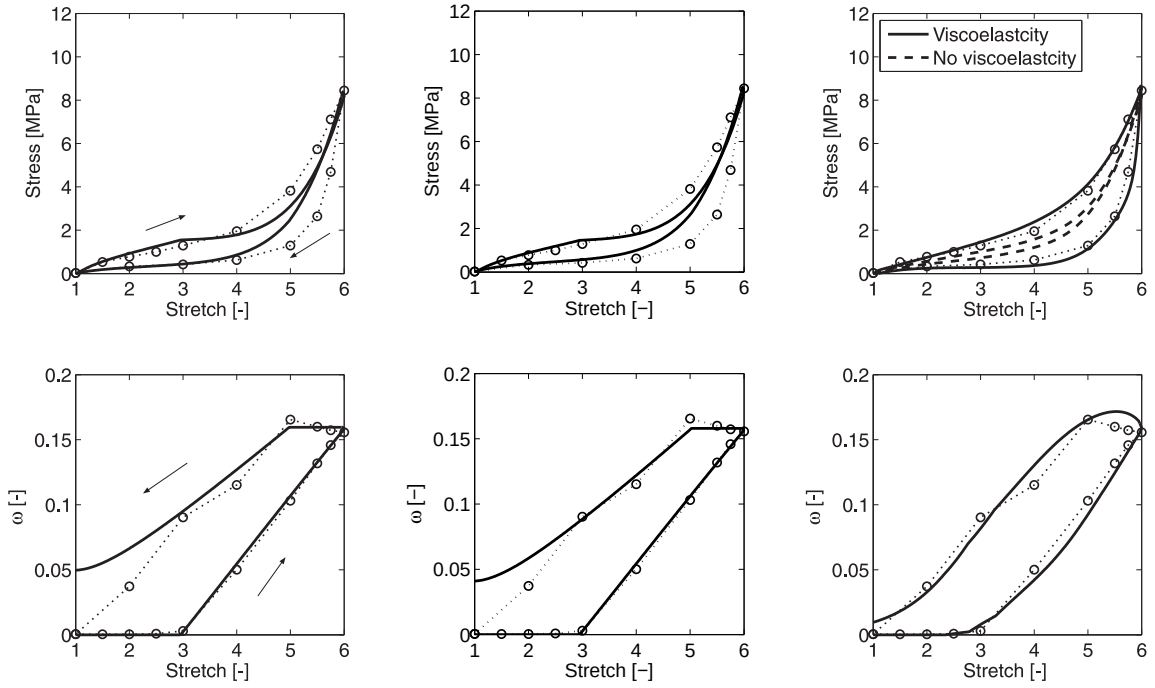


(a) Gaussian model (b) Non-Gaussian model (c) Kroon's model

Figure 6.1: Comparison of the sulfur vulcanized NR data (dotted line) to: (a) the Gaussian model; (b) the non-Gaussian model; and (c) Kroon's model with (solid line) and without (dashed line) viscoelasticity. The curve for the degree of crystallinity is only plotted once because it stays the same for both cases. Optimized parameters for (a) and (b) can be found in Table 6.3 under NR-S.

### 6.2.2 Model compared to Kroon's model

As mentioned in Chapter 1 a similar model was recently developed by Kroon (2010). One of the core differences between the two models is in how they view the increase of the degree of crystallinity. In the proposed model the increase in crystallinity stems from the growth of the extended-chain crystallites, which is supported by Chenal et al. (2007). Kroon uses the idea of Murakami et al. (2002), where the crystallite size is thought to be constant and the growth driven by nucleation. However, it is also mentioned in Murakami et al. (2002) that the induced crystallites are well packed, which can be seen as a growing crystallite provided the definition of a crystallite is loosened a bit. In any case, researchers do not seem to fully agree on the mechanism that governs the increase in crystallinity.

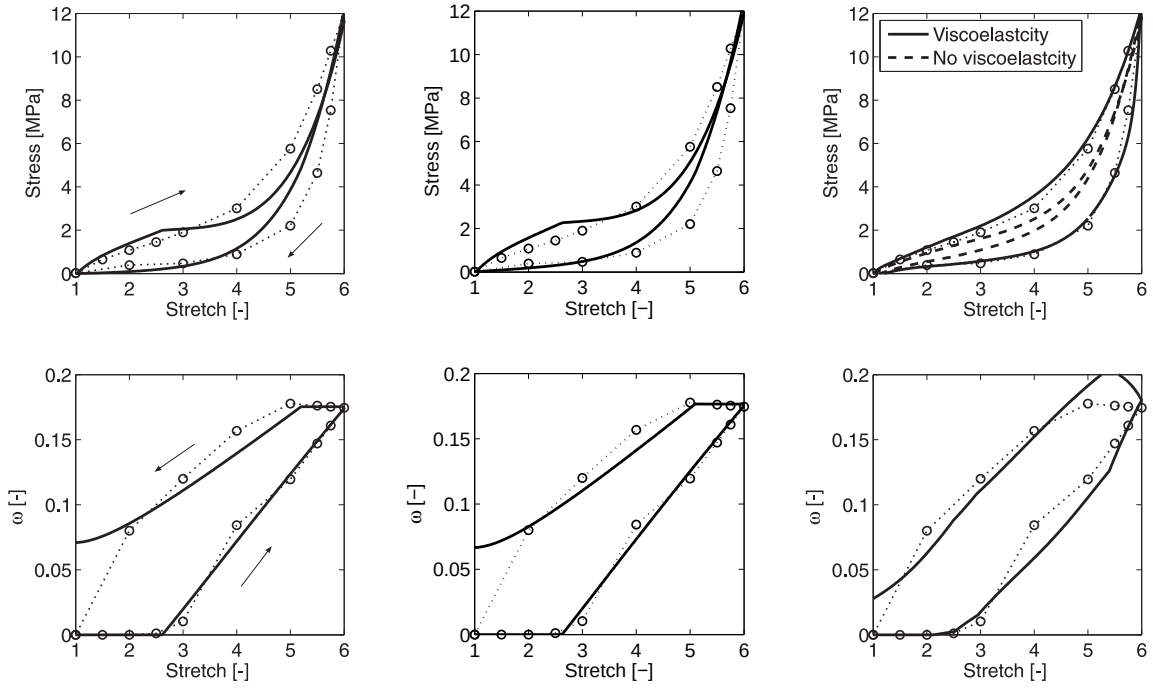


(a) Gaussian model (b) Non-Gaussian model (c) Kroon's model

Figure 6.2: Comparison of the peroxide vulcanized NR data (dotted line) to: (a) the Gaussian model; (b) the non-Gaussian model; and (c) Kroon's model with (solid line) and without (dashed line) viscoelasticity. The curve for the degree of crystallinity is only plotted once because it stays the same for both cases. Optimized parameters for (a) and (b) can be found in Table 6.3 under NR-P .

Another important point is viscoelasticity. In order to be able to predict the stress-strain hysteresis, Kroon uses a phenomenological viscoelastic component. However Murakami et al. (2002) and Trabelsi et al. (2003) clearly note that the hysteresis is entirely due to the phenomenon of crystallization and not due to viscoelastic effects. Toki's loading rate is also observed to be rather slow. Kroon's predictions with and without the viscoelastic component are plotted in Figures 6.1(c), 6.2(c), and 6.3(c). The plots show that without the viscoelastic component only a slight stress-strain hysteresis is observable. In the proposed model no viscoelastic component is used. This issue is clearly important if the model is to be utilized for fracture prediction where energy balance issues are of paramount interest.

Another difference in the models is the evolution law for the degree of crystallinity.

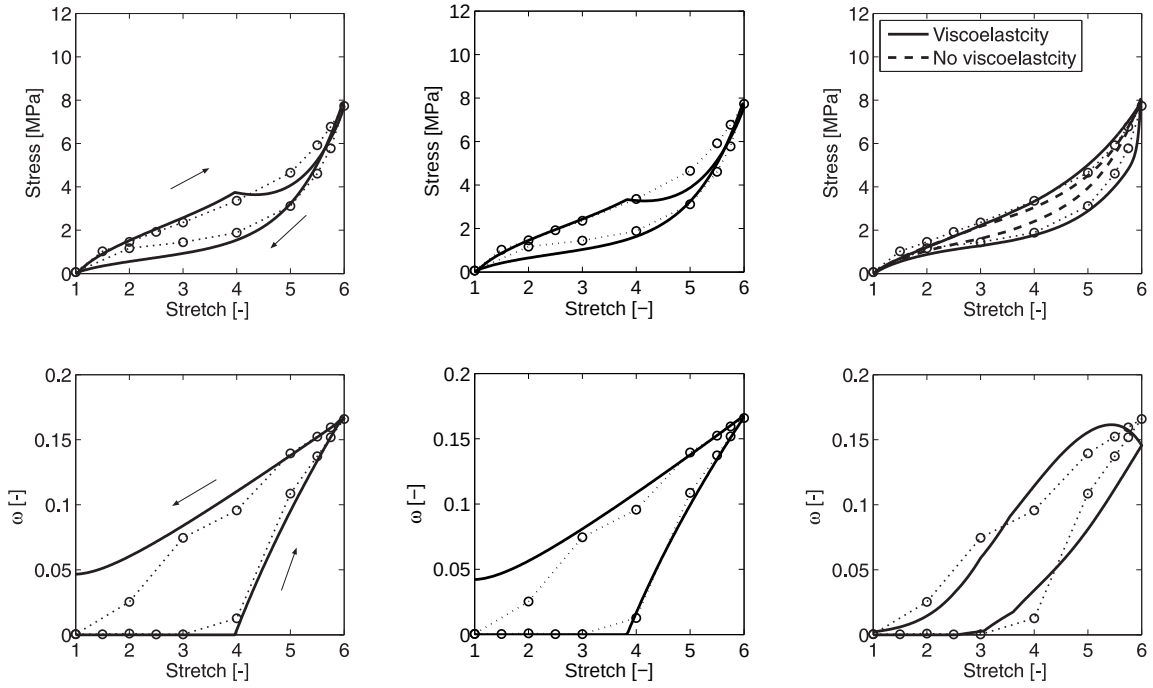


(a) Gaussian model (b) Non-Gaussian model (c) Kroon's model

Figure 6.3: Comparison of the sulfur vulcanized synthetic polyisoprene rubber data (dotted line) to: (a) the Gaussian model; (b) the non-Gaussian model; and (c) Kroon's model with (solid line) and without (dashed line) viscoelasticity. The curve for the degree of crystallinity is only plotted once because it stays the same for both cases. Optimized parameters for (a) and (b) can be found in Table 6.3 under IR-S.

In Kroon's model a phenomenological Arrhenius equation is implemented to govern the crystallinity. However in the proposed model it is felt that the approach using the chemical potential as a driving force is more physical and provides the better predictions for the degree of crystallinity, especially if compared in the case of IR-S in Figure 6.3.

A further modeling difference is found in the way the non-affine deformation is introduced. Kroon uses a phenomenological compliance stretch on the microscopic scale to incorporate non-affine deformation. Computationally it is equivalent to the introduction of an *ad hoc* penalty constraint, which is used to penalize non-affine deformation. In the proposed model the non-affine deformation is derived from a principle of minimum free energy and a simple closed-form result is obtained (Miehe et al., 2004). It is noted that Kroon's methodology

| | | Viscoelasticity | | | No viscoelasticity | | |
|---|---|---|---|---|---|---|---|
| | | NR-P | IR-S | NR-S | NR-P | IR-S | NR-S |
| $n$ | [-] | 22.0 | 20.0 | 23.3 | 22.0 | 27.6 | 22.4 |
| $n_c$ | [-] | 9.3 | 11.0 | 11.0 | 9.9 | 13.1 | 11.0 |
| $N$ | [-] | 0.1 | 0.1 | 0.1 | 0.1 | 0.1 | 0.1 |
| $\mu_c$ | [MPa] | 1.05 | 1.20 | 0.60 | 1.00 | 1.35 | 0.6 |
| $\alpha$ | [MPa] | 0 | 0 | 0 | 0 | 0 | 0 |
| $\mu_{nc}$ | [MPa] | 180 | 63 | 170 | 245 | 270 | 200 |
| $\mu_v$ | [MPa] | 1 | 1 | 1 | 0 | 0 | 0 |
| $\eta$ | [MPa min] | 0.25 | 0.12 | 0.20 | - | - | - |
| $g_c$ | [$\text{min}^{-1}$] | 0.088 | 0.047 | 0.044 | 0.073 | 0.066 | 0.051 |
| $g_a$ | [$\text{min}^{-1}$] | 0.31 | 0.74 | 0.50 | 0.31 | 0.59 | 0.48 |

Table 6.4: The material parameters used for the reproduced results of Kroon's model.

can lead to unstable behavior at large stretches.

As a last point, the model parameters regarding the crystallite size are mentioned. Kroon uses a parameter $N$ as the number of participating chains in the crystallite and a parameter $n_c$ as the number of links in the extended-chain crystal. The first value turns out to be $N = 0.1$, which is not physical and the second value is around $n_c = 11$, which is physically quite low. In the proposed model however, the predicted size of the crystallite fully agrees with experimentally reported values.

**Remark 6.1.** *The predictions in Figures 6.1(c), 6.2(c), and 6.3(c) are reproduced results from Kroon (2010) and might slightly differ from the original predictions, since here a 21-point integration scheme (Bazant and Oh, 1986) is used to integrate over a spherical surface instead of the 50-point integration scheme mentioned in Kroon (2010). The material parameters used for the reproduced results of Kroon's model curves are listed in Table 6.4.*

# Chapter 7

# Concluding Remarks

The goal of this thesis was to develop a computationally-accessible micro-mechanically motivated continuum model for SIC in NR. To this end, a micro-mechanical model of a constrained partially crystallized polymer chain was derived and subsequently connected to the macroscopic level using the non-affine micro-sphere model. On the macroscopic level, a thermodynamically consistent framework for strain-crystallizing materials was developed, and a description of the crystallization kinetics was introduced. For that matter, an evolution law for crystallization based on the gradient of the macroscopic Helmholtz free energy function (chemical potential) in combination with a simple threshold function was used. The key here was the addition of a softening of the critical chemical potential driving force with advancing crystallization. The predictive performance of the proposed model was shown by fitting available experimental data for various cured natural rubber samples, and as a last step the model was compared to a recently developed constitutive model to highlight its physical features. It is seen that both the coarse scale stress-strain response is reasonably reproduced as is the internal state degree of crystallinity. Further the fitted model parameters are seen to correctly fit in the physical range seen in experiments. The good behavior occurs despite this rather basic model of SIC. This simplicity warrants further discussion.

Three key issues were encountered during the development of this model. Firstly, as mentioned in Section 5.3.2, the proposed model is isotropic, and the addition of anisotropy with relaxation over the micro-sphere is non-trivial but a desirable next step. However, there is only little experimental work available on anisotropic effects of SIC on the macroscopic scale, such that the testing of an anisotropic model would be difficult.

A second relevant issue is viscoelasticity. Researchers do not seem to agree completely on whether the hysteretic behavior is entirely due to the phenomenon of crystallization or due to viscoelastic effects. More work has to be done to understand thoroughly the energetic and dissipative effects. This is especially important with regard to the current work of the author on fracture prediction, where energy balance issues are of utmost interest.

Thirdly, the mechanisms that govern the evolution of the degree of crystallinity are not entirely clear. Chenal et al. (2007) suggests that there are a fixed amount of nuclei in the amorphous polymer and the increase in crystallinity stems from crystal growth. However,

Murakami et al. (2002) states that the size of the crystallites is constant and a growth in crystallinity is achieved through the formation of nuclei. Again, more experimental work has to be done to fully understand the underlying physics of crystallization in NR.

Finally, a further suggestion to improve the predictive ability of the proposed model, is to use a rate-dependent crystallization "flow-rule" as seen in viscoplasticity formulations by Perzyna and Duvaut-Lions (see e.g. Simo and Hughes (1998, Section 2.7)) instead of a rate-independent ones.

# Appendix A

# Non-Gaussian Model

## A.1 Probability Density $\bar{p}_f$

The probability density of the conformation in Figure 5.1 using the Non-Gaussian probability density (3.128) is given as

$$\begin{aligned}
\bar{p}_f(\lambda;\omega) &= -\frac{1}{3200N^4\pi^{3/2}(-1+\omega)^8\sqrt{\frac{1}{N-N\omega}}}3\sqrt{\frac{3}{2}}e^{\frac{3(\lambda-\sqrt{N}\omega)^2}{2(-1+\omega)}}(3(243\lambda^8-828\lambda^6(-1+\omega)\\
&- 2346\lambda^4(-1+\omega)^2-900\lambda^2(-1+\omega)^3-485(-1+\omega)^4)-72\sqrt{N}\lambda(81\lambda^6\\
&- 207\lambda^4(-1+\omega)-391\lambda^2(-1+\omega)^2-75(-1+\omega)^3)\omega-5832N^{7/2}\lambda\omega^7\\
&+ 729N^4\omega^8-72N^{5/2}\lambda\omega^3(-160+\omega(480+(-273+567\lambda^2-47\omega)\omega))\\
&+ 36N^3\omega^4(-80+\omega(240+\omega(-171+567\lambda^2+11\omega)))-24N^{3/2}\lambda\omega(1701\lambda^4\omega^2\\
&- 30\lambda^2(-1+\omega)(-16+\omega(32+53\omega))-(-1+\omega)^2(1120+\omega(-2240+2293\omega)))\\
&+ 12N(1701\lambda^6\omega^2-225(-1+\omega)^3\omega^2-15\lambda^4(-1+\omega)(-16+\omega(32+191\omega))\\
&- \lambda^2(-1+\omega)^2(1120+\omega(-2240+4639\omega)))-2N^2(800+\omega(-4800+\omega(18720\\
&- 25515\lambda^4\omega^2+270\lambda^2(-1+\omega)(-32+\omega(64+37\omega))+\omega(-42880+\omega(55839\\
&+ \omega(-38718+11039\omega)))))),
\end{aligned}$$

where $N_1$ and $N_2$ are assumed to be $N(1-\omega)/2$, since the position of the extended crystal within the chain does not change the result. The probability density $\bar{p}_f$ was calculated using Mathematica.

# Bibliography

Albouy, P., Marchal, J., Rault, J., 2005. Chain orientation in natural rubber, part i: The inverse yielding effect. European Physical Journal E 17, 247–259.

Allen, P., 1952. The kinetics of the crystallization of hexamethylene adipamide polymer. Transactions of the Faraday Society 48, 1178–1185.

Arlman, J., 1949. On the degree of crystallinity in natural rubber iii. Applied Scientific Research 1, 347–352.

Arlman, J., Goppel, J., 1951. On the degree of crystallinity in natural rubber .v. a discussion of the x-ray results on natural rubber in connection with the work of flory, gee and wildschut. Applied Scientific Research Section A-Mechanics Heat Chemical Engineering Mathematical Methods 2, 1–8.

Avrami, M., 1939. Kinetics of phase change I - General theory. The Journal of Chemical Physics 7, 1103–1112.

Avrami, M., 1940. Kinetics of phase change. II. Transformation-time relations for random distribution of nuclei. The Journal of Chemical Physics 8, 212–224.

Avrami, M., 1941. Granulation, phase change, and microstructure - kinetics of phase change. III. The Journal of Chemical Physics 9, 177–184.

Bazant, Z., Oh, B., 1985. Microplane model for progressive fracture of concrete and rock. Journal of Engineering Mechanics 111, 559–582.

Bazant, Z., Oh, B., 1986. Efficient numerical-integration on the surface of a sphere. Zeitschrift fuer Angewandte Mathematik und Mechanik 66, 37–49.

Becker, R., 1938. Die Keimbildung bei der Ausscheidung in metallischen Mischkristallen. Annalen der Physik 424, 128–140.

Bishop, R., Goldberg, S., 2012. Tensor Analysis on Manifolds. Dover Books on Mathematics. Dover Publications.

Boyce, M., Arruda, E., 2000. Constitutive models of rubber elasticity: A review. Rubber Chemistry and Technology 73, 504–523.

Bunn, C., 1942a. Molecular structure and rubber-like elasticity. I. The crystal structure of $\beta$ gutta-percha, rubber and polychloroprene. Proceedings of the Royal Society A 180, 40–66.

Bunn, C., 1942b. Molecular structure and rubber-like elasticity. III. Molecular movements in rubber-like polymers. Proceedings of the Royal Society A 180, 82–99.

Casey, J., 1998. On elastic-thermo-plastic materials at finite deformations. International Journal of Plasticity 14, 173 – 191.

Casey, J., Krishnaswamy, S., 1998. A characterization of internally constrained thermoelastic materials. Mathematics and Mechanics of Solids 3, 71–89.

Chadwick, P., 1999. Continuum Mechanics: Concise Theory and Problems. Dover books on physics. Dover Publications.

Chandler, D., 1987. Introduction to Modern Statistical Mechanics. Oxford University Press Inc.

Chenal, J.-M., Chazeau, L., Guy, L., Bomal, Y., Gauthier, C., 2007. Molecular weight between physical entanglements in natural rubber: A critical parameter during strain-induced crystallization. Polymer 48, 1042–1046.

Coleman, B., Noll, W., 1963. The thermodynamics of elastic materials with heat conduction and viscosity. Archive for Rational Mechanics and Analysis 13, 167–178.

Doi, M., Edwards, S., 1986. The Theory of Polymer Dynamics. The International Series of Monographs on Physics Series. Oxford University Press Inc.

Ericksen, J., 2008. On the Cauchy-Born rule. Mathematics and Mechanics of Solids 13, 199–220.

Evans, U., 1945. The laws of expanding circles and spheres in relation to the lateral growth of surface films and the grain-size of metals. Transactions of the Faraday Society 41, 365–374.

Flory, P., 1947. Thermodynamics of crystallization in high polymers. 1. crystallization induced by stretching. The Journal of Chemical Physics 15, 397–408.

Flory, P., 1953. Principles of Polymer Chemistry. Cornell University Press, Ithaca, New York.

Flory, P., 1961. Thermodynamic relations for high elastic materials. Transactions of the Faraday Society 57, 829–838.

Flory, P., 1969. Statistical Mechanics of Chain Molecules. Wiley-Interscience, New York.

Gaylord, R., 1976. A theory of the stress-induced crystallization of crosslinked polymeric networks. Journal of Polymer Science. Part B, Polymer Physics 14, 1827–1837.

Gaylord, R., Lohse, D., 1976. Morphological changes during oriented polymer crystallization. Polymer Engineering and Science 16, 163–167.

Gee, G., Stern, J., Treloar, L. R. G., 1950. Volume changes in the stretching of vulcanized natural rubber. Trans. Faraday Soc. 46, 1101–1106.

Gent, A., 1954. Crystallization and the relaxation of stress in stretched natural rubber vulcanizates. Transactions of the Faraday Society 50, 521–533.

Gibbs, J., 2010. Elementary Principles in Statistical Mechanics: Developed with Especial Reference to the Rational Foundation of Thermodynamics. Cambridge Library Collection - Mathematics. Cambridge University Press.

Göktepe, S., Miehe, C., 2005. A micro-macro approach to rubber-like materials: Part III: The micro-shpere model of anisotropic Mullins-type damage. Journal of the Mechanics and Physics of Solids 53, 2259–2283.

Goppel, J., 1949a. On the degree of crystallinity in natural rubber i. Applied Scientific Research 1, 3–17.

Goppel, J., 1949b. On the degree on crystallinity in natural rubber ii. Applied Scientific Research 1, 18–26.

Goppel, J.M. and Arlman, J.J., 1949. On the degree of crystallinity in natural rubber .iv. the degree of crystallization in frozen raw rubber and stretched vulcanized rubber. Applied Scientific Research Section A-Mechanics Heat Chemical Engineering Mathematical Methods 1, 462–474.

Govindjee, S., 2006. Nonlinear continuum mechanics. Lecture notes.

Govindjee, S., 2007. Statistical mechanics of elasticity. Lecture notes.

Govindjee, S., Miehe, C., 2001. A multi-variant martensitic phase transformation model: formulation and numerical implementation. Computer Methods in Applied Mechanics and Engineering 191, 215–238.

Govindjee, S., Simo, J., 1991. A micro-mechanically based continuum damage model for carbon black-filled rubbers incorporating mullins effect. Journal of the Mechanics and Physics of Solids 39, 87–112.

Green, A., Naghdi, P., 1977. On thermodynamics and the nature of the second law. Proceedings of the Royal Society of London. A. Mathematical and Physical Sciences 357, 253–270.

Guilie, J., Lê, T., Le Tallec, P., 2013. Microsphere model for strain-induced crystallization in rubber. In: Alonso, G.-N. . (Ed.), Proceedings of the 8th conference on constitutive models in rubbers. Taylor & Francis, San Sebastian, Espagne, pp. 467–472.

Gurtin, M., 1982. An Introduction to Continuum Mechanics. Mathematics in Science and Engineering. Elsevier Science.

Gurtin, M., Fried, E., Anand, L., 2010. The Mechanics and Thermodynamics of Continua. The Mechanics and Thermodynamics of Continua. Cambridge University Press.

Hoffman, J., Weeks, J., 1962. Rate of spherulitic crystallization with chain folds in polychlorotrifluoroethylene. Journal of Chemical Physics 37, 1723–&.

Holzapfel, G., 2000. Nonlinear Solid Mechanics: A Continuum Approach for Engineering. John Wiley & Sons.

Katz, J., 1925. Was sind die Ursachen der eigentümlichen Dehnbarkeit des Kautschuks? Kolloid-Zeitschrift 36, 300–307.

Khinchin, A., 2013. Mathematical Foundations of Statistical Mechanics. Dover Books on Mathematics. Dover Publications.

Kroon, M., 2010. A constitutive model for strain-crystallising rubber-like materials. Mechanics of Materials 42, 873–885.

Landau, L., Lifshitz, E., 1980. Statistical Physics. Pergamon Press, Oxford.

Le Cam, J.-B., Toussaint, E., 2010. The mechanism of fatigue crack growth in rubbers under severe loading: the effect of stress-induced crystallization. Macromolecules 43, 4708–4714.

Marchal, J., 2006. Cristallisation des caoutchoucs chargés et non chargés sous contrainte: Effet sur les chaînes amorphes. Ph.D. thesis, University of Paris XI, Orsay.

Mark, J., 1981. Rubber elasticity. Journal of Chemical Education 58, 898–903.

Marsden, J., Hughes, T., 1994. Mathematical Foundations of Elasticity. Dover Civil and Mechanical Engineering Series. Dover.

Menzel, A., Waffenschmidt, T., 2009. A microsphere-based remodelling formulation for anisotropic biological tissues. Philosophical Transactions of the Royal Society A 367, 3499–3523.

Miehe, C., Goktepe, S., Lulei, F., 2004. A micro-macro approach to rubber-like materials - Part I: The non-affine micro-sphere model of rubber elasticity. Journal of the Mechanics and Physics of Solids 52, 2617–2660.

Mielke, A., 2004. Deriving new evolution equations for microstructures via relaxation of variational incremental problems. Computer Methods in Applied Mechanics and Engineering 193, 5095–5127.

Mielke, A., Ortiz, M., 2008. A class of minimum principles for characterizing the trajectories and the relaxation of dissipative systems. ESAIM: Control, Optimisation and Calculus of Variations 14, 494–516.

Mistry, S., Govindjee, S., 2014. A micro-mechanically based continuum model for strain-induced crystallization in natural rubber. International Journal of Solids and Structures 51, 530 – 539.

Murakami, S., Senoo, K., Toki, S., Kohjiya, S., 2002. Structural development of natural rubber during uniaxial stretching by in situ wide angle x-ray diffraction using a synchrotron radiation. Polymer 43, 2117–2120.

Naghdi, P., 2001. Introduction to continuum mechanics. Lecture notes.

Ogden, R., 1997. Non-linear Elastic Deformations. Dover Civil and Mechanical Engineering Series. Dover Publications.

Papadopoulos, P., 2013. Introduction to continuum mechanics. Lecture notes.

Penrose, O., 1979. Foundations of statistical mechanics. Reports on Progress in Physics 42, 1937–2006.

Reif, F., 1965. Fundamentals of Statistical and Thermal Physics. McGraw Hill Higher Education.

Rivlin, R., 1973. Comments on some recent researches in thermomechanics. Recent Advances in Engineering Science 8, 1–23.

Rivlin, R., 1975. The thermomechanics of materials with fading memory. Theoretical Rheology, 83–103.

Rivlin, R., Barenblatt, G., Joseph, D., 1997. Collected Papers of R.S. Rivlin. No. v. 1 in Collected Papers of R.S. Rivlin. Springer.

Roe, R.-J., Krigbaum, W., 1965. Application of irreversible thermodynamics to the kinetics of polymer crystallization from seeded nuclei. Polymer 6, 231–236.

Rudin, W., 1976. Principles of mathematical analysis. International series in pure and applied mathematics. McGraw-Hill.

Serrin, J., 1996. The equations of continuum mechanics and the laws of thermodynamics. Meccanica 31, 547–563.

Simo, J., Hughes, T., 1998. Computational Inelasticity. Interdisciplinary applied mathematics: Mechanics and materials. Springer Verlag.

Smith, Jr, K., 1976. Crystallization of networks under stress. Polymer Engineering and Science 16, 168–175.

Toki, S., Fujimaki, T., Okuyama, M., 2000. Strain-induced crystallization of natural rubber as detected real-time by wide-angle x-ray diffraction technique. Polymer 41, 5423–5429.

Toki, S., Sics, I., Hsiao, B., Tosaka, M., Poompradub, S., Ikeda, Y., Kohjiya, S., 2005. Probing the nature of strain-induced crystallization in polyisoprene rubber by combined thermomechanical and in situ x-ray diffraction techniques. Macromolecules 38, 7064–7073.

Toki, S., Sics, I., Ran, S., Liu, L., Hsiao, B., 2003. Molecular orientation and structural development in vulcanized polyisoprene rubbers during uniaxial deformation by in situ synchrotron x-ray diffraction. Polymer 44, 6003–6011.

Trabelsi, S., Albouy, P., Rault, J., 2003. Crystallization and melting processes in vulcanized stretched natural rubber. Macromolecules 36, 7624–7639.

Treloar, L., 1975. The Physics of Rubber Elasticity. Clarendon Press, Oxford.

Treloar, L., Riding, G., 1979. A non-Gaussian theory for rubber in biaxial strain. I. Mechanical properties. Proceedings of the Royal Society A 369, 261–280.

Truesdell, C., Noll, W., 1965. The Non-Linear Field Theories of Mechanics. Springer Verlag, New York.

Truesdell, C., Toupin, R., 1960. The Classical Field theories. Springer.

Turnbull, D., Fisher, J., 1949. Rate of nucleation in condensed systems. Journal of Chemical Physics 17, 71–73.

Wang, M., Guth, E., 1952. Statistical theory of networks of non-gaussian flexible chains. The Journal of Chemical Physics 20, 1144–1157.

Weiner, J., 1983. Statistical Mechanics of Elasticity. John Wiley & Sons, Inc.

Wildschut, A. J., 1946. On the proportion of crystalline and amorphous components in stretched vulcanized rubber. Journal of Applied Physics 17, 51–60.

Wu, P., van der Giessen, E., 1993. On improved network models for rubber elasticity and their applications to orientation hardening in glassy polymers. Journal of the Mechanics and Physics of Solids 41, 427–456.